CHALMERS

Optimization of the Quasi Dynamic Method for Solar Collector Testing

Master of Science Thesis in Sustainable Energy Systems (MPSES)

GAËL SEENÉ, PATRIK OLLAS

Department of Energy and Environment
Division of Building Services Engineering
CHALMERS UNIVERSITY OF TECHNOLOGY
Gothenburg, Sweden, 2012
Report No. E2012:05

THESIS FOR THE DEGREE OF MASTER OF SCIENCE

Optimization of the quasi dynamic method for solar collector testing

Master of Science Thesis in Sustainable Energy Systems (MPSES)

GAËL SEENÉ, PATRIK OLLAS

SUPERVISORS:
Peter Kovacs
Martin Persson

EXAMINER:
Jan-Olof Dalenbäck

CHALMERS

Department of Energy and Environment
Division of Building Services Engineering
CHALMERS UNIVERSITY OF TECHNOLOGY
Gothenburg, Sweden, 2012

Optimization of the quasi dynamic method for solar collector testing

Master's Thesis within the Sustainable Energy System programme

GAEL SEENÉ
PATRIK OLLAS

Department of Energy and Environment
Division of Building Services Engineering
Chalmers University of Technology
SE-412 96 Göteborg
Sweden
Telephone + 46 (0)31-772 1000

Cover:
Test installation for two evacuated tube collectors at SP Technical Research Institute of Sweden.

Chalmers Reproservice
Göteborg, Sweden 2012

Optimization of the quasi dynamic method for solar collector testing
Master's Thesis within the Sustainable Energy System (MPSES) programme
GAËL SEENE, PATRIK OLLAS

Department of Energy and Environment
Division of Building Services Engineering
Chalmers University of Technology

ABSTRACT

The aim of this Master Thesis work is to optimize the Quasi-Dynamic Test (QDT) method used to evaluate the thermal performance of solar collectors. Three main areas of improvement are identified; increasing the angular resolution in the evaluation process, using a dynamic inlet temperature variation, both to increase the accuracy and the latter in combination with night time measurements to shorten the required test period. These options are tested, on one side with simulated data from TRNSYS, and on the other through experiments on a flat plate collector and a heat pipe evacuated tube collector.

The results from analytical testing on simulated collector data show that an increased angular resolution, a dynamic inlet temperature change and night measurements are valid options for improving the QDT method. Experimental trials conducted on one type of flat-plate collector show that increasing the angular resolution in the evaluation is useful for detecting measurement errors caused by external factors and confirm the theoretical findings of using a dynamic inlet temperature variation coupled with night time measurements.

Key words: Solar collector testing, quasi-dynamic, QDT, QAiST, TRNSYS, FPC, ETC, CPC, night time measurement, optimization, dynamic inlet temperature, EN 12975-Standard

Optimering av den quasi-dynamiska testmetoden för solfångare
Examensarbete inom masterprogrammet Sustainable Energy Systems (MPSES)
GAËL SEENE, PATRIK OLLAS
Institutionen för Energi och Miljö
Avdelningen för installationsteknik
Chalmers Tekniska Universitet

SAMMANFATTNING

Syftet med detta examensarbete är att optimera den quasi-dynamiska testmetoden som används för utvärdering av den termiska prestandan hos solfångare. Tre huvudområden för optimering identifierades – högre vinkelupplösning för användning i utvärderingsprocessen, användandet av en dynamiskt varierade inloppstemperatur, båda för att öka noggrannheten vid mätningarna, den senare också tillsammans med mätningar under natten för att korta ner testtiden. Dessa tre alternativ utvärderades dels med hjälp av simulerad data från TRNSYS och dels med hjälp av experimentell data från mätningar på en plan solfångare och en vakuumsolfångare.

Resultaten från de analytiska testerna på simulerad data visade att en högre vinkelupplösning, en dynamisk varierande temperaturprofil och mätningar från natten är giltga metoder som kan användas vid optimering av QDT metoden. Experimentella tester på en plan solfångare bekräftade också att användandet av en högre vinkelupplösning och en dynamisk ingångstemperatur tillsammans med mätdata från natten kan förbättra testmetoden.

Nyckelord: Solfångare, quasi-dynamisk, QDT, QAiST, TRNSYS, FPC, ETC, CPC, nattmätningar, optimering, dynamisk ingångstemperatur, EN 12975-Standard

ACKNOWLEDGEMENTS

This Master Thesis has been financed by SP Technical Research Institute of Sweden in collaboration with QAiST[1].

We would first of all like to thank our supervisors at SP; Martin Persson and Peter Kovacs for their helpfulness, inspiration and knowledge. They have been a great part of the completion of this Thesis. Further on at SP we would like to thanks Torbjörn Eliasson that helped us with the programming of our configuration used for measurements.

A special thanks to Bengt Perers, Senior researcher at the Technical University of Denmark that has been a priceless source of expert knowledge and guidance. He has also been providing us with the TRNSYS simulation data that has been used as a validation of our findings.

Thanks also to our examiner Jan-Olof Dalenbäck professor at Chalmers University of Technology for good collaboration and feedback on the report and for taking care of all administrative parts.

[1] QAiST: http://www.qaist.org/

TABLE OF CONTENTS

1 INTRODUCTION

Solar collectors need to be tested in order to determine their characteristics in terms of thermal performance and durability. The thermal evaluation tests can be done either outdoors or indoors under static or dynamic ambient conditions respectively. While outdoor testing under static weather conditions can be hard to achieve in some locations, there is a need for varying conditions to accurately determine the collector characteristics. Owing to this, Sweden has, together with Dr. Bengt Perers and SP Technical Research Institute of Sweden developed one of the two certificated test models that are being used today by the European test facilities and included in the EN 12975 Standard; the Quasi Dynamic Testing, QDT. This method allows a wider range of acceptance regarding the transient outdoor conditions (Perers, 1997).

Standardized test methods of the solar collectors thermal output developed with acceptable accuracy are crucial in the maturity and wide spreading of the solar collector technology. This gives the ability to universally and fairly compare collector performance and enables a way of communication between customer and supplier. As a result, the producers strive to be on top by trying to create the best performing collectors at minimum costs, thus stimulating the market and enhancing the solar collector development. Today's testing and evaluation is however relatively complicated and expensive, especially for small companies trying to reach the market.

An optimization of the existing Quasi Dynamic Test model aims at reducing the test time required without compromising on the accuracy of the results. This would enable test institutes to make collector testing more efficient and readily available for their costumer, thus increasing the internal market turnover and creating a positive feedback.

2 BACKGROUND

The world's final energy consumption today is very much dependent on non-renewable energy sources such as oil, gas and coal/peat which are associated with environmentally hazardous emissions. The fact is that out of the total final demand of 518 EJ, 71.8 % was produced from these non-renewable sources in 2009 (IEA, 2010). Some scientists argue that the future energy demand will increase due to the population growth and more energy intensive needs. As some of these energy sources previously mentioned have reached, or are close to reaching their peak supply, man-kind could possibly be heading towards a major energy crisis if no applicable substitutions are found; not to mention the creation of a contaminated environment for our future generations (Mandil, 2008).

The solution to this problem is to find technologies that achieve substantial emission reductions in the most cost-effective way possible. One source of energy that seems free of charge, emission free[2] and almost unlimited is the one extracted from the sun. Today however, solar collectors are a high cost emission abatement option for creating heat and will remain so in the short-term future unless progress within this area is made in cost-reductions and technology development. Competing energy sources such as gas, coal and oil are much cheaper and have already penetrated the market, thus making them hard and expensive to phase out. More research within the solar industry needs to be done to increase the knowledge and enhance the internal positive feedback to the system.

Standardisation enables a uniform way of communicating within the solar energy business and a fair way of evaluating the thermal performance of collectors. However, further improvements in the existing test method could enhance the market diffusion of thermal solar power since it would be possible to cut down costs and testing time, and thus embrace a broader clientele.

[2] Solar collectors are assumed to be emission free when looking at them from a local usage perspective

2.1 MAIN SOLAR COLLECTOR DESIGNS

The basic function of a solar collector is to convert the energy extracted from the solar radiation into useful heat, e.g. hot water or residential heating. This is done by the solar collector through conversion of solar short wave radiation into heat which is then exchanged from absorber surface to the working fluid. Following is a description of the basic configuration for the three most commercially available collector types; flat-plate, evacuated tube and concentrating collectors.

2.1.1 FLAT-PLATE COLLECTORS

A flat-plate solar collector has the simplest designs and requires neither tracking nor as much maintenance as the other collector designs. Figure 2.1 shows a principle sketch of all main components of a flat-plate solar collector. The cover box contains insulation to prevent losses, the main pipe to transfer the heating media, a dark-coloured absorber and a cover glass.

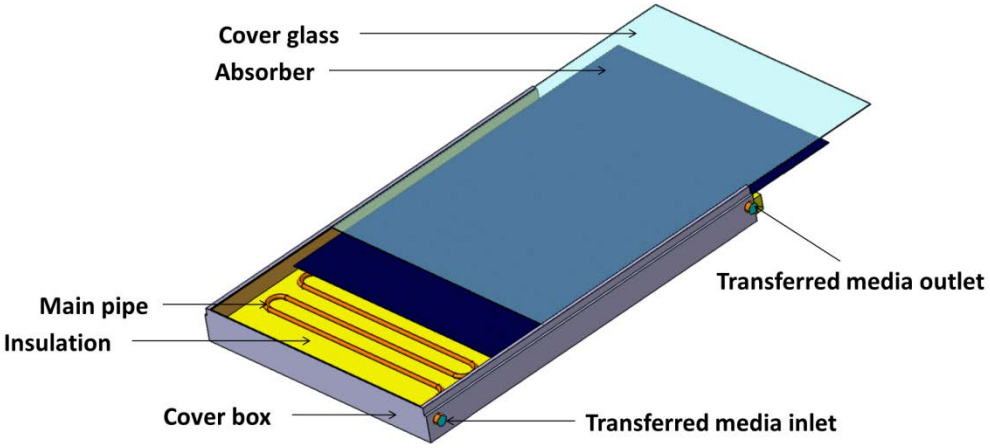

Figure 2.1 Principle layout of a typical flat-plate solar collector with a serpentine piping configuration

Direct and diffuse solar radiation is absorbed by the absorber and heat transfer is done to the heating media through a heat exchange where the solar energy is converted to useful heat. The absorber plate is usually made out of metal, typically copper or aluminium for their good heat conduction properties. To further enhance the heat retaining effects, the absorber is usually treated with a selective coating, such as titanium oxynitride or aluminium oxide.

The cover glazing must be designed to withstand high operating temperatures and tough mechanical strains, proposed by wind, hail, snow or external vandalism. Furthermore, it should transmit incoming solar radiation well and keep the low wavelength radiation trapped once reflected by the absorber to minimize losses. A number of different materials are possible in that sense and

the selection of the best one is merely a trade-off between those properties. Examples of glazing materials used are; glass, different types of polymers and fibreglass. There are also varieties of solar collectors without any glazing, typically used for low temperature operations referred to as unglazed collectors.

A number of different absorber-media configurations are on the market but the most commonly used type is to separate them by the use of a media transferring pipe. These piping configurations come mainly in two different varieties; harp and serpentines, see Figure 2.2. In the harp piping configuration, the media is transferred once through the collector and continuously heated by the sun from the bottom pipe to the upper collecting pipe (manifold) where it is heat exchanged. Serpentine collectors use a continuous S-shaped piping configuration where the media is transferred through the whole collector.

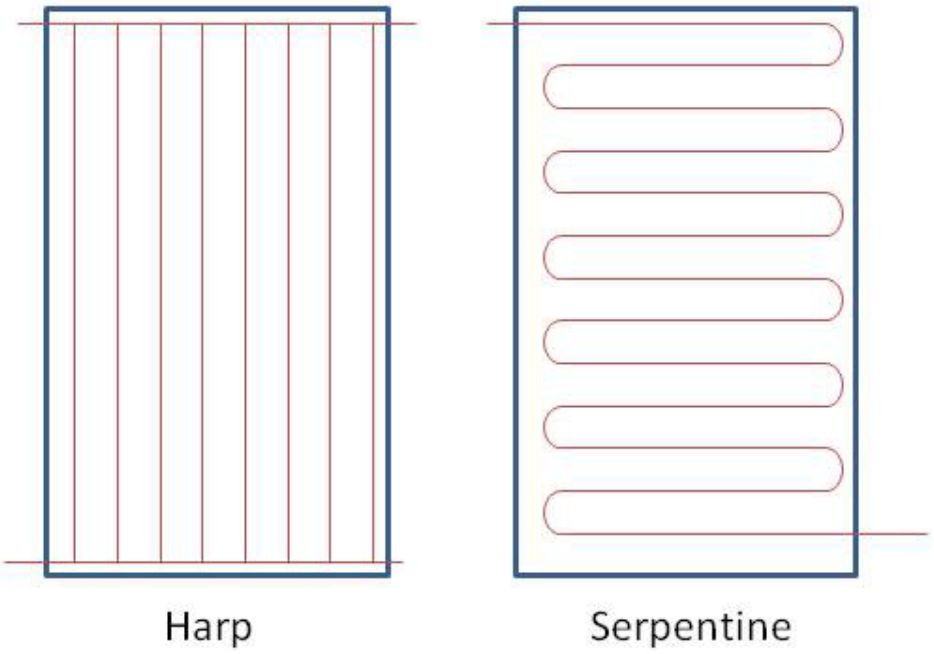

Figure 2.2 Harp and serpentine piping configuration for flat plate collectors

As any other object with a temperature above ambient, the collector wants to return to its thermal equilibrium. This is done by thermal losses to the surrounding air, for further elaboration around these, see *2.3 Collector performance*. To minimize these losses, insulation is added to the cover box and thereby preventing the heat to escape.

2.1.2 EVACUATED TUBE COLLECTORS

An evacuated-tube collector is characterized by the use of encapsulated vacuum for minimizing the convective and radiation heat losses. It can be composed either by an inner and outer layer of strong borosilicate glass joined together and containing the vacuum (double-glazed), or by covering the

absorption surface in vacuum (single-glazed). Within these two types, three main configurations can be distinguished; direct-flow evacuated-tubes consisting of only one circuit of the same fluid, heat pipe evacuated-tube collector characterized by the heat exchange between two closed streams, and the integrated tank solar collector based on the same principle as the direct-flow tubes but with an integrated liquid storage (GreenTerraFirma, 2007).

For the direct-flow evacuated tubes type, the evacuated glass tubes contain aluminium fins covered by a selective coating. These fins are attached to an absorber pipe (usually in copper) in which water circulates. Three different types of direct-flow evacuated collectors can be distinguished depending on the water pipes arrangement,

- A single absorber pipe contains the water inlet and outlet and can be rotated in order to orientate the fin. This results in a glass-metal contexture between the glass tube and the metal absorber pipe.
- Secondly, the absorber pipe can include a U-shaped pipe with one end for the water inlet and the other end for water outlet, similar to the harp configuration for the flat plate collector, see Figure 2.2. The absorber pipe can therefore be flat or curved. This the most common type of flow-direct tube. This is also a glass-metal assembly type of collector.
- The last type is made by the fusion of the absorber pipe made of glass, this time with the other glass tube. Hence, the inner tube is coated with a cylindrical metal absorber. This type is therefore a glass-glass assembly type.

Concerning the heat pipe configuration, the media transferring pipe is mounted into a fin for heat conduction and surrounded by a cylindrical absorber coating the inner tube. A condenser is situated at the top of the heat pipe and is inserted into a main copper pipe containing a set of sleeves in which a heating fluid (such as water or a mixture of glycol and water) is circulating. Each sleeve contains the condenser of each heat pipe and the set acts as a heat exchanger between the acetone flow and the heating fluid (Solar Heating Canada , 2009). The main pipe is covered by an insulated manifold to limit the conduction losses with the outside, see Figure 2.3.

Regarding the heat pipe thermal performance, it consists of thin copper and containing a heat transferring liquid with a boiling point around 30 °C (Enviko, 2009). As this liquid is heated up, through the absorption of solar radiation, it evaporates within the pipe and dissipates heat to a separate liquid flow in the bulb (located in the manifold) through heat exchange. When the heat is dissipated the condensate liquid returns down to the bottom of the pipe (evaporator) and the process is repeated, see Figure 2.4 for a principle sketch of the sequence. Due to this natural flow caused by the thermal properties, there is no need for any external pumps.

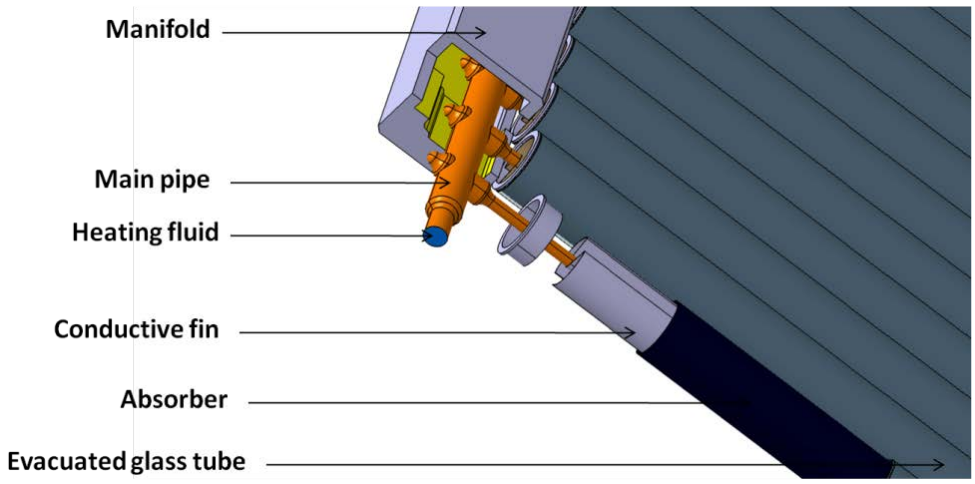

Figure 2.3 Principle layout of an evacuated glass tube collector with a Heat pipe

The integrated storage tank collector, as mentioned before, is based on the direct-flow evacuated tubes collector. One substantial difference with this type of collector compared to the conventional collectors is that it combines the actual solar panel (including absorber, coating, insulation, etc.) with its storage tank, and thus the name *integrated storage tank*. This type of collector can however not be tested according to EN 12975 Standard. Instead, it needs to be tested as a complete system.

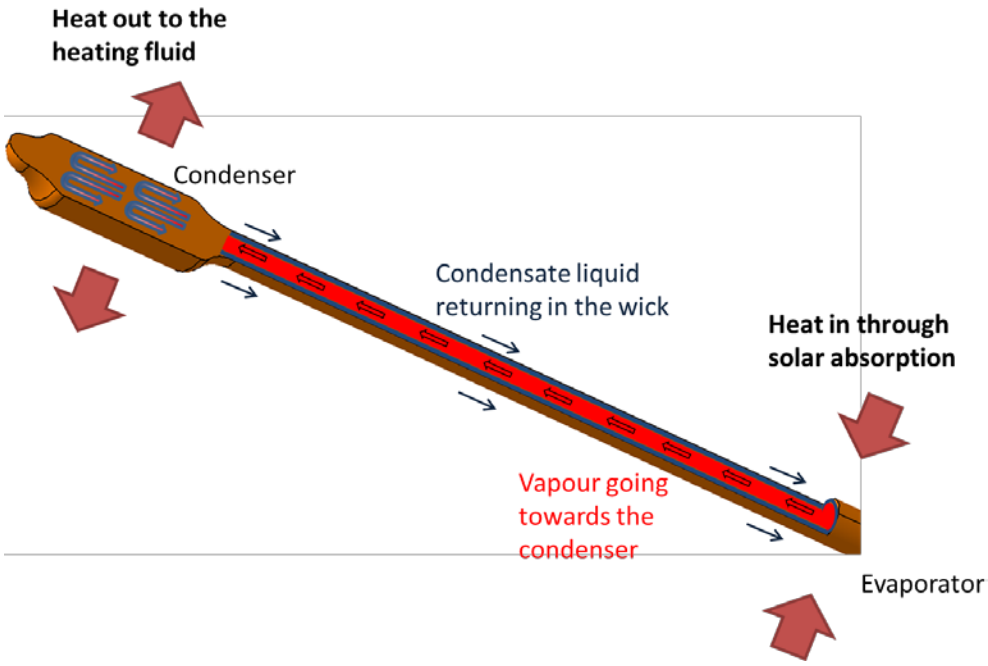

Figure 2.4 Sketch of the basic heat pipe principle describing the natural flow of the confined acetone

2.1.3 CONCENTRATING COLLECTORS

Concentrating collectors are different from the conventional flat-plate and evacuated tube collectors previously mentioned in the way that they use concentrators to direct the sun onto the absorber. The reason for using these concentrated systems is to increase the radiation concentration per area. As the sun beam is concentrated to a smaller absorption area, heat losses are reduced. This however, puts a constraint on the quality and positioning of the optical system, proportional to the concentration ratio (CR) (Duffie & Beckman, 1991).

The concentration ratio is defined as the ratio between ingoing and outgoing energy density (ρ and ρ' respectively), see Figure 2.5 for a schematic illustration. Provided that there are no optical losses in the actual concentration stage (ρ equal to ρ'), the concentration ratio can be expressed by the inverse area ratio between the aperture and absorption area as shown by Equation (2.1).

$$CR = \frac{\rho'}{\rho} = \frac{A_p}{A_r} \tag{2.1}$$

More specifically, the concentration ratio describes the factor of how much the radiation flux on the energy-absorbing surface is increased and can vary from unity to 10^5 depending on the concentration configuration.

When reducing the collector absorption area to minimize heat losses the optical losses will increase and thus creating a trade-off between these two aspects when designing a concentrating solar collector for long-term usage. Studies have shown that the optimal receiver size will intercept 90 to 95 % of the radiation, thus having optical losses in the range of 5 to 10 % (Löf & Duffie, 1963).

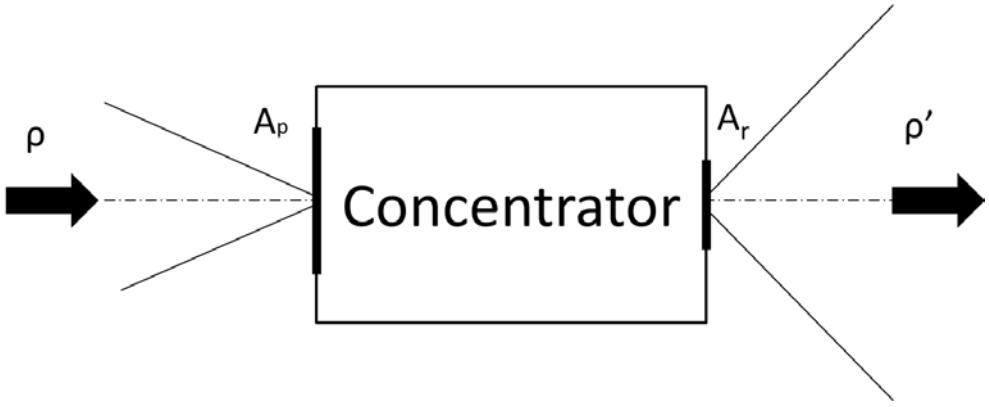

Figure 2.5 Explanatory picture of the concentration stage

To clarify the terminology, the **receiver** is the element where radiation absorption takes place and is converted to another form of energy through heat exchange. It includes the absorber, associated cover and insulation. The **concentrator** (optical system) is the part of the collector that concentrates the solar radiation onto the receiver. The collector is the total system including

receiver and the concentrator, see Figure 2.6. Concentrated solar collectors have various designs; concentrators can be reflectors or refractors, cylindrical or surface of revolution and continuous or segmented. Receivers can be convex, concave or flat, covered or uncovered. This gives a lot of different configurations when it comes to defining the collector. Thus, a distinction has been made between imaging and nonimaging collectors depending on their optical properties (Duffie & Beckman, 1991). The nonimaging collector do not produce any clear imaging picture of the sun on the absorber but rather distribute the solar radiation onto all parts of the receiver, whilst the imaging, as the name suggests, works as a camera lens and reproduces the solar image onto the absorber. More details about these types and their characterization can be found in *2.3.3 Concentrating collector behaviour.*

Due to a wide range of different designs, collector performance of concentrating solar collectors differs much more within the genre than the conventional flat-plate and evacuated tube collectors. The concentration ratio is much different depending on the collector design whether it is a three-dimensional circular concentrator (parabolic) or a two-dimensional linear concentrator (cylindrical parabolic concentrator). Requirements of higher operating temperature create a need for a larger concentration ratio and thus more precise optics. Due to these high operating temperatures, all collector components have to withstand higher temperature levels due to higher irradiance concentration and keep good absorption and emittance properties.

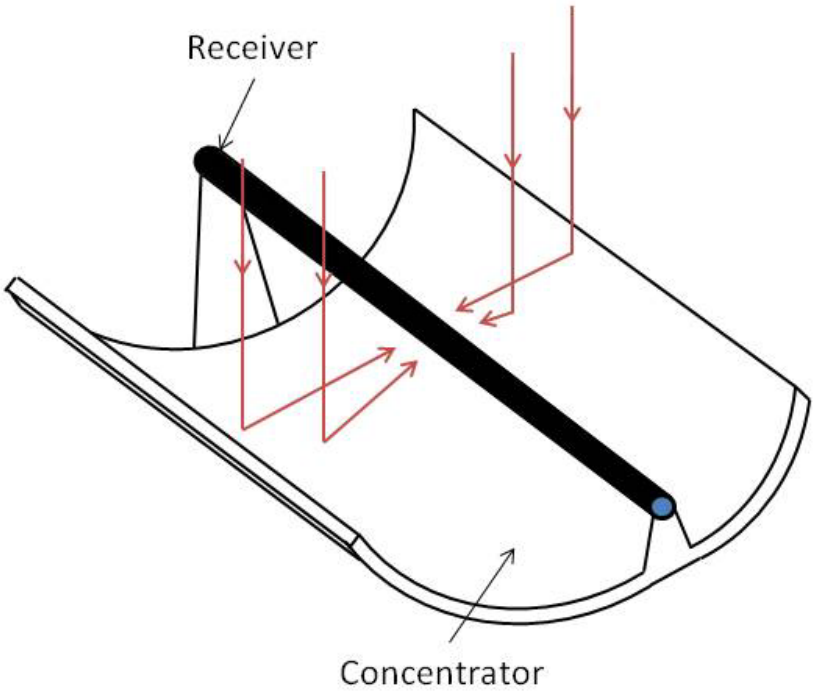

Figure 2.6 Illustration of a concentrated imaging solar collector including receiver and concentrator

These kinds of collectors can present a different mechanical setup than the conventional solar collectors in the way that they need specific solar tracking to ensure that the beam radiation is always directed onto the absorbing surface. This requirement becomes more significant as the concentrating ratio (CR) increases and can be performed in many different ways, depending on the level of importance. For collectors with low CR it is sometimes enough to intermittently adjust their position, weekly, monthly or even seasonal. As the CR increases, the collector's performance becomes more and more reliant on the solar beam radiation on the absorber surface and in that case, mechanical systems with sun-seekers that detects and adjust the solar misalignment could be used. Tracking is done in both the transversal and longitudinal axis plane of the collector, either continually or by fixing on axis according to the earth's axis of rotation (Duffie & Beckman, 1991).

2.2 SOLAR THEORY

For explaining the principles behind the absorption of the sun by solar collectors, some basic properties regarding the sun position are needed. Most of the theory is explained in detail in Solar Engineering of Thermal Processes, Second Edition (Duffie & Beckman, 1991). However, it is interesting here to sum up some of the important points mentioned in this book for a better understanding of the calculations later on.

2.2.1 SOLAR RADIATION

When considering a surface receiving sun radiation, three types of radiation can be distinguished. Firstly, the beam (also called direct) radiation G_b is the radiation received from the sun without having been scattered by the atmosphere. Secondly, the diffuse radiation G_d is the one received after the sun radiation direction has been changed when scattering in the atmosphere. Finally, the total radiation is the sum of beam and diffuse radiation received on the collector surface. The fraction of beam and diffuse radiation received will mainly depend on the weather conditions and the sun position in the sky (see *3.2.1 A zoom into the Quasi-Dynamic Testing method*).

2.2.2 SUN POSITION RELATIVE TO THE COLLECTOR SURFACE

To evaluate the direction of the incident beam radiation on the surface, a couple of parameters need to be introduced for determining the sun position relative to the collector surface.

Firstly, the position of the surface on earth must be known. It will be identified via the **longitude L** or the angular location from the prime meridian and the **latitude φ**, i.e. the angular location of the equator with north positive. Then, the **solar time** can be distinguished from the **standard time**. It is defined as the time based on the apparent angular motion of the sun across the sky, with solar noon being the time when the sun crosses the meridian of the observer.

Used in all the sun-angle relations, it can be expressed according to Equation (2.2).

$$Solar\ time = Standard\ time + 4 * (L_{st} - L_{loc}) + E \quad (2.2)$$

Here, L_{st} is the standard meridian for the local time zone in degrees west and L_{loc} is the longitude of the observer in degrees west. E is in minutes and given by Equation (2.3),

$$\mathrm{E} = 229{,}2 * (0.000075 + 0.001868*\cos(\mathrm{B}) - 0.032077*\sin(\mathrm{B}) - 0.014615*\cos(2\mathrm{B}) - 0.04089*\sin(2\mathrm{B})) \quad (2.3)$$

where B is given by Equation (2.4) with n the number of the day of the year ($1 \leq n \leq 365$),

$$B = \frac{(n-1)360}{365} \quad (2.4)$$

Secondly, two angles are necessary to determine the orientation of the surface; a) the **slope $\boldsymbol{\beta}$** or the angle between the plane of a surface (here the collector) and the horizontal and b) the **surface azimuth angle γ**, i.e. the deviation of the projection on a horizontal plane of the normal to the surface from the local meridian with zero due south and west positive.

Finally, angles are identified in order to position the sun and determine the beam radiation direction. The **hour angle $\boldsymbol{\omega}$** will be the angular displacement of the sun due to the earth rotation on its axis with 15° per hour. Hence, it is expressed by Equation (2.5), giving a negative angle for the morning and a positive one for the afternoon,

$$\omega = 15 * (Solar\ time - 12) \quad (2.5)$$

The angular position of the sun at solar noon must also be known. It is called the **declination $\boldsymbol{\delta}$** and can be expressed by Equation (2.6) with respect to the plane of the equator and north positive,

$$\delta = 23{,}45 * \sin(360 * \frac{284 + n}{365}) \quad (2.6)$$

The **solar altitude angle $\boldsymbol{\alpha_s}$** or the angle between the horizontal and the line to the sun is shown in Equation (2.7),

$$\alpha_s = \arcsin(\cos(\omega) * \cos(\delta) * \cos(\varphi) + \sin(\delta) * \sin(\varphi)) \quad (2.7)$$

This angle is the complement of the **zenith angle $\boldsymbol{\theta_z}$,** i.e. the angle between the vertical and the line to the sun. The relation between those angles is therefore given in Equation (2.8),

$$\theta_z = 90 - \alpha_s \tag{2.8}$$

A last angle for locating the sun is necessary for further calculation; the solar **azimuth angle $\boldsymbol{\gamma_s}$**, or the angular displacement from south of the beam radiation projection on the horizontal plane. It can be expressed as seen in Equation (2.9), with displacements east of south negative and west of south positive,

$$\gamma_s = SIGN(\omega) * \left|\arccos\left(\frac{cos(\theta_z) * sin(\phi) - sin(\delta)}{sin(\theta_z) * cos(\varphi)}\right)\right| \tag{2.9}$$

With $SIGN(\omega) = \begin{cases} 1\ if\ \omega \geq 0 \\ -1\ otherwise \end{cases}$

Most of the previous angles are illustrated in Figure 2.7,

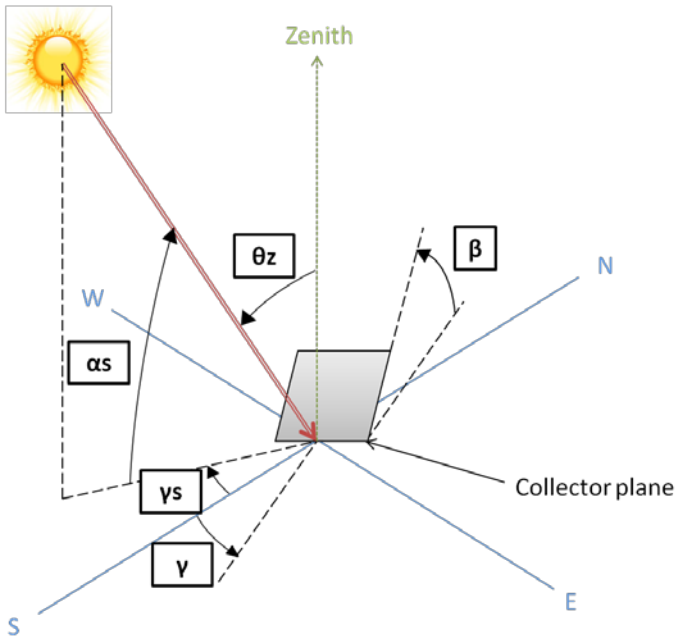

Figure 2.7 Illustration of the different solar and collector angles

Now that all the necessary parameters have been identified, a crucial angle using previous data can be introduced; the **angle of incidence $\boldsymbol{\theta_i}$** (illustrated in Figure 2.8) or the angle between the beam radiation on a surface (here the collector) and the normal to that surface. This angle will be used later in the calculations especially due to its impact on the radiation received by the collector (see *3.2.2 The regression tool*) and can be derived from Equation (2.10).

$$\theta i = \arccos(cos(\theta_z) * cos(\beta) + sin(\theta_z) * sin(\beta) * cos(\gamma_s - \gamma)) \tag{2.10}$$

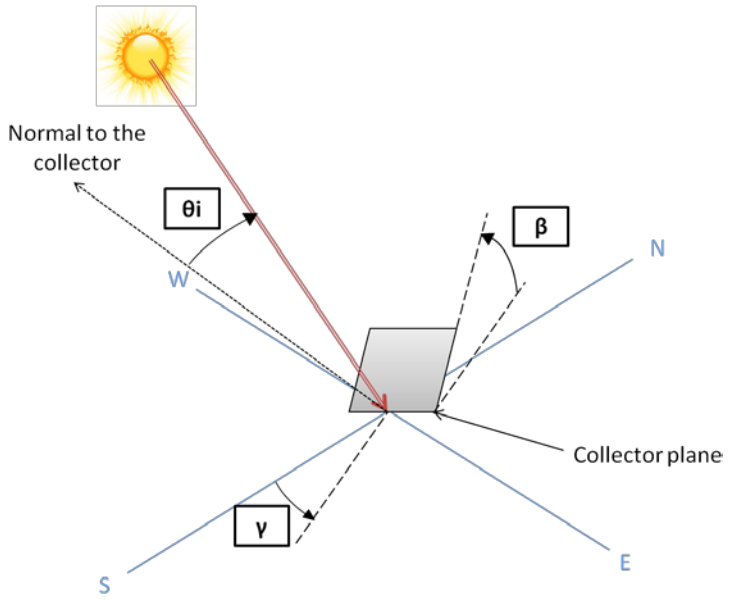

Figure 2.8 Illustration of the incidence angle and the different collector angles

2.2.3 TWO ADDITIONAL ANGLES FOR SPECIAL COLLECTOR DESIGNS

The angle of incidence θ_i can be used for symmetrical plane surfaces such as flat plate collectors. However, when it comes to special collector designs, two new directions have to be implemented for characterizing the non-symmetry of the collector. On one hand, the **longitudinal plane** is defined as the plane perpendicular to the collector plane and containing the collector's optical axis direction. On the other hand, the **transversal plane** is defined as the plane perpendicular to both the collector plane and the longitudinal plane.

As illustrated in Figure 2.9, the angle of incidence can be projected in two new angles; the **longitudinal incidence angle $\boldsymbol{\theta_L}$** or the projection of θ_i on the longitudinal plane and **the transversal incidence angle $\boldsymbol{\theta_T}$** being the projection of θ_i on the transversal plane.

Those two new angles can also be expressed as a function of the previous parameters via trigonometric projections equations as shown by Equations (2.11) and (2.12),

$$\theta_L = \begin{cases} |\arctan(\tan(\theta_z) * \cos(\gamma_s - \gamma) - \beta| \\ if\ \theta_z < 90 - and\ \theta_i < 90 \\ 90\ otherwise \end{cases} \quad (2.11)$$

$$\theta_T = \begin{cases} \left|\arctan\left(\frac{sin(\theta_z) * sin(\gamma_s - \gamma)}{cos(\theta_i)}\right)\right| \\ if\ \theta_z < 90 - and\ \theta_i < 90 \\ 90\ otherwise \end{cases} \quad (2.12)$$

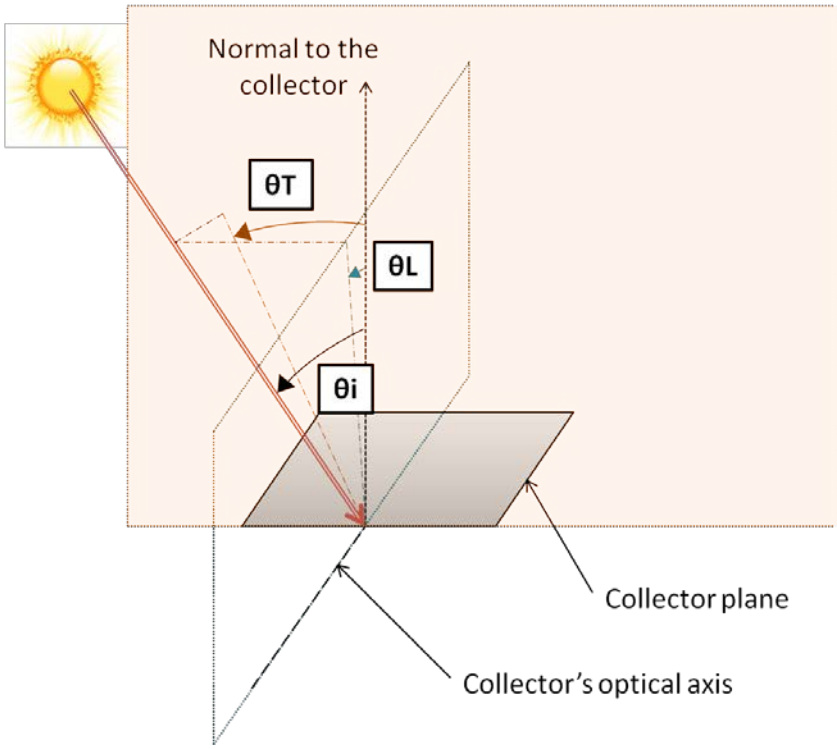

Figure 2.9 Illustration of the incidence angle and its projections

2.3 COLLECTOR PERFORMANCE

This part deals with the ability of different collector designs to absorb solar irradiance and describes their thermal performance.

2.3.1 FLAT-PLATE COLLECTOR PERFORMANCE

The flat plate collector is the simplest design which makes it perfect for introducing the basic calculations and can be re-used or modified for other collector designs. Two aspects of this collector type can be identified, its ability to absorb sun energy on one side and its losses with the surrounding on the other. This part will briefly introduce the different factors present in basic QDT equation (see *3.1 Test methods: From the real collector to its model*).

As mentioned in *2.1 Main solar collector designs*, the incident solar radiation will reach the absorber after passing through the glass cover of the collector. It is therefore necessary to define the absorber capability of receiving energy from the sun. It will be described by a product between the glass transmittance τ or the glass ability to transmit energy from the sun and the absorber angular absorptance α, i.e. its aptitude for absorbing radiation from the glass cover. Then, this product $\tau\alpha$ has to be thought of as a combination of those two characteristics more than just a strict mathematical product (Duffie & Beckman, 1991). As illustrated by Figure 2.10, the fraction of radiation reflected by the absorber will hit the glass cover and another fraction ξ of this radiation will be once again reflected back to the absorber and so on.

The factor $(\tau\alpha)$, defined by Equation (2.13), will then characterize the incident energy ultimately absorbed after the multiple reflection of diffuse radiation,

$$(\tau\alpha) = \tau\alpha * \sum_{n=0}^{\infty} \left((1-\propto) * \xi_d\right)^n = \frac{\tau\alpha}{1-(1-\alpha)*\xi_d} \tag{2.13}$$

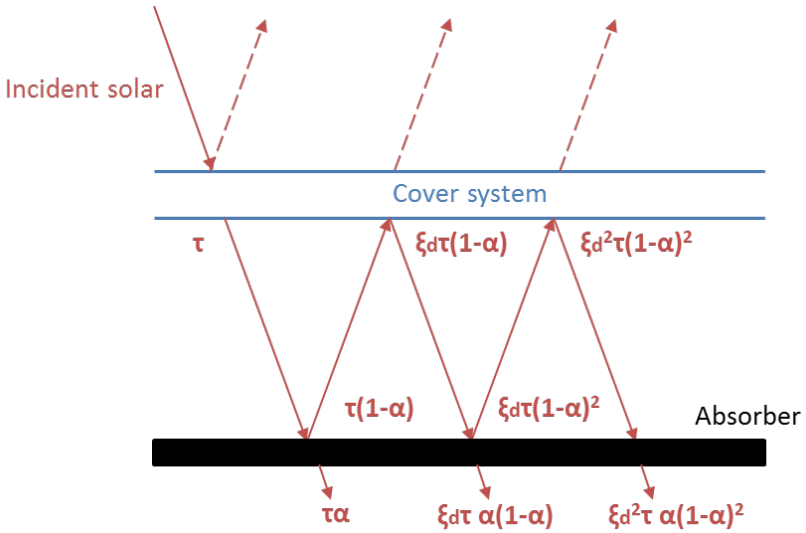

Figure 2.10 Illustration of the multiple reflection of the direct radiation for a single glazed flat plate collector

The factor $(\tau\alpha)$ depends on the angle of incidence of the radiation. Hence, the transmittance-absorptance product for normal incidence angle of radiation noted $(\tau\alpha)_n$ is distinguished from the one at any given incidence angle $(\tau\alpha)$. An Incidence Angle Modifier K (IAM) is then introduced as the quotient between $(\tau\alpha)$ for a given incidence angle and $(\tau\alpha)_n$ for radiation normal to the collector, as shown by Equation (2.14),

$$K = \frac{(\tau\alpha)}{(\tau\alpha)_n} \tag{2.14}$$

The transmittance-absorptance product $(\tau\alpha)$ also depends on the wavelength of the incident radiation through the dependency of the transmittance factor. Hence, as mentioned in *2.1.1 Flat-plate collectors*, films of low refractive index can be added at a specific optical thickness onto a transparent slab to decrease the reflectance and boost the transmittance (Duffie & Beckman, 1991). This is nowadays applied in many collector designs and better known as “anti-reflective coating”.

As previously mentioned, collectors naturally strive to reach equilibrium through different types of thermal losses with its surrounding; conduction, convection and infrared radiation. All those losses can be modelled by the

general heat transfer coefficient U_L multiplied by the difference between the mean absorber temperature T_{pm} and the ambient temperature T_a. Since T_{pm} is hard to estimate, a general expression of the useful energy gain has to be reformulated using inlet and outlet fluid temperatures. By isolating an elemental region of the tube and solving the equation obtained from an energy balance, a general expression for the useful gain of energy for the tube and fin per unit of length can be obtained, see Equation (2.15).

$$q'_u = W * F' * \left(S - U_L * \left(T_f - T_a\right)\right) \tag{2.15}$$

W being the distance between two tubes and S the energy absorbed by the absorber from diffuse, beam and horizon brightening radiation. The collector overall heat loss coefficient, represents the heat transfer from the absorbing surface to the surroundings via convection, conduction and radiation losses, called U_L.

As seen in Equation (2.16) the collector efficiency factor F' (used later on in *3.1 Test methods: From the real collector to its model*) or the ratio of the actual useful gain to the useful gain obtained if the absorber surface had been at the local fluid temperature,

$$F' = \frac{U_0}{U_L} \tag{2.16}$$

This factor has to be distinguished from average heat removal factor F_R which relates the actual energy again to the useful gain if the whole collector surface were at the fluid inlet temperature. Later on in *3.1 Test methods: From the real collector to its model*, the arithmetic average of inlet and outlet temperatures is used as well as the average heat removal factor. However, if a linear temperature rise with distance through the collector is assumed like it is the case here, F' is equal to F_R (Duffie & Beckman, 1991). That is why the factor F' is used in the QDT model.

2.3.2 EVACUATED TUBE COLLECTOR PERFORMANCE

The behaviour of an evacuated tube collector is to some extent similar to the flat collector type. Indeed, the useful gain of energy can be identified as the energy absorbed from the sun lowered by the losses to the surrounding.

When it comes to the energy absorbed by the sun, the first main difference with the flat plate type comes from the tubular geometry. As shown by Herrick (1982), the transmittance τ present in the factor $(\tau\alpha)$ has a completely different behaviour compared with a flat plate, depending on the angle of incidence of beam radiation and the position of the plane containing this angle (perpendicular or parallel to the optical axis). By introducing the IAM behaviour for both

longitudinal and transversal incidence angles mentioned in *2.2 Solar theory*, Beckman and Theunissen (1985) completed Herrick's study and investigated both beam and diffuse transmittance dependency on the tube orientation. However, a whole collector includes several tubes and a peculiar manifold/absorber/tubes configuration (as mentioned in *2.1 Main solar collector designs*). Thus, Yong and Taebeom (2007) investigated the performances of different evacuated tube collectors considering the angle of incidence of radiation, the effect of both beam and diffuse radiation, the spacing between the tubes and the shadowing between adjacent tubes, the absorber design and the tube configuration.

As detailed by Hardling *et al.* (1985), the thermal losses of an evacuated tube collector are more complex than for a flat plate collector and occur at different locations of the collector. A first type of losses is due to the thermal conduction occurring through the insulation at the header pipe. This thermal conduction can be modelled by Equation (2.17),

$$Q_{k1} = k_1 * (T_f - T_a) \tag{2.17}$$

k_1 being a function of the inner and outer diameters of the tube and the thermal conductivity of the insulating material.

Other conduction losses occur at the absorber tubes. As shown by Equation (2.18), this is represented by the factor k_2 including the conduction losses at the open end of the tube, losses through the residual gas in the evacuated volume (non-perfect void) and the conduction through the steel retainer and the glass envelope,

$$Q_{k2} = k_2 * (T_s - T_a) * N_{tubes} \tag{2.18}$$

Here, T_s is the temperature of the selective surface and N_{tubes} the number of absorbing tubes.

Finally, radiation losses from the absorber to the envelope can be identified by introducing the coefficient k_3 as described by the Equation (2.19),

$$Q_{k3} = k_3 * (T_s^4 - T_a^4) * N_{tubes} \tag{2.19}$$

k_3 being a function of the area of the selective surface, its emittances and the radii of inner and outer tubes.

Even if some of the optical and loss properties had to be mentioned here, it can be seen that this present report does not go into detail for the different models of evacuated tube collectors losses and absorptance. This is because the model used in the later sections (see *3.2.1 A zoom into the Quasi-Dynamic Testing method*) is general enough to be applied to a wide range of collector

types and this report focuses more on the test methods than on the equation models.

2.3.3 CONCENTRATING COLLECTOR BEHAVIOUR

The optical properties of a concentrated solar collector vary substantially with the geometry of the device. Equation (2.20) can be applied for all types of collectors within this genre but it varies with the type of configuration,

$$S = G_b \rho (\gamma \tau \alpha)_n K_{\gamma \tau \alpha} \tag{2.20}$$

where S is the absorbed collector radiation per unit area of unshaded aperture, G_b the effective incident radiation on the aperture plane (includes only beam radiation, except for those collectors with very low CR as part of the diffuse radiation will be reflected onto the receiver), ρ the specular reflected on the concentrator. The three factors ϒ, τ and α are functions of the solar incidence angle to the collector. The fraction of reflected radiation that is incident on the absorbing surface of the receiver is called the intercept factor ϒ. Transmittance, τ, and emittance, α, have been previously defined.

The behaviour of the incidence angle modifier, $K_{\Upsilon\tau\alpha}$, mentioned in *2.1.3 Concentrating collectors*, can be very different in the longitudinal and transversal plane for biaxial concentrated collectors compared to the other collectors due to its symmetry, as seen in Figure 2.11.

Despite its dependency on solar tracking, it is still possible to achieve good performance with a limited tracking with nonimaging collectors due to its capability to reflect radiation in a much broader spectrum of incidence angles to the receiver. The limit of the acceptable angle is defined by the acceptance half-angle, θc. Even the diffuse part of the radiation is utilized in a nonimaging collector since its reflected to the receiver and acts as a useful input to the collector. Figure 2.12 shows a principle sketch of a compound parabolic concentrator (CPC) to illustrate the acceptable half-angle and the basic layout. The parabola lines eventually become perpendicular to the receiver area and thereby give a low contribution to the radiation that reaches the absorber. By truncating the parabola it is possible to save reflector area whilst not compromising too much on the collector performance, at the same time as it lowers the number of beam radiation reflections needed to reach the receiver.

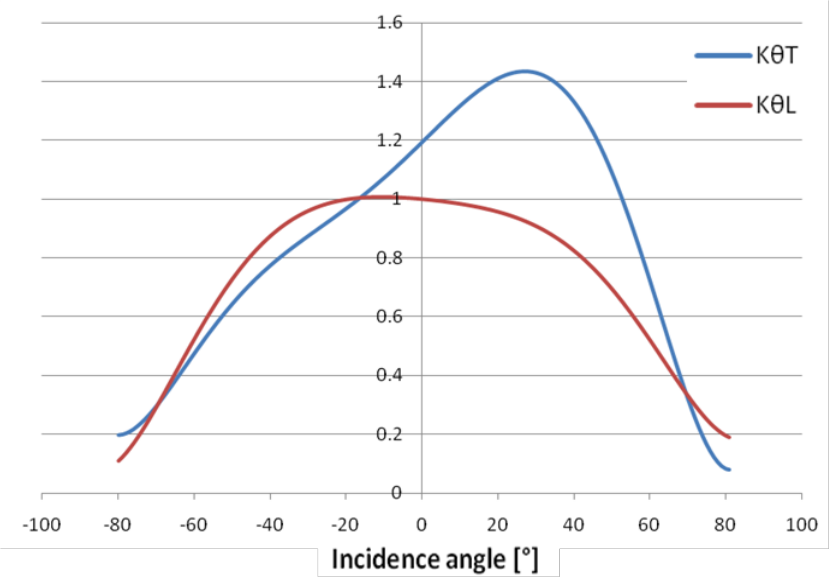

Figure 2.11 Incidence Angle Modifier for one type of CPC collector with a non-symmetrical IAM behaviour

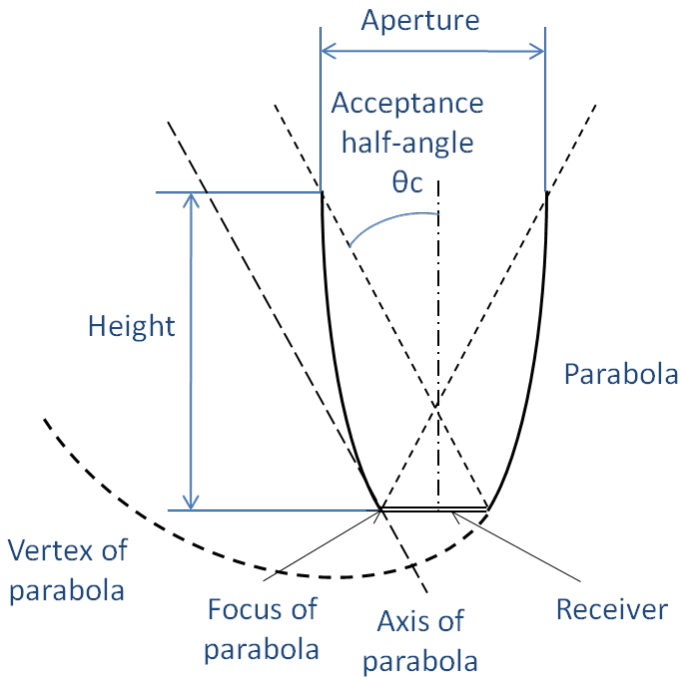

Figure 2.12 Cross section of a CPC showing the basic layout showing θc and collector aperture area

To determine the total radiation that hits the collector receiver, regards have to be taken for not only beam radiation, but also for diffuse and ground-reflected radiation that lie within the acceptance half-angle according to Equations (2.21) - (2.24),

$$S = A_p(G_{b,CPC} * \tau_{c,b} * \tau_{CPC,b} * \alpha_b + G_{d,CPC} * \tau_{c,d} * \tau_{CPC,d} * \alpha_d + G_{g,CPC} * \tau_{c,g} * \tau_{CPC,g} * \alpha_g) \quad (2.21)$$

$$G_{b,CPC} = F * G_{bn} * cos\theta \quad (2.22)$$

$$G_{d,CPC} = \begin{cases} \frac{G_d}{C} & if\ (\beta + \theta_c) < 90° \\ \frac{G_d}{C}\left(\frac{1}{C} + cos\beta\right) & if\ (\beta + \theta_c) > 90° \end{cases} \quad (2.23)$$

$$G_{g,CPC} = \begin{cases} 0 & if\ (\beta + \theta_c) < 90° \\ \frac{G_g}{C}\left(\frac{1}{C} - cos\beta\right) & if\ (\beta + \theta_c) > 90° \end{cases} \quad (2.24)$$

where the first term is the beam radiation contribution, second one is from diffuse radiation and the last from ground-reflections. The first part in the first term, $G_{b,CPC}$ is the beam radiation within the acceptance half-angle θ_c, $\tau_{c,b}$ and α_b the transmittance and absorptance. Reflection losses as a function of the number of reflections are taken into account by the term $\tau_{CPC,b}$. The same terminology goes for the terms for diffuse and ground-reflecting radiation. Note that the ground-reflection, $G_{g,CPC}$ is only affecting if the collector "sees" the ground $(\beta + \theta_c) < 90$, see Figure 2.13. Equation (2.22) is called the control function F and it is set to 1 if beam radiation is within the acceptable angle and 0 otherwise, according to Equation (2.25),

$$(\beta - \theta_c) \leq \tan^{-1}(tan\theta_z cos\gamma_s) \leq (\beta + \theta_c) \quad (2.25)$$

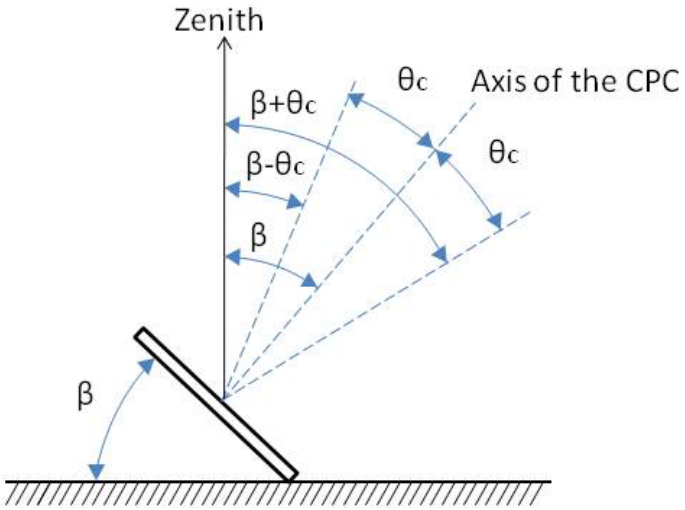

Figure 2.13 Angular definition for a CPC collector

Using Equation (2.20) for the determination of the absorbed radiation, it is possible to determine the collector output for a CPC according to (2.26),

$$Q_u = F'A_p\left[S - \frac{A_r}{A_p}U_L(T_f - T_a)\right] \tag{2.26}$$

Another type of compound parabolic collector (CPC) is the imaging solar collector aiming at concentrating the solar beam to the focal point/plane where energy conversion is made to the heat exchange media; see Figure 2.6. Due to its dependence on direct beam radiation, as previously discussed in *2.1.3 Concentrating collectors*, the need for solar tracking is crucial for its performance; ensuring that it always lies within incidence of the sun. Concentration ratios for these kinds of collectors are intermediate and temperatures in the focal point reach values of a few hundred degrees Celsius (Duffie & Beckman, 1991).

Figure 2.14 shows a cross section of a linear parabolic concentrating collector and its geometry. If a solar beam hits point B on the reflector rim at its maximum radius, r_r, the rim angle φ_r is described by AFB in Figure 2.14 and Equation (2.27).

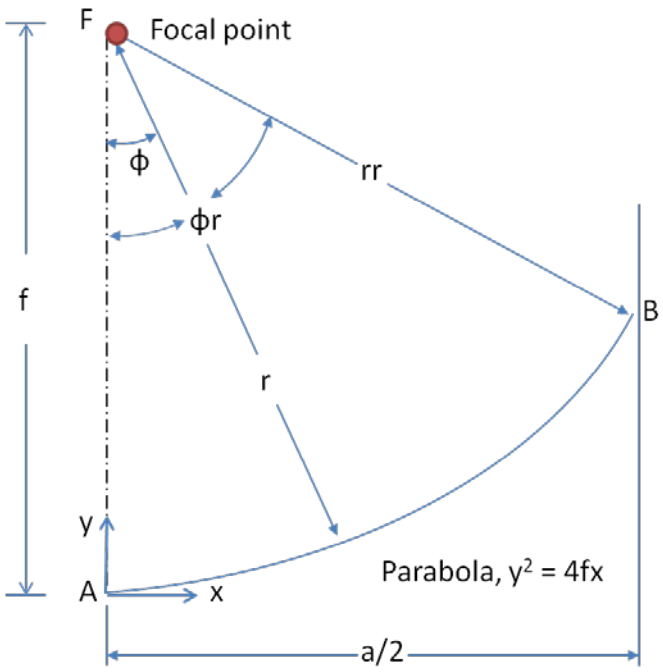

Figure 2.14 Cross section of linear parabolic concentrator

$$\phi_r = \tan^{-1}\left[\frac{8 * \left(\frac{f}{a}\right)}{16 * \left(\frac{f}{a}\right)^2 - 1}\right] = \sin^{-1}\left(\frac{a}{2r_r}\right) \tag{2.27}$$

where f is the distance from vertex to the focal point.

The width of the solar image projected onto the focal point is a function of the rim angle and increases with increasing angles. Determining the width of flat-plate, semicircular and circular receiver located in the focal points is given by Equations (2.28) and (2.29).

$$D = 2r_r * sin0.267 = a * \frac{sin0.267}{sin\phi_r} \tag{2.28}$$

$$\begin{aligned} W_r &= 2 * \frac{r_r sin0.267}{\cos(\phi_r + 0.267)} \\ &= a * \frac{sin0.267}{sin\phi_r * cos(\phi_r + 0.267)} \end{aligned} \tag{2.29}$$

Where D is the diameter of the circular receiver and W_r the width of the flat and the semicircular receiver see Figure 2.15. Note that as φ increases from 0 to φ_r, the radius increases from f to r_r and the image size increases from D to W_r.

A special type of imaging concentrating solar collector is the "power tower" where a central focal point receives concentrated solar beams from a number of individual concentrators (heliostats). Problems occurring with these types of collectors are shading of other collectors and collector prevention of radiation reaching the receiver. To cope with this, the heliostats are spaced apart, leaving room for maintenance and other practical issues.

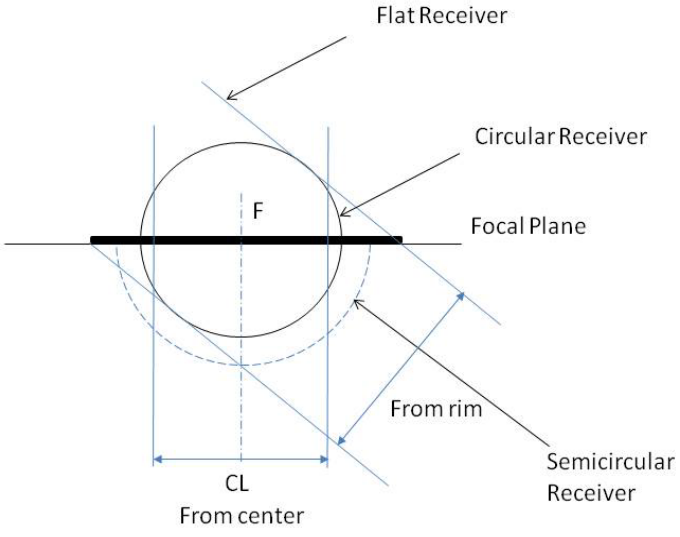

Figure 2.15 Schematics of receiver width for different configurations

3 METHOD

The following section describes the analytical and experimental method used when evaluating thermal performance of solar collectors. It also describes the optimization possibilities found for improving the QDT method.

3.1 TEST METHODS: FROM THE REAL COLLECTOR TO ITS MODEL

The main goal for test methods of solar collectors is to characterize the behaviour of a collector as accurately as possible regarding its energy thermal performance and durability. Since the output from a solar collector depends on many factors such as the weather conditions, the materials or the fluid properties, there is a requirement for finding valid coefficients that can illustrate the collector performance for a wide range of conditions and collectors types. Therefore, a model is required for providing those coefficients that are identified via data from real measurements. This will constitute the basis for comparison between collectors in terms of performances and economic viability.

3.1.1 MEASUREMENT OF THE COLLECTOR PERFORMANCE

The performance of a solar collector is characterized by the useful gain in power the media acquires while passing through the collector. This can also be illustrated in Equation (3.1) by the change of temperature between the fluid inlet and outlet:

$$Q_{coll} = \dot{m} * C * (T_{out} - T_{in}) \tag{3.1}$$

This equation is the basis for measuring collector performance by exposing the device to solar radiation and at the same time measuring the fluid inlet and outlet temperature as well as the fluid flow rate.

As for any other energy generation device, the energy or power output has to be compared with the provided input energy. Hence, other data characterizing the surrounding conditions are recorded as well during the measurement, i.e. the radiation on the collector G_{tot}, the ambient temperature T_a, the wind speed w and in addition, the sky temperature T_{sky} , for covering all types of collectors.

3.1.2 INSTALLATION REQUIRED FOR MEASUREMENTS

In order to measure the different parameters mentioned previously, some elements are required to provide accurate data for further exploitation. Those requirements are provided by the EN 12975 Standard (2006) method involving a compulsory set of essential components used for the measurement. Here is a list of those main components and their respective roles, also illustrated in Figure 3.1,

- The solar collector orientated carefully depending on the requirements of the test (i.e. angular position and orientation of the collector regarding the sun path) and connected to one closed-loop system.
- The temperature sensors situated at the inlet and at the outlet of the collector but also next to it for measuring the ambient air temperature surrounding the collector surface.
- The pump providing the required flow rate.
- The flow-meter measuring the flow within the circuit.
- The set of heat exchanger, electric heater and storage tank controlling the inlet temperature of the collector.
- The pyranometers measuring the total solar irradiance, the diffuse radiation when equipped with a shadow ring but also the incident long wave radiation (for sky temperature).
- The anemometer measuring the wind velocity.

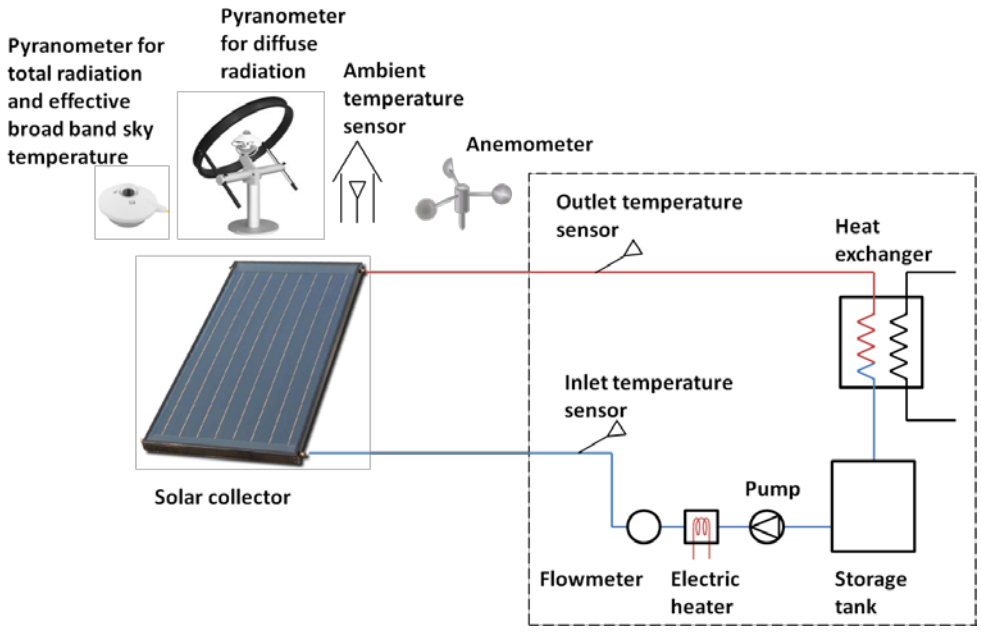

Figure 3.1 Main components for a closed-loop test installation setup for solar collectors according to the EN 12975 Standard

3.1.3 THE MODELS

Once those data are measured, the characterization of how the collector absorbs and loses energy to the surrounding can be done. This characterization is made via a mathematical model that differs depending on the test method and the solar collector type. Hence, two test methods can be distinguished; the steady-state testing method which describes the performances of the collector under stationary conditions and the QDT, a method including a dynamic part identified simultaneously with the other parameters together with an IAM dependency for diffuse radiation.

As mentioned previously, the useful gain in energy can be described as the sum of two terms; one describing the solar absorption by the collector and the other one the losses to the surrounding. Under steady-state conditions for European practice, the energy absorbed from the sun is estimated for the best useful output, i.e. when the transmittance-absorptance product $(\tau\alpha)$ is estimated for the incidence angle of the sun radiation θ close to 0˚ and the radiation mainly composed by beam radiation (Duffie & Beckman, 1991). The collector thermal output can be expressed according to Equation (3.2).

$$Q_{coll} = A_{coll} * F_{av} * \left[G_{tot} * (\tau\alpha)_n - U_L * \left(T_{f,av} - T_a\right)\right] \quad (3.2)$$

It can be noticed here that the arithmetic average of fluid inlet and outlet temperatures and the heat removal factor are used. The instantaneous efficiency can then be obtained from Equation (3.3).

$$\eta_i = \frac{Q_{coll}}{A_{coll} * G_{tot}} = F_{av} * (\tau\alpha)_n - \frac{F_{av} * U_L * \left(T_{f,av} - T_a\right)}{G_{tot}} \quad (3.3)$$

Steady state tests can be performed indoor or outdoor but the results must be interpreted carefully for indoor testing since the difference in diffuse fraction and long-wave radiation exchange compared to outdoor conditions can affect the outcome. Since the radiation must have a normal incidence on the surface and be composed mainly of beam radiation, outdoor tests will be done in the midday hours and within clear sky conditions. While the term F_{av} is a weak function of the temperature, U_L varies depending on the wind speed and the temperature. Hence, the Standard imposes a given wind speed for measurements or an additional term for wind speed influence and a linear temperature dependence of the overall loss coefficient $U_L$is assumed according to Equation (3.4).

$$U_L = a_1 + a_2 * (T_{f,av} - Ta) \quad (3.4)$$

This gives a second order fit equation for the useful gain of energy as it can be seen on Equation (3.5) where η_0 is the Zero Loss Efficiency and defined in Equation (3.6).

$$\eta_i = \eta_0 - a_1 * \frac{\left(T_{f,av} - T_a\right)}{G_{tot}} - a_2 * \left(\frac{\left(T_{f,av} - T_a\right)}{G_{tot}}\right)^2 \quad (3.5)$$

$$\eta_0 = F_{av} * (\tau\alpha)_n \quad (3.6)$$

When it comes to the Quasi-Dynamic Testing method, the main difference concerns the consideration of the effects of the incidence angle of radiation on the transmittance-absorptance product $(\tau\alpha)$ as mentioned in *2.3 Collector*

performance. According to the EN 12975 Standard (2006), this factor is also introduced in the Steady-State method but has to be evaluated only for specific given angles depending on the collector type. The QDT model distinguishes the contribution of the diffuse radiation G_d from the beam radiation G_b and includes other loss factors such as the wind speed dependence of the heat loss coefficient or the effective thermal capacitance in order to cover glazed, unglazed, evacuated tube and concentrating collectors (Perers, 1993). The complete model can hence be described by Equation (3.7).

$$\begin{aligned} Q_u = {} & F'(\tau\alpha)_n * K_{\tau\alpha b}(\theta) * G_b + F'(\tau\alpha)_n * K_{\alpha\tau d} * G_d - c_6 * G_{tot} * w \\ & -c_1 * \left(T_{f,av} - T_a\right) - c_2 * \left(T_{f,av} - T_a\right)^2 \\ & -c_3 * \left(T_{f,av} - T_a\right) * w - c_4 * (E_L - \sigma T_a^4) - c_5 * \frac{dT_f}{dt} \end{aligned} \tag{3.7}$$

with the following parameters; $F'(\tau\alpha)_n$ as the Zero Loss Efficiency for beam radiation at normal incidence, $K_{\tau\alpha b}(\theta)$ the Incidence Angle Modifier for beam radiation and $K_{\tau\alpha d}$ the Incidence Angle Modifier for diffuse radiation. It has to be noticed that $K_{\tau\alpha d}$ is considered constant for all incident angles. This is not absolutely true since it also depends on the collector slope β, the ground reflectance and the anisotropy of the sky (Brandemuehl & Beckman, 1980). This dependency can however be neglected due to the low influence of $K_{\tau\alpha d}$. The loss factors are described as,

$c_1 = F' * U_0$ is the Heat Loss coefficient at $\left(T_{f,av} - T_a\right) = 0$.

$c_2 = F' * U_1$ is the Temperature dependence of the Heat Loss coefficient.

$c_3 = F' * U_w$ is the Wind Speed Dependence of the Heat Loss coefficient.

$c_4 = F' * U_{sky}$ is the Sky Temperature Dependence of the Heat Loss coefficient.

$c_5 = (m * C)_n$ is the Effective Thermal Capacitance including piping for the collector array.

$c_6 = B_w$ is the Wind Dependence in the Zero Loss Efficiency.

The input factors described in Equation (3.7) can be related to the term S mentioned in *2.3* Collector *Collector performance* via Equation (3.8).

$$S = (\tau\alpha)_n(K_{\tau\alpha b}(\theta) * G_b + K_{\alpha d} * G_d) \tag{3.8}$$

For a plate collector only, it is possible to express the beam IAM behaviour as a function of the incidence angle by introducing the factor b_0 as shown in Equation (3.9) (Souka & Safwat, 1966). It has to be noticed that using such an approximation implicitly involves that $K_{\tau\alpha b} \leq 1$.

$$K_{\tau\alpha b} = 1 + b_0 * \left(\frac{1}{\cos(\theta)} - 1\right) \quad (3.9)$$

3.2 EXPLOITATION OF THE MEASURED DATA

This study focuses on the Quasi-Dynamic Testing method. Hence, the following section will present the characteristics, standards and calculations behind the QDT method as well as the main differences with the steady-state method in terms of test conditions and results.

3.2.1 A ZOOM INTO THE QUASI-DYNAMIC TESTING METHOD

As evoked by the name, this method allows dynamic measurements with varying conditions and exploitation of a multitude of data points. Unlike the Steady-State method which consists of only measurements for specific conditions (see *3.1.3 The models*), this type will characterize collectors performances with less strict requirement for stable climatic conditions and hence give more realistic results during a fairly short testing period (Perers, 1997). The EN 12975 Standard (2006) provides all the requirements and descriptions for proceeding to the measurements. Following are the key points mentioned in the standards, the important measurement characteristics and their impact on the results.

Besides the parameters mentioned in part *3.1.3 The models*, other parameters have to be known; the aperture, absorber and gross collector areas[3], the angle of incidence of beam radiation θ_i, the azimuth angle γ and the slope β of the collector and the time derivative of the mean temperature $\frac{dT_f}{dt}$ expressed in Equation (3.10).

$$\frac{dT_f}{dt} = \frac{T_{f,new} - T_{f,old}}{Sampling\ interval} \quad (3.10)$$

In order to properly fit the characteristics of the solar collector, the test sequence has to be performed during four to five days with each of the following conditions.

- Day type 1: The inlet temperature must be set at a value giving the Zero Loss Efficiency conditions, i.e. when $(T_{f,av} - T_a) = 0$ and under clear sky radiation. When looking at Equation (3.7), those days mainly provide data for estimating $F'(\tau\alpha)_n$, B_w and IAM factors. More specifically, since the incident radiation will mostly be composed of beam radiation (as illustrated in Figure 3.2), the fitting here will mainly concern the beam radiation IAM $K_{\tau\alpha b}(\theta)$.

[3] The aperture area corresponds to the area on which solar beam enters the collector and the gross collector area is the area based on outer dimensions of the collector, i.e. the area needed for installation.

- Day type 2: The inlet temperature must also be set at a value giving the Zero Loss Efficiency conditions but under broken clouds conditions. On one hand, this will provide enough solar radiation variability for making the time derivative of the mean temperature term react and hence making the thermal capacitance effects $(m * C)_n$ significant (phenomenon described later on in *3.3.1 Dynamic inlet temperature change*). On the other hand, the fitting will principally concern the diffuse radiation IAM $K_{\tau\alpha d}$ with a total radiation significantly composed by diffuse radiation (see Figure 3.3).

- Day type 3: The measurements have to be carried out under mean operating temperature conditions with partly cloudy days including both broken clouds and clear sky. Those data will be used for partly evaluating the loss factors in Equation (3.7) multiplied to the temperature difference $(T_{f,av} - T_a)$ or $(T_{f,av} - T_a)^2$, i.e. c_1, c_2 and c_3.

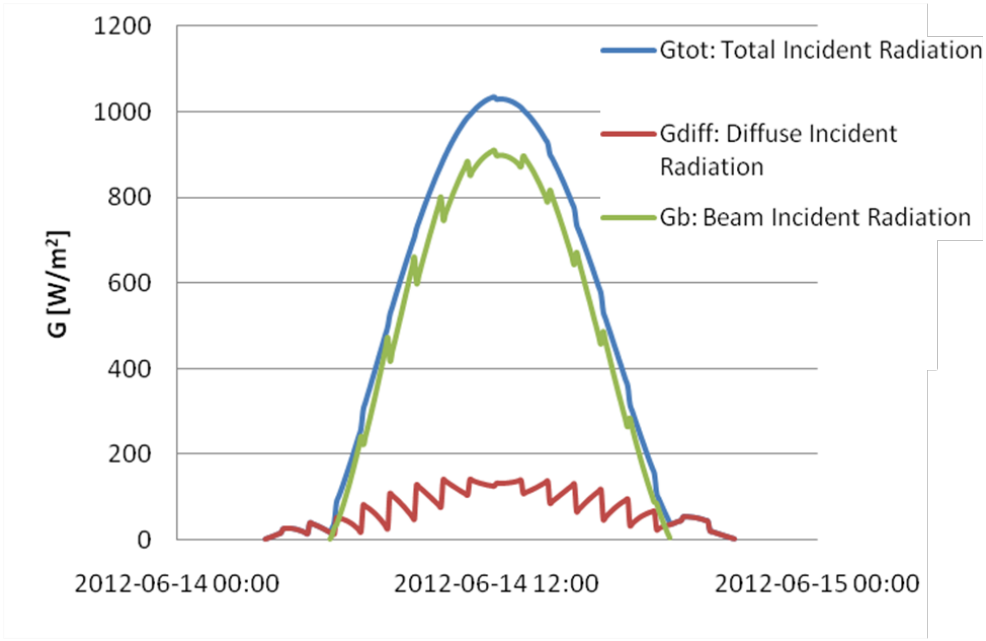

Figure 3.2 Total, beam and diffuse incident radiation for a typical clear sky day during summer – day type 1

- Day type 4: This day is used for completing the fitting of the factors in day type 3 by operating the collector under the same weather conditions but with a high operating temperature. This provides together with other day types a fitting of all the parameters for at least four ranges of temperature difference or four different inlet temperatures.

When it comes to complicated designs such as unglazed collector types, special requirements are specified in the standards for the evaluation of the Wind Speed Dependence factors c_3 and c_6 and the Sky Temperature

Dependence of the Heat Loss coefficient c_4. Moreover, for non-symmetric designs, $K_{\tau\alpha b}$ can no longer be considered as a function of the angle of incidence θ but must be generalized as $K_{\tau\alpha b}(\theta_T, \theta_L)$, i.e. a function of the two angles $\theta_T$and θ_L (defined previously in *2.2.3 Two additional angles for special collector designs*). When evaluating separately $K_{\tau\alpha b}(\theta_L)$ and $K_{\tau\alpha b}(\theta_T)$, the general expression of $K_{\tau\alpha b}$ can be obtained thanks to Equation (3.11).

$$K_{\tau\alpha b} = K_{\tau\alpha b}(\theta_T) * K_{\tau\alpha b}(\theta_L) \tag{3.11}$$

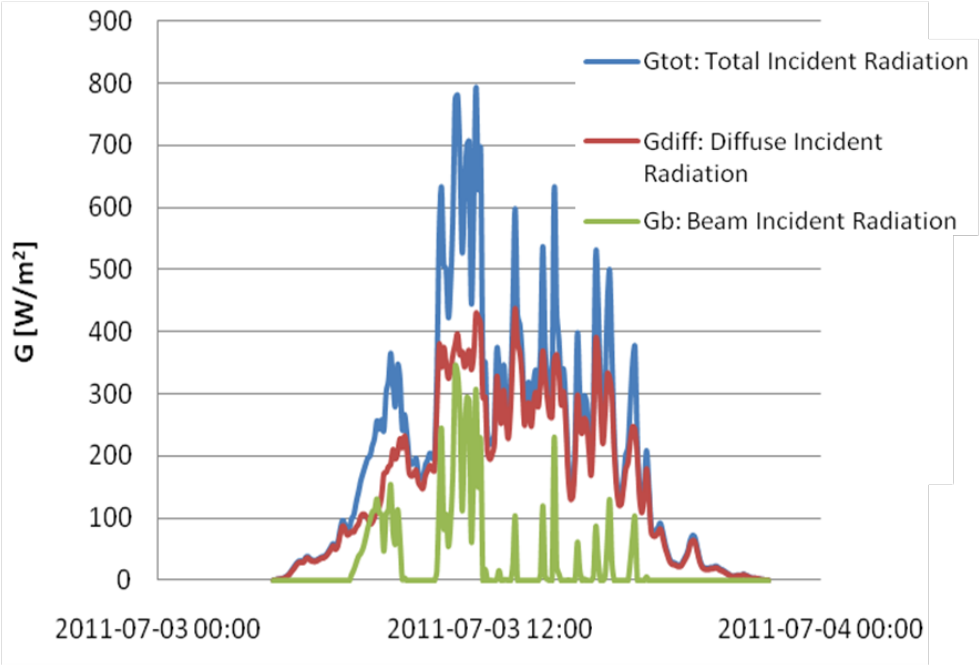

Figure 3.3 Total, beam and diffuse radiation for a measured broken clouds day during summer – day type 2

3.2.2 THE REGRESSION TOOL

During the testing, the parameters mentioned in part *3.1.2 Installation required for measurements* and *3.2.1 A zoom into the Quasi-Dynamic Testing method* have to be measured. When it comes to the mass flow, a particular attention on the accuracy is needed since the disparity can have a considerable influence on the measured energy output. Hence, careful consideration has to be taken when calibrating and installing the flow meters. The only parameter that can be fully controlled by the user is the inlet temperature to the collector. Thus, the test sequence will require a set of data points obtained dynamically for different wind velocity and solar radiation at different levels of temperature difference $(T_{f,av} - T_a)$ (Perers, 1997). The sampling rate and averaging interval will also have an influence on the results, especially on $\frac{dT_f}{dt}$ that has to be calculated on-line. Thus, the EN 12975 Standard (2006) requires a sampling rate of 1-6 seconds and an averaging interval of 5-10 minutes. Special calculations

must be carried out for the evaluation of the IAM factor. Indeed, since it will characterize the variation of the received radiation depending on the incidence angle, intermediate calculations will be performed. First, the different angles will be determined via the equations mentioned in part *2.2 Solar theory*. As shown in Equation (3.12), the transversal and the longitudinal incidence angles of radiation will be then used for separating the beam radiation term on different angles interval. This equation is valid for the separation relative to the transversal incidence angle with a fixed longitudinal incidence angle to insure a one-axis dependency of the beam radiation. For a separation relative to the longitudinal incidence angle at fixed transversal angle, this equation can be reused just by interchanging the subscripts T and L.

$$Gb_{\theta_{T(i)}} = \begin{cases} G_b * \left(1 - \left|\frac{\theta_{Tmean(i)} - \theta_{T(j)}}{\theta_{Tlow(i+1)} - \theta_{Tlow(i)}}\right|\right) \\ if\ \theta_{T(j)} \geq \theta_{Tlow(i)}, \theta_{T(j)} < \theta_{Tlow(i+1)}, \theta_{L(j)} \leq \theta_{L\ limit} \\ 0\ otherwise \end{cases} \quad (3.12)$$

$\theta_{Tlow_{(i)}}$ is the lower limit of the angle interval (i) and $\theta_{Tlow(i+1)}$ is the lower limit of the angle interval (i+1). $\theta_{T(j)}$is the actual measured transversal incidence angle at a given time with $0 \leq \theta_{T(j)} \leq 90$. The angle range $\theta_{Tlow(i+1)} - \theta_{Tlow(i)} = \Delta\theta_T$ is chosen by the observer (e.g. $\Delta\theta_T = 0, 10, 20$ ...). It has to be noticed that if $\Delta\theta_T$ is set at 1° (see *3.3.2 Increased angular resolution*), this separation is not used anymore. Instead, the value of the transversal angle is rounded to the nearest integer and $Gb_{\theta_{T(i)}}$ is just expressed for each rounded value of the transversal angle. $\theta_{Tmean(i)} = \frac{\theta_{Tlow(i+1)} + \theta_{Tlow(i)}}{2}$ is the theoretical value of θ_T compared with the measured value $\theta_{T(j)}$. For all the terms, (i) and (j) are indexes $(i, j \geq 1)$ with (i) indexing the angle step and (j) the measurement value (e.g. on Excel (j) would correspond to a particular row). At last, $\theta_{L(j)}$ is the actual measured longitudinal incidence angle at a given time with $0 \leq \theta_{L(j)} \leq 90$ and $\theta_{L\ limit}$ the limit within which this angle is considered to have no influence on the beam radiation value. It has to be noticed that this value will depend on the type of collector tested (e.g., for a flat plate collector $\theta_{L\ limit} = 45°$).

Equation (3.12) shows the separation of the transversal incidence angle. For an ideal situation, the separation for the longitudinal incidence angle would use a similar equation with a test on $\theta_{L(j)}$ and a restriction on $\theta_{T(j)}$. However, practical issues need to be considered here. For having radiation levels high enough to respect the standards (>300 W/m^2), the tests are performed during the summer. Due to sun's apparent motion within the day from east to west, there will be high variations of the angular displacement of the sun from east to west

θ_{EW}, for reasonable beam radiation levels G_b and a low angular displacement from north to south θ_{NS} as illustrated in Figure 3.4.

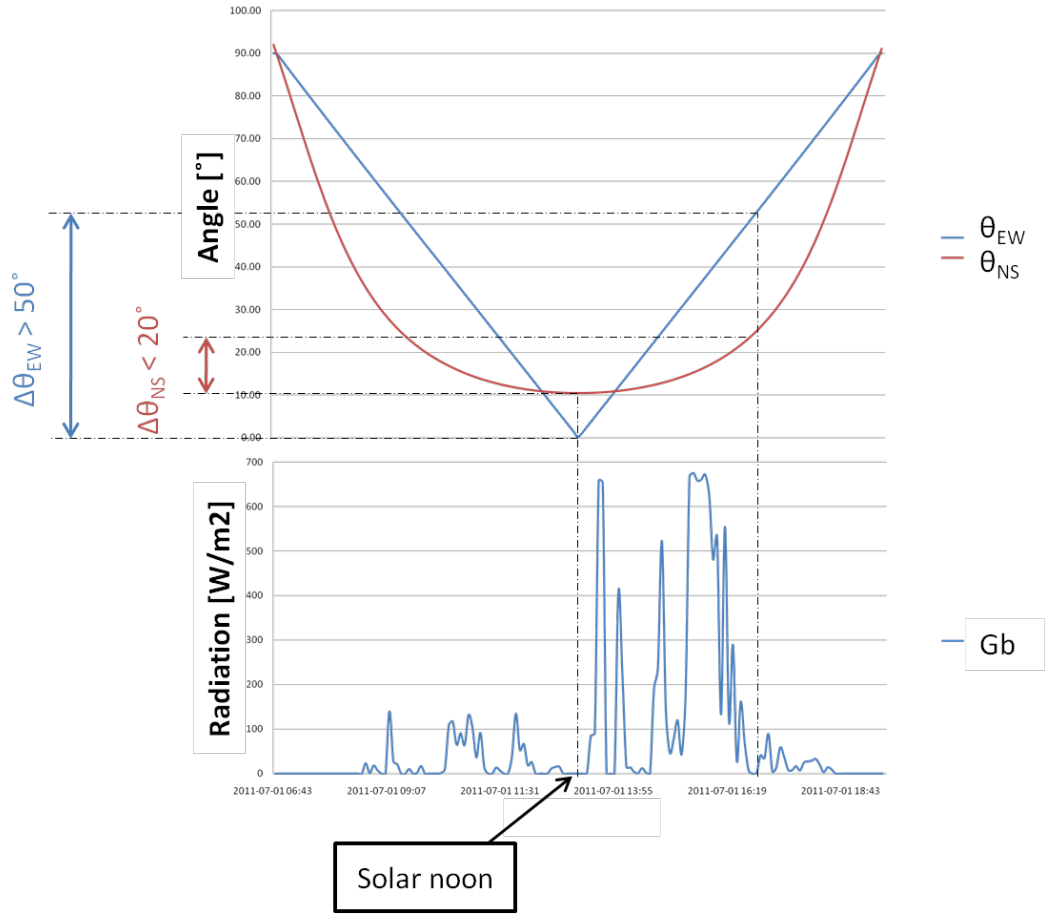

Figure 3.4 Illustration of the angular displacement of the sun in two directions during a mid-summer day for a surface slope of 45˚

As a result, in normal summer conditions, the transversal and longitudinal IAM cannot be evaluated with one single collector orientation because of inadequate variation of θ_{NS}. However, when testing a flat plate collector, the collector can stay in one position since the design is symmetric, the behaviour of the IAM will therefore remain the same in the both transversal and the longitudinal planes. The surface will then be orientated facing South making the transverse direction of the collector match the East-West direction and the longitudinal direction of the collector match the North-South direction. When it comes to non-symmetric designs such as tube collectors or concentrating collectors, two sets of measurement will be needed; one with the transverse direction matching the East-West direction for evaluating $K_{\tau\alpha b}(\theta_T)$ and the second one with the longitudinal direction matching the East-West direction for evaluating $K_{\tau\alpha b}(\theta_L)$ (after rotating the collector). Another solution, used for heat-pipe collectors for gravity issues, would be to increase the slope β of the

collector to get a sufficient variation of the longitudinal angle for fixed transversal angles.

Once the data have been measured and collected, they are filtered to meet the EN 12975-2 Standard requirements (filter on G_{tot}, $\frac{dT_f}{dt}$, the angular separation of the beam radiation). The method used here for modeling the collector from the previous measurement data is the Multiple Linear Regression (MLR). It is a non-iterative matrix method giving one parameter fitting p_n for each set of input data $f_i(X)$ (Perers, 1997). Equation (3.13) is used to fit the collector output equation.

$$Y = p_0 + p_1 * f_1(X) + p_2 * f_2(X) + p_3 * f_3(X) + \cdots + p_n * f_i(X) \qquad (3.13)$$

The linear term might be misleading since each of the functions $f_i(X)$ can actually be non-linear functions of X. Equation (3.7) is the one used for the MLR and the correspondence with the linear equation is illustrated in Figure 3.5.

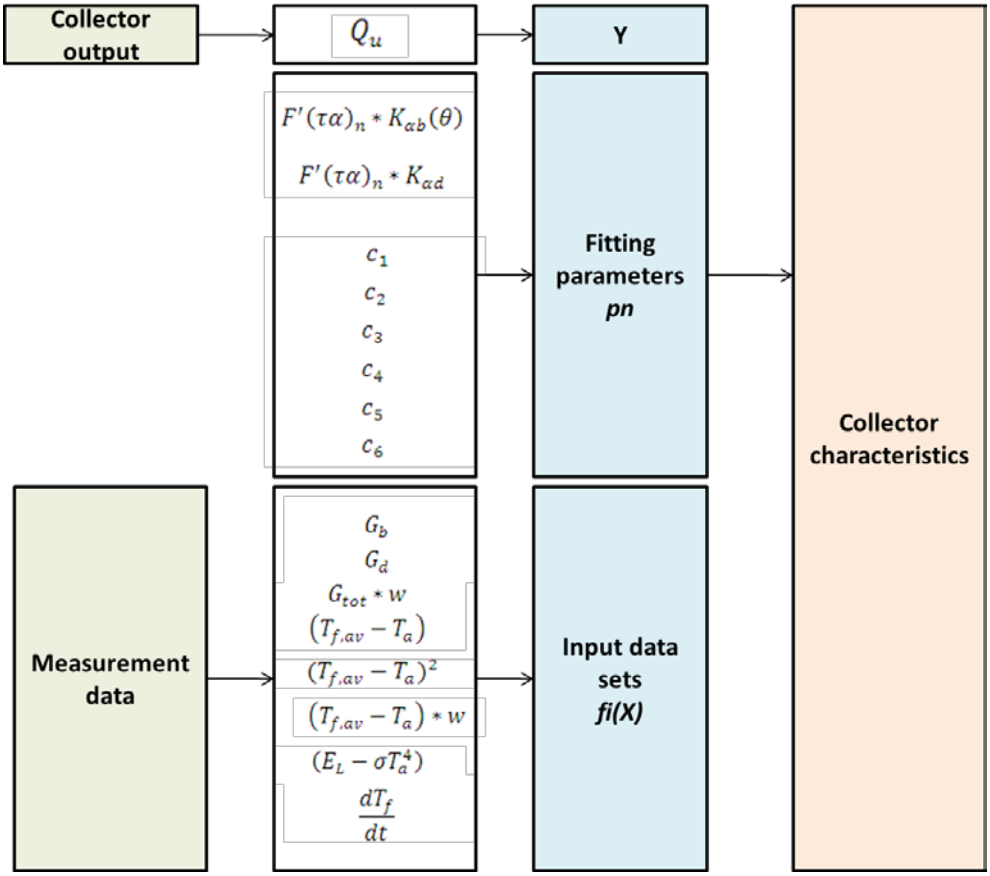

Figure 3.5 Relation between measured data and the MLR model

One of the main advantages of the MLR method is its availability in many spread sheet or statistical programs (Perers, 1997). In this study, two programs are used for this regression; Excel 2007 and the open source software R. Excel is

a really convenient tool since it includes all the required functions; gathering of data in tables, implementation of formulas for calculations, filtering, and a regression function. However, when it comes to the regression itself, Excel has a limit of 16 columns for calculations (i.e. maximum 16 input data sets). This can be limiting when separating the beam radiation in smaller step angles, used to create a higher angular resolution (see *3.3.2 Increased angular resolution*) and/or including all the loss factors in Equation (3.7). Hence, R is used in complement of Excel since it does not have any restrictions for the number of input data, yet R is mainly a regression tool so it needs to be used together with spread sheet software.

As it can be seen in the EN 12975 Standard (2006), there is a need for summarizing and representing the results. The QDT method includes the variation of so many parameters that it is hard to represent the results without fixing some parameters at a constant value. Moreover, both methods; the Steady State tests and the QDT, are still used and detailed in collectors testing reports. Hence, it can be interesting to convert the results from the QDT regression into Steady State factors. Firstly the Zero Loss Efficiency factor can be expressed as a function of the IAM factors for a given incidence angle of 15˚ and radiation fraction of 85% of beam radiation and 15% of diffuse radiation according to Equation (3.14).

$$\eta_0 = F'(\tau\alpha)_n * (K_{\alpha b}(\theta_T = 15°) * 0{,}85 + K_{\alpha d} * 0{,}15) \tag{3.14}$$

As shown in equations (3.15) and (3.16). A correlation between the Steady State and the QDT loss factors is also used when assuming an average wind speed of 3 m/s,

$$a_1 = c_1 + 3 * c_3 \tag{3.15}$$
$$a_2 = c_2 \tag{3.16}$$

Finally, the IAM constant b_0 for a flat plate collector is determined at an incidence angle of 50˚ as expressed in Equation (3.17).

$$b_0 = \frac{1 - K_{\alpha b}(\theta_T = 50°)}{\frac{1}{\cos(\theta_T = 50°)} - 1} \tag{3.17}$$

Once the regression is done, it is really important to have tools for evaluating the validity of the results. An obvious method is to simply compare the characteristics obtained from the regression with the actual collector characteristics if those ones are well-known (typically the case for computer simulated data). When the collector's parameters are unknown, the MLR proposes statistical factors that can be analysed to investigate the validity of the

model through the fitting. One important factor is the coefficient of determination R^2. This factor gives an idea of how well the model can predict the actual outcome with $R^2 = 1$ corresponding to a perfect fit. Additionally, the t statistic $tstat$, or the value of the coefficient divided by its standard error, represents the significance of each parameter with high values for high significance. Thus, $|tstat| > 2$ is necessary to consider a parameter relevant.

Another option could be a graphical representation of the fitting. Hence, two additional curves can be analysed to investigate the fitting with all the measurement data. The residuals or the difference between $Q_{coll\,measured}$ and $Q_{collmodel}$ can be plotted to evaluate the deviation of the model together with $Q_{coll\,measured}$ as a function of $Q_{collmodel}$ to check the fitting for different range of the collector output value. Some other useful curves are also recommended by the standards (European Standard EN, 2006). Among them, it is really useful to plot ΔT as a function of G_{tot}. Indeed, the more scattered the plot is, the more valid are the results since it prevents an implicit correlation between the two variables ΔT and G_{tot} in the regression.

3.3 OPTIMIZATION POSSIBILITIES FOR THE QUASI DYNAMIC TEST METHOD

The importance of solar collector thermal output testing has previously been mentioned in 1 *Introduction* as one of the crucial parts of technology development. However, today's test methods are relatively complicated and costly, especially for small companies trying to penetrate the market. Optimizing this method with regards to costs and complexity enables a greater diffusion of solar panels, thus favouring a sustainable development. However, careful consideration should be taken so that accuracy of the tests is not reduced due to cost reductions. Ideally, a shortened test sequence with a better or equal accuracy would be a preferable outcome. Following are optimization possibilities that could be used to reduce the time required for testing different types of solar collectors and thus lowering the costs.

3.3.1 DYNAMIC INLET TEMPERATURE CHANGE

One of the few parameters that allow regulation from outside the test system is the fluid inlet temperature that is determined by the operator and regulated by heaters and coolers. To fulfil the requirements of EN 12975 Standard (see *3.2.1 A zoom into the Quasi-Dynamic Testing method*), measurement data points should be obtained for at least 4 different fluid temperature intervals spaced evenly over the collector operating interval in order to accurately determine the efficiency characteristics. Furthermore, it is stated that at least one of the fluid inlet temperature intervals should be set so that the collector mean temperature lays ±3K from the ambient air temperature around solar noon, to enable a good estimation of the collector Zero Loss Efficiency, η_0. The inlet temperature

should however be kept above the ambient air dew point to eliminate condensation on the absorber that otherwise would have generated false data points.

As the temperature interval should cover the whole collector temperature range, another measurement should be done at the highest operating temperature of the collector around solar noon. The two remaining temperature interval measurements should be placed evenly spaced between the two previously mentioned points. For unglazed collectors, only 3 intervals are needed and the third one should therefore be placed in between the highest and lowest collector operating points. After completion of each temperature measurement interval, the inlet temperature should be regulated and data during these "step-changes" should not be included in the data used for evaluation (European Standard EN, 2006).

One possible way of optimizing the quasi dynamic test method is by dynamically regulating the fluid inlet temperature to enable a better fitting of the efficiency curve since data points are continuously taken along the collector operating interval. Instead of using 4 individual temperature points and reconstructing the efficiency curve through a multiple linear regression, a dynamic temperature regulation of the inlet fluid would more or less fit the curve itself as it goes on. This would give a more accurate representation of the actual efficiency curve and exclude requirement for the mean fluid temperature to be kept ±3K around the ambient temperature. This requirement can be really inconvenient since the inlet temperature must be controlled depending on the weather predictions and can prolong the test period if the necessary conditions for the ambient temperature are not met. A test of a dynamic inlet temperature change is theoretically achieved by using the transient system simulation tool TRNSYS[4] with a sinusoidal variation of the collector inlet temperature as an input to the system. In experimental trials, a controller is used to regulate the inlet temperature through heating and cooling cycles.

The collector instantaneous thermal output is given by Equation (3.18),

$$\dot{m}C\frac{dT_f}{dt} = Q_{in} - Q_{loss} = \Delta Q \tag{3.18}$$

Determining the collector thermal inertia parameter, $\dot{m}C_p$ in the quasi dynamic test method described in the EN 12975 Standard, requires a variation in $\frac{dT_f}{dt}$. This is done by measurements during partly cloudy days (day type 2) when $\frac{dT_f}{dt}$ is said to vary the most (European Standard EN, 2006) due to the variation in solar collector input, Q_{in}. This means that this parameter determination is very weather dependent. By regulating this dynamic

[4] TRNSYS - http://www.trnsys.com/

temperature change manually instead (independent of the weather condition), a more accurate evaluation of the collector thermal inertia is possible since more data points are presented over a much broader interval.

3.3.2 INCREASED ANGULAR RESOLUTION

For collector types with symmetrical angular dependency in the east-west and north-south directions, namely the flat-plate collectors, an angular step size of 10° is enough to use in the angular separation for the regression to accurately determine the incidence angular modifier, see Figure 3.6.Thanks to this symmetry, only the absolute value of θ_T is considered in the evaluation process, avoiding the need for a distinction between east and west..

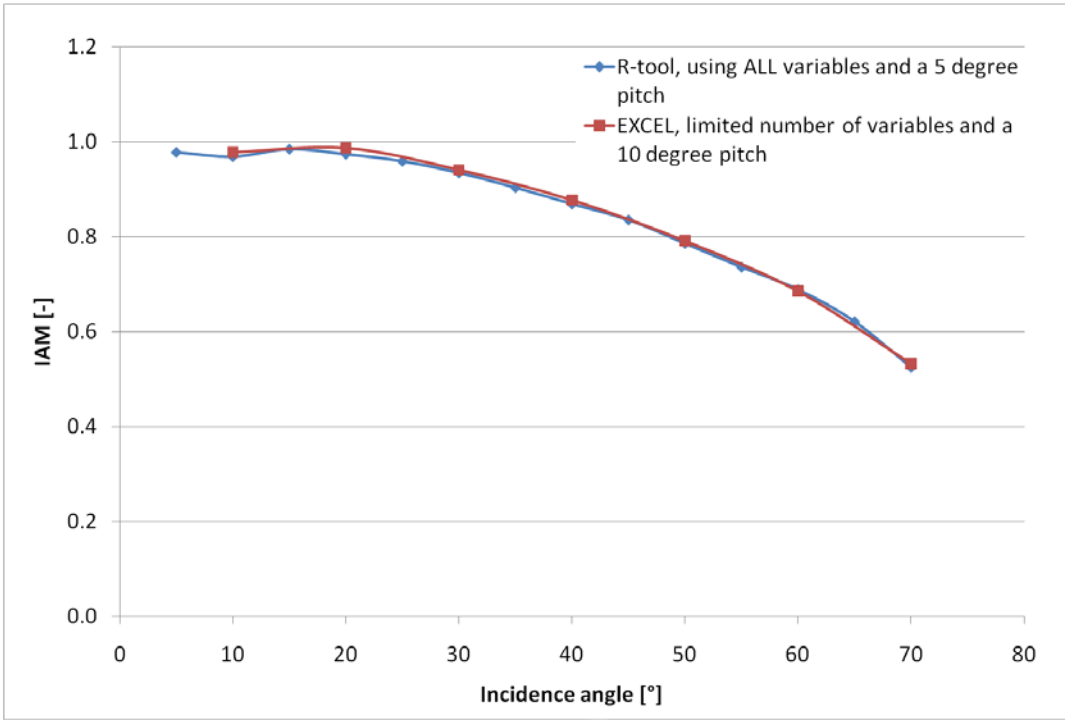

Figure 3.6 Incidence Angle Modifier for a flat-plate collector using different step sizes

As the collector design becomes more complex, (concentrated solar collectors and evacuated tube collectors) the determination of the incidence angle modifier measurements has to be performed in two directions (transversal and longitudinal) to fully characterize the incidence angle modifier dependency for non-symmetric collector designs.

Deviations in the angular dependency from its actual value can be crucial when evaluating the performance of a solar collector and thus a high angular resolution can be desirable. This is especially true for concentrated solar collectors that have big instantaneous changes in the transversal IAM around an incidence angle of 0° (Duffie & Beckman, 1991). Since these changes occur around solar noon, it has a big impact on the annual collector output when doing

the evaluation, hence making it crucial to get as accurate values as possible when evaluating the collector thermal performance.

By lowering the angular step size and thus increasing the angular resolution, it is possible to get more accurate values, especially around 0° incidence angle for concentrated solar collectors. It also gives the possibility for error checking of the measurements in the evaluation stage. Since EXCEL 2007 has a built-in regression limitation of only 16 parameters, the open source software R has been used for this purpose.

3.3.3 NIGHT TIME MEASUREMENTS

In today's QDT method, data points that are measured during the night are filtered away when determining the collector performance since there is a required minimum irradiance condition and a need for a positive output for the useable data points stated in the EN 12975 Standard (2006). This means that a lot of data points are measured without being used. Previous studies, (Perers, 1995), have suggested further investigation in using the night measurements to optimize the test method of quasi dynamic testing and thereby reducing the required test time.

When referring to the equation for the collector thermal output for quasi dynamic testing, see Equation (3.7), the use of night measurements would mean that there is no sun irradiance; G_b and G_d are then set to zero and only the losses are determined during this measurement. By setting the fluid inlet temperature above the ambient, the collector will generate thermal losses to the ambient air that can be determined during the night. However, to accurately determine all loss factors, there is a need for a variation in $\frac{dT_f}{dt}$ to get a correct value of the collector's thermal inertia, c_5. This is done by feeding the collector with a sinusoidal fluid inlet temperature change, as described in *3.3.1 Dynamic inlet temperature change*, which also gives a good fitting of the curve since it is possible to cover the whole temperature range with data points instead of a few at 3-4 different temperature intervals.

As the focus of these measurements is merely on the collector losses (irradiance terms negligible) it is possible to achieve a better estimate of the loss terms. Equation (3.7) is now narrowed down to only focus on the thermal losses of the collector and the corresponding loss factors as shown in Equation (3.19).

$$\begin{aligned} Q_{coll} &= Q_{in} - Q_{loss} = -Q_{loss} \\ Q_{coll} &= -c_1 * \left(T_{f,av} - T_a\right) - c_2 * \left(T_{f,av} - T_a\right)^2 \\ &\quad -c_3 * \left(T_{f,av} - T_a\right) * w - c_4 * (E_L - \sigma T_a^4) - c_5 * \frac{dT_f}{dt} \end{aligned} \tag{3.19}$$

However, this conjunction of configurations (using night time measurements together with a dynamical inlet temperature) gives rise to a problem associated

with the direction of the heat-flux and its impact on the loss factors, as identified by Rockendorf (1993). As illustrated by Figure 3.7, solar irradiance heats the collector absorber during the day. This heat is then transferred from the absorber to the heating fluid on one side and to the surrounding on the other. During the night when there is no irradiance, the heating fluid is warmer than the absorber and the ambient air. This causes a reversed heat-flux from the fluid to the absorber fins and out to the ambient surrounding.

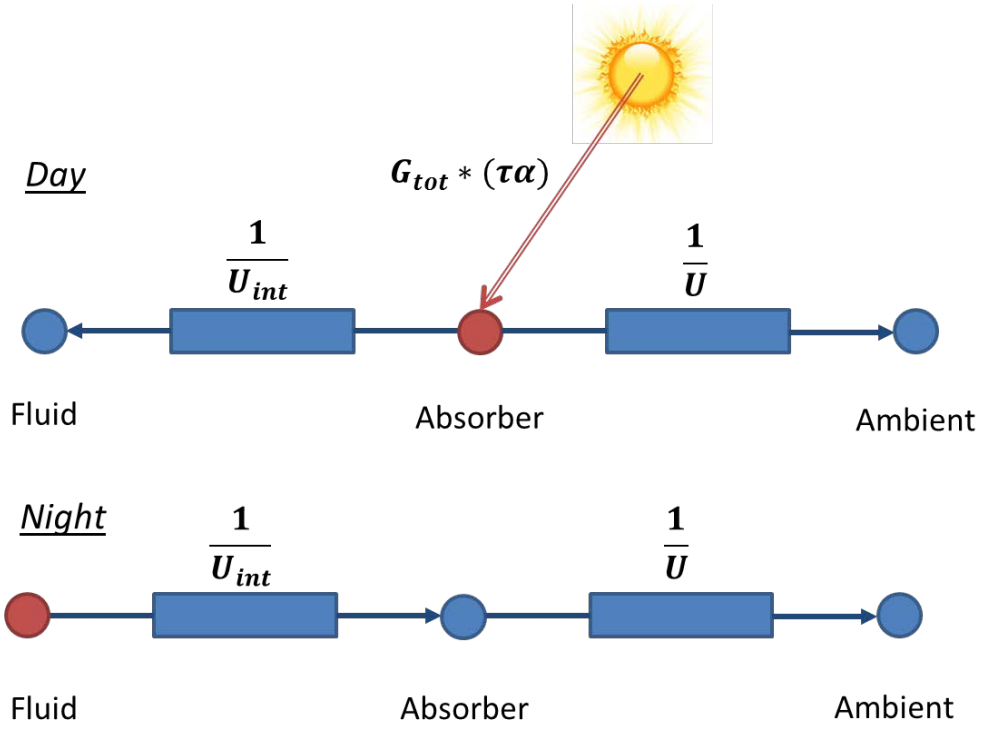

Figure 3.7 Heat-flux direction for day and night conditions

In the basic QDT equation (see Equation (3.7)), a solar collector is modelled as a 1-node system, where absorber, insulation and heat transfer fluid is combined into one resistance, thus neglecting the influence of the heat-flux direction. Consequently, the EN-12975 Standard only takes measurements into account when there is a positive collector output and irradiance (European Standard EN, 2006). Two solutions are identified for solving this problem. On one hand, Fischer & Müller-Steinhagen (2009) propose a new equation, modelling the collector as a 2-node system. On the other hand, Rockendorf (1993) introduces an additional term B_{irr} which characterizes c_1's dependency on the total solar irradiance, as illustrated in Equation (3.20), with c_{10} being the loss factor at no solar irradiance (case a). B_{irr} can be described as a function of the internal resistance of the collector U_{int} according to Equation (3.21).

$$c_1 = c_{1_0} + B_{irr} * G_{tot} \tag{3.20}$$

$$B = \frac{2 * F'U_1}{(U_{int} + U_0)} \tag{3.21}$$

Table 3.1 Different collector behaviours using day and night time measurements and a dynamical inlet temperature change

Case	Qcoll	Gtot
a)	>0	>0
b)	<0	>0
c)		0

In Table 3.1 the three different cases of collector behaviour are shown,

- Case a) has a positive collector output due to a heat-flux from the absorber to the fluid, thus (T_m > T_{amb}). This is the normal collector behaviour and what is being used in the EN 12975 Standard for collector testing.
- Case b) is described by Fischer & Müller-Steinhagen (2009) when modelling the collector as a 2-node system with negative thermal output in the presence of irradiance. This is contradictive to what is stated in the EN 12975 Standard but allows for a reduced test time as long as the heat transfer capacity rate is independent of the transfer direction.
- Case c) represents night time behaviour where there is no solar irradiance to the collector and the output is dependent on the mean temperatures' relationship to the ambient air. In the latter case, no subdivision has been made between positive and negative collector outputs as the collector will present a negative output in the majority of times.

This solution of using night time measurements to determine the loss factors assumes a natural flow of the medium during operation and is therefore not applicable for collectors using the heat pipe principle since it requires external irradiance to move the internal gas/fluid, see *2.1.2 Evacuated tube collectors.*

4 RESULTS

The flat plate collector remains the simplest design of collector and thus, it can be used as a basis for testing the optimization options and detailing the results. This section firstly introduces the detailed analysis and observation of the results on a simulated flat plate collector. The same tests have been applied on other designs such as unglazed collectors or evacuated tube collectors. As a result, a brief summary of the findings is provided when those complex designs confirm the points developed for flat plate collectors. Additionally, a detailed analysis of the results is given when the behaviour for these collectors actually differs from the flat plate collector model.

4.1 THEORETICAL FINDINGS FOR IMPROVING THE QUASI-DYNAMIC TEST METHOD

As mentioned in 3 *Method,* the data used for this analysis are obtained from simulated flat plate, unglazed, evacuated tubes and concentrated collectors in TRNSYS. The weather data correspond to the ones in Borås during a typical summer. The data is treated using a 12 seconds sampling time with 5 minutes averages. The QDT reference parameter sets of the collectors are already known since they are used in the software as input data and will be referred in the following tables and figures as Collector characteristics.

4.1.1 DYNAMIC INLET TEMPERATURE CHANGE

Regressions have been made for three different types of measurement. The first method follows the EN 12975 Standard, i.e. the use of constant inlet temperatures (at 25, 55, 85˚C). The second one uses a sinusoidal dynamic inlet temperature change covering a temperature range from 10 to 90˚C providing a variation of $(T_{f,av} - T_a)$ wide enough to meet the standards requirements. The last method also uses a sinusoidal dynamic inlet temperature change but covers a smaller temperature interval from 25 to 85˚C to investigate the need for $(T_{f,av} - T_a) = 0$. Table 4.1 presents the results obtained from the MLR regression of those three methods compared with the actual characteristics of the collector.

When looking at the results, it can be seen that the three methods in general give reasonable approximation of the factors with less than 10% deviation, except for the Effective Thermal Capacitance when using the three constant inlet temperature levels. This confirms the theory explained in *3.3.1 Dynamic inlet temperature change* by showing a more accurate estimation of $(m * C)_n$ when using a controlled variation of $\frac{dT_f}{dt}$ (via the sinusoidal variation of T_{in}) instead of using the random daily variation of the solar radiation.

Table 4.1 Results comparison between different temperature inlet configurations for a flat plate collector

Parameters	Collector characteristics	Results from the MLR					
		3 different constant inlet temperature levels (25˚C, 55˚C, 85˚C)		Sinusoidal variation of the inlet temperature from 10˚C to 90˚C		Sinusoidal variation of the inlet temperature from 25˚C to 85˚C	
		Results	Deviation	Results	Deviation	Results	Deviation
F´(τα)n [-]	**0.800**	0.785	-1.91%	0.791	-1.08%	0.786	-1.80%
b0 [-]	**0.200**	0.199	-0.48%	0.195	-2.40%	0.194	-3.08%
Κταd[-]	**0.900**	0.905	0.61%	0.911	1.17%	0.913	1.43%
c1 [W/(m^2.K)]	**3.50**	3.38	-3.29%	3.62	3.38%	3.49	-0.36%
c2 [W/(m^2.K^2)]	**0.0200**	0.0195	-2.62%	0.0188	-5.81%	0.0202	1.12%
c5 [J/(m^2.K)]	**9500***	11942	25.71%	9314	-1.96%	9256	-2.57%

**With 8000 J/(m2.K) for the absorber and the solid materials and 1500 J/(m2.K) for the fluid*

One can also notice that the sinusoidal variation from 25 to 85˚C provides a good estimation for the IAM coefficients and the Zero Loss Efficiency even though $(T_{f,av} - T_a) = 0$ is not reached. The deviation is a bit higher than for the model using a sinusoid variation between 10 and 90˚C (providing values for $(T_{f,av} - T_a) = 0$) but still remains within a reasonable range. This can be explained by the accuracy offered by the dynamic inlet change of temperature when fitting the curve as illustrated in Figure 4.1. This figure shows a 3D-curve of Q_{coll} as a function of the transversal incidence angle θ_T and the temperature difference ΔT for a fixed radiation level of $G_{tot} = 800\ W/m^2$. The scattered points represent the measured points only for a certain range of θ_T that allows the selected radiation level. The surface represents the three different models obtained after the regression considering only the main contributors, i.e. c_1 and c_2 for the losses, and a total radiation composed by 85% of beam radiation and 15% of diffuse radiation. The first series of curves show a general overview and the second series a zoom on the temperature range.

It can be seen that more data points are available to fit the output energy curve when using the sinusoidal inlet temperature change than for fixed inlet temperature levels. Hence, there is no need to cover the whole temperature

range to get a satisfying trend and even the Zero Loss Efficiency and IAM factors can be obtained without measurement points at $(T_{f,av} - T_a) = 0$.

It can be argued here that evaluating the previous deviations is not relevant if the impact of those factors variation on the yearly performance is unknown. Hence, a program developed by SP to calculate the collector's annual thermal output (SEnOCalc) has also been used in order to simulate the previous models over a year in Stockholm and compare their yearly output. For input data, the program requires the location, the collector operating mean temperatures, the area of the collector and its characteristics (the user can choose between QDT or steady state factors). For outputs, the program provides the energy output of the collector at different operating temperatures and the total available irradiance for a year neglecting the impact from the Effective Thermal Capacitance. The results are illustrated in Figure 4.2 and show that the previous deviations in collector factors have a negligible impact on the yearly output of the collector.

Those findings have to be confirmed also for other types of collectors. Table A.1 in Appendix shows data from MLR with dynamic inlet temperature changes for typical evacuated tube, concentrating and unglazed collectors simulated with TRNSYS. For all types of collectors, it can be seen that the previous statements are confirmed. Indeed, the use of a smaller interval of sinusoidal variation of the temperature gives reasonable results despite the deviations for the factors estimated with the MLR. As a result, Table 4.2 shows the low impact of those deviations on the yearly output, with a maximum deviance of 3% for the evacuated tube collector, 1.5% for the unglazed collector and 3.5% for the concentrating collector.

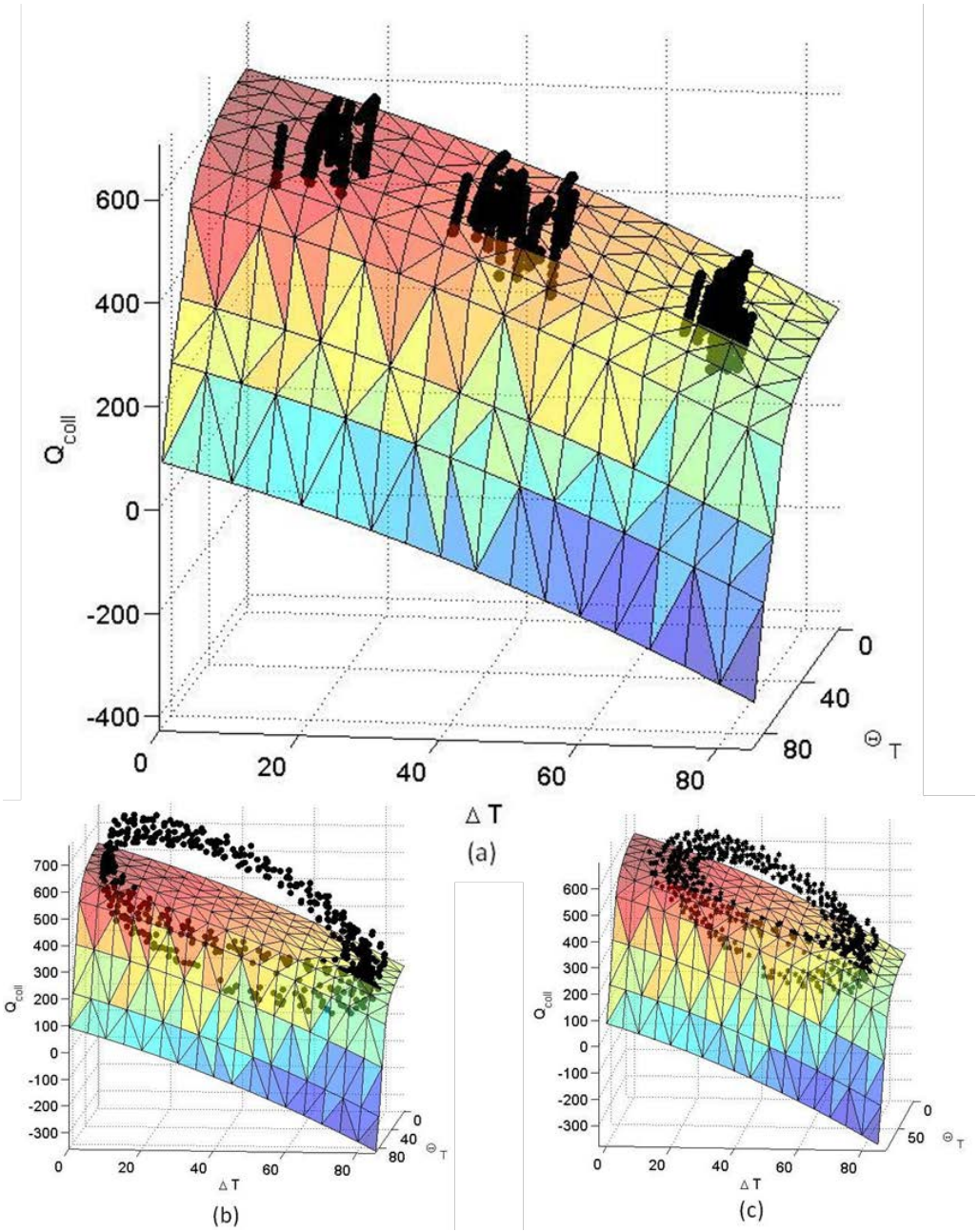

Figure 4.1 Energy output as a function of the transversal angle and the temperature difference for three different models of a flat plate collector. Case (a) is using MLR factors with three fixed temperature inlets, case (b) using MLR factors with a sinusoidal variation of the inlet temperature between 10-90˚C and case (c) with a variation between 25-85˚C

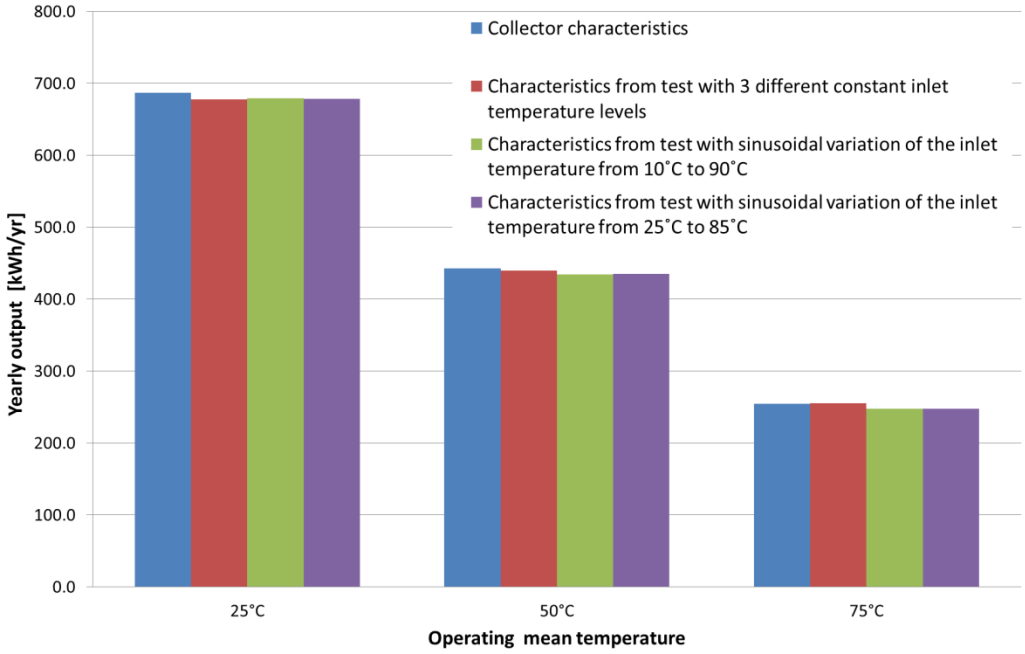

Figure 4.2 Annual output at different operating mean temperatures for different parameter sets describing the same flat plate collector

Table 4.2 Annual output based on rerefence parameter sets for different collector types

	Evacuated Tube Collector energy output using the reference parameter sets [kWh]	Evacuated Tube Collector energy output from MLR with sinusoidal variation of the inlet temperature from 25˚C to 85˚C [kWh]	Deviation
25°C	**862**	852	-1.23%
50°C	**742**	726	-2.08%
75°C	**613**	595	-3.01%
	Unglazed Collector energy output using the reference parameter sets [kWh]	Unglazed collector energy output from MLR with sinusoidal variation of the inlet temperature from 15˚C to 45˚C [kWh]	Deviation
15°C	**721**	723	0.32%
20°C	**511**	514	0.58%
45°C	**61**	62	1.48%
	Concentrating Collector energy output using the reference parameter sets [kWh]	Concentrating collector energy output from MLR with sinusoidal variation of the inlet temperature from 25˚C to 85˚C [kWh]	Deviation
25°C	**477**	489	2.49%
50°C	**321**	331	3.05%
75°C	**210**	217	3.38%

4.1.2 HIGHER ANGULAR RESOLUTION

As mentioned in *3.3.2 Increased angular resolution*, it can be interesting to increase the angular resolution for non-symmetrical collector designs, especially for the low incidence angles where there is a rapid change in efficiency. When evaluating the concentrating collector simulated previously on TRNSYS (see *4.1.1 Dynamic inlet temperature change*), Figure 4.3 shows the comparison between the IAMs curve for a regression with 1˚ angular step at lower incidence angles ($-40^{\circ} \leq \theta_T \leq 40^{\circ}$) and the IAMs curve for the actual characteristics of the collector. It can be observed that there is a match between those two curves for both $K(\theta_T)$ and $K(\theta_L)$.

This regression with higher angular resolution can then provide valid results. While this separation can be limited on theoretical data with enough relevant data points for each angle, its benefits will be further investigated when it comes to MLR on real test data (*4.2.2 Higher angular resolution*).

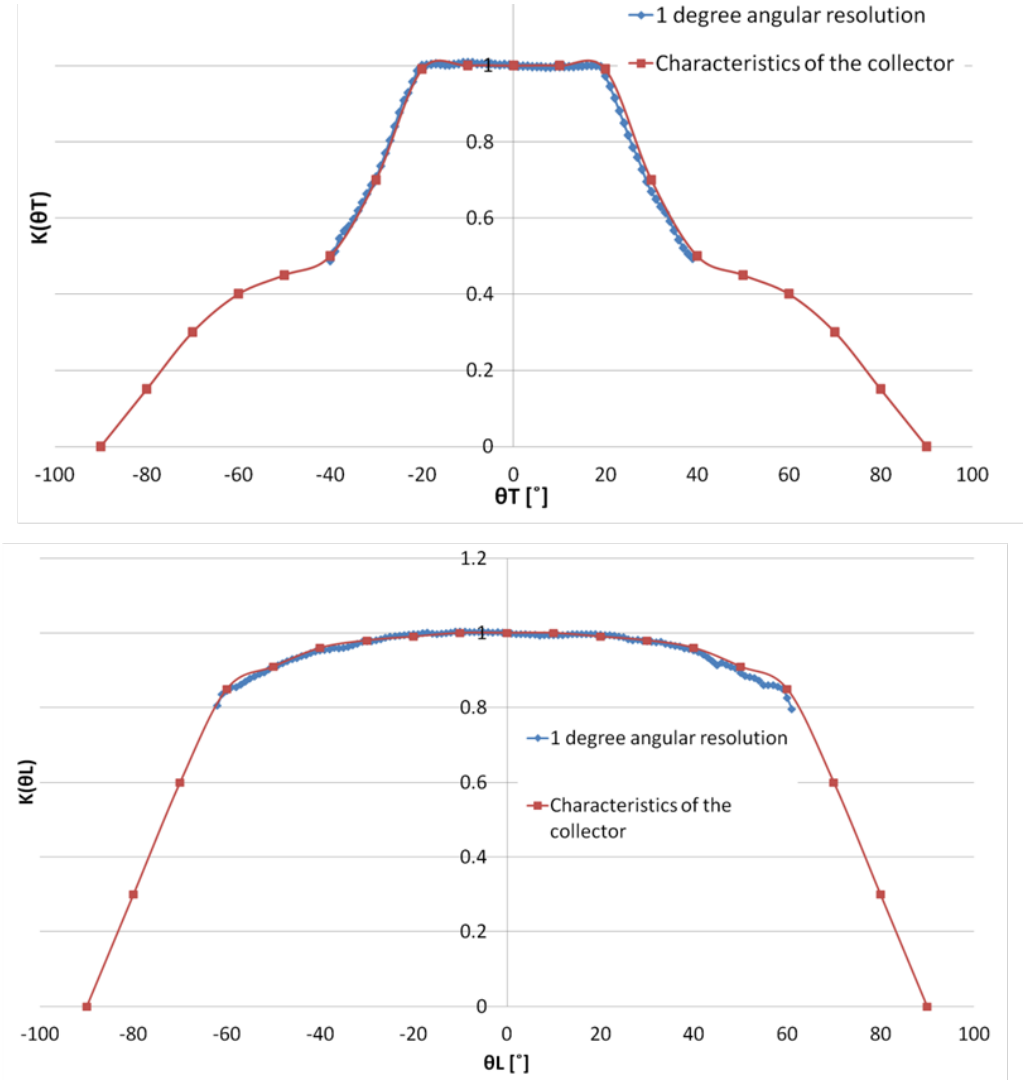

Figure 4.3 Comparison of the transversal and longitudinal IAMs from an MLR using an increased angular resolution with the reference parameter sets for a CPC collector

4.1.3 NIGHT TIME MEASUREMENTS

Night time measurements can possibly be used together with a dynamic inlet temperature change to give a good estimation of the solar collector thermal loss coefficients. Data that otherwise would have been redundant and filtered away can thus be utilized to shorten the required test time. Following are the results achieved in the theoretical stage using simulated collector test data by TRNSYS for four different kinds of collectors; flat-plate, evacuated tube, unglazed and compound parabolic collector (CPC).

Theoretical trials have been made for a flat-plate solar collector using night time measurement where the number of nights and corresponding days as well as the weather conditions have been altered to see the impact on the collectors coefficients, see Table 4.3. The results are compared to the actual collector coefficients used when simulating the collector behaviour in TRNSYS (labelled 'Collector characteristics'). Here, the collector design has been simulated as a 1-node system, so no consideration has been taken to the separation of c_1 described in *3.3.3 Night time measurements.*

Table 4.3 Result comparison of using day and night time measurement for different configurations on a flat-plate collector

Parameters	**Collector characteristics**	**Results from the MLR**			
		Tin ϵ (25-85°C) for 2 bad days and 1 night		Tin ϵ (25-85°C) for 1 good day, 1 bad day and 1 night	
		Results	Deviation	Results	Deviation
F´(τα)n [-]	**0.800**	0.678	-15.23%	0.779	-2.67%
b0 [-]	**0.200**	-0.145	-27.29%	0.196	-1.95%
Κταd [-]	**0.900**	1.051	16.75%	0.915	1.62%
c1 [W/(m^2.K)]	**3.500**	3.364	-3.90%	3.338	-4.63%
c2 [W/(m^2.K^2)]	**0.0200**	0.0203	1.32%	0.0205	2.27%
c5 [J/(m^2.K)]	**9500***	9197	-3.19%	9165	-3.52%

**With 8000 J/(m2.K) for the absorber and the solid materials and 1500 J/(m2.K) for the fluid*

Using 2 days with bad weather (a lot of diffuse radiation) and the measurements for the night between those two days, gives an underestimation of $F'(\tau\alpha)_n$ as the fraction of beam radiation is not adequate to give a good approximation. This also reflects the determination of the IAM constant, b_0, as it is dependent on the incidence angle modifier at 50°, see Equation (3.17). As the measurements are taken during days with a high fraction of diffuse radiation, the collector output is referred to the diffuse coefficient (as the beam radiation is so low). This results as an overestimation of $K(\tau\alpha)_d$. So, without a day with enough fraction of beam radiation it is not possible to accurately determine the day time parameters, $F'(\tau\alpha)_n, K(\tau\alpha)_d$and b_0. On the other hand, using these measurements together with a dynamic inlet temperature variation gives relatively accurate results when determining the thermal losses; this confirms that night time measurements can be used for this purpose. The coefficient deviation of the loss factors from the collector characteristics lies within an acceptable range of 4%.

By instead including measurements from one good day (with a high share of beam radiation) together with data from 1 bad day and the corresponding night, the collector parameters are accurately determined (deviation < 5%), Table 4.3 column 5.

The impact of these parameter deviations on the annual collector output has to be analysed to confirm the validity of the night time configuration. The IAM is modelled using a b_0 dependency with mirrored east-west and north-south behaviour and the output is taken at three different collector operating temperatures, (25, 50 and 75°C)[5]. The impact, shown in in Table 4.4 and Appendix Figure A.6, confirms that 1 good day with high enough beam radiation, 1 bad day and the night in between is adequate to give a good approximation of the collector parameters. In the case of using only bad days for parameter approximation, the underestimation of the day time parameters, mainly $F'(\tau\alpha)_n$ and $K_{\tau\alpha d}$ has a significant impact (up to 11%) on the collector output performance as previously acknowledged by Perers (1995).

[5] Please note that all computations of the annual output is done assuming a collector aperture area of 1 m2 located in Stockholm, Sweden without any solar tracking

Table 4.4 Annual collector output comparison for a flat-plate collector for different configurations using day and night time measurements

	Energy output using the reference parameter sets [kWh]	Energy output from MLR with Tin ϵ (25-85°C) [kWh]			
		Day types = two "bad" days and one night measurement, all with dynamic temperature change [kWh]	Deviation	Day types = 1 good day (clear), 1 moderate day (cloudy) and one night, all with dynamic temperature change [kWh]	Deviation
25°C	**687**	680	-0.94%	676	-1.56%
50°C	**443**	426	-3.89%	438	-1.17%
75°C	**255**	228	-10.49%	252	-0.99%

Results of using the night time configuration for an unglazed collector is shown in Table 4.5.

Table 4.5 Comparison of collector parameters for an unglazed collector using day and night time measurements

Parameters	**Collector characteristics**	**Results from the MLR**	
		Tin ϵ (15-45°C) for 1 good day, 1 bad day and 1 night	
		Result	Deviation
F´(τα)n [-]	**0.850**	0.849	-0.10%
b0 [-]	**0.200**	0.203	1.53%
Κταd [-]	**0.900**	0.916	1.77%
c1 [W/(m^2.K)]	**15.000**	14.914	-0.57%
c2 [W/(m^2.K^2)]	**0.020**	0.023	13.24%
c3 [W.s/(m^3.K)]	**2.000**	2.006	0.30%
c4 [W/(m^2.K)]	**0.500**	0.503	0.61%
c5 [J/(m^2.K)]	**12000***	11913	-0.72%
c6 [W/(m.s)]	**0.010**	0.011	14.97%

** With 10500 J/(m2.K) for the absorber and the solid materials and 1500 J/(m2.K) for the fluid*

It is seen that it gives a very good estimation of the collector parameters when using data from 1 good, 1 bad day and 1 night and a dynamic inlet temperature. This confirms the use of this setup for unglazed collectors. The impact of these parameter deviations is seen in Table 4.6. It is evident that the deviation in the annual output is very low in comparison with the collector characteristics.

Table 4.6 Annual output comparison for an unglazed collector using measurements from 1 good day, 1 bad day and 1 night

	Energy output using the reference parameter sets [kWh]	Energy output from MLR with Tin ϵ (15-45°C) using 1 good day, 1 bad day and 1 night [kWh]	Deviation
15°C	**721**	0.11%	0.11%
20°C	**511**	0.23%	0.23%
45°C	**61**	0%	0%

The night time configuration has also been performed on an evacuated tube collector to test its validity. As previously mentioned in *3.3.3 Night time measurements*, the principle of using night time measurements is not possible to perform on heat pipe evacuated tube collectors since it requires a natural fluid flow through the collector, independent of the irradiance. Instead, these tests are performed on simulated data from a direct-flow evacuated tube collector using TRNSYS simulation tool with a dynamically varying collector inlet temperature. Please note that the regression is only made on the collector's transversal direction for the determination of the incidence angle modifier, θ_T. When comparing the results of the annual output in SEnOCalc, the same longitudinal IAMs as the ones from the simulation in TRNSYS, θ_L, have been used.

As seen in Figure 4.4, the IAM dependency fits very well to the collector characteristics. However, there is a significant deviation, seen in Table 4.7, occurring in the two loss factors c_1 and c_2. This impact on the collector performance is analysed once again using SEnOCalc and seen in Table 4.8. It is shown that the annual collector output does not deviate significantly despite these parameter offsets. This confirms the theoretical validity of using night time measurements for an evacuated tube collector with a U-pipe direct through flow.

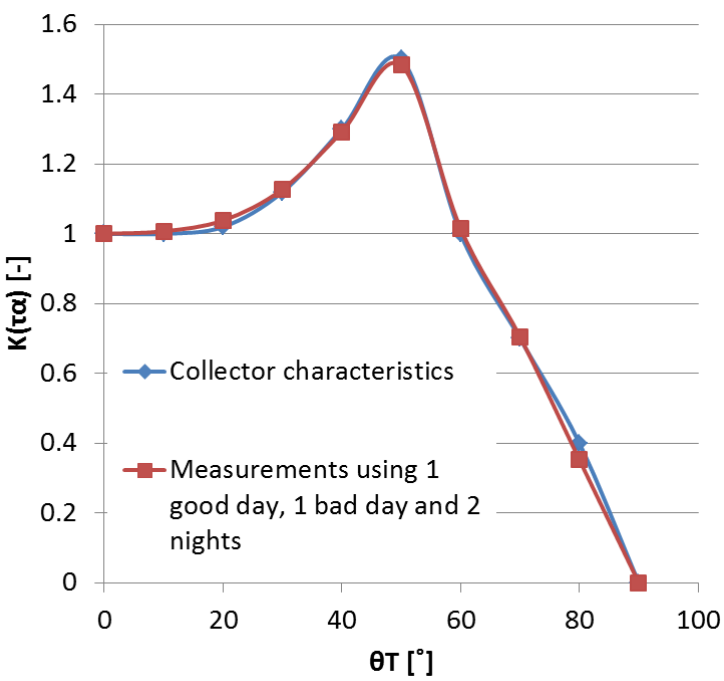

Figure 4.4 Comparison of IAMs between collector characteristics and results from MLR using day and night time measurements on an evacuated tube collector taking only the transversal incident angle dependency into account

Table 4.7 Result comparison of collector coefficient when using night time measurements on an evacuated tube collector taking only the transversal incident angle dependency into account

Parameters	**Collector characteristics**	**Results from the MLR**	
		Tin ϵ (25-85°C) using 1 good day, 1 bad day and 2 nights	
		Results	Deviation
F´(τα)n [-]	**0.70**	0.69	-2.05%
Κταd [-]	**1.20**	1.26	4.96%
c1 [W/[m^2.K)]	**1.00**	1.11	11.10%
c2 [W/[m^2.K^2)]	**0.0100**	0.0090	-10.16%
C5 [J/[m^2.K)]	**6500***	6215	-4.39%

**With 5000 J/(m2.K) for the absorber and the solid materials and 1500 J/(m2.K) for the fluid*

Table 4.8 Annual collector output comparison for an evacuated tube collector using night time measurement

	Energy output using the reference parameter sets [kWh]	Energy output from MLR with Tin ϵ (25-85°C) using 1 good day, 1 bad day and 2 nights [kWh]	Deviation
25°C	**862**	862	0%
50°C	**742**	735	-0.94%
75°C	**613**	603	-1.66%

A fourth type of collector (the CPC) is tested using night time measurements and the coefficient comparison is shown in Table 4.9. It is seen that there are negligible deviations for analysed parameters. In Figure 4.5, it can be observed that large deviations occur for high incidence angles in both the transversal and longitudinal direction. This is due to the necessary limitation of the incidence angle θ_{limit}, mentioned in *3.2.2 The regression tool*, that eliminates data for higher incidence angles.

Table 4.9 Collector coefficients for a compound parabolic collector (CPC) collector using day and night time measurements

Parameters	**Collector characteristics**	**Results from the MLR on transversal IAMs**		**Results from the MLR on longitudinal IAMs**	
		Tin ϵ (25-85°C) using 1 good day, 1 bad and 1 night			
		Results	Deviation	Results	Deviation
F´(τα)n [-]	**0.75**	0.74	-1.08%	0.74	-1.12%
Κταd [-]	**0.60**	0.64	6.34%	0.61	1.40%
c1 [W/(m^2.K)]	**2.50**	2.43	-2.96%	2.51	0.36%
c2 [W/(m^2.K^2)]	**0.0100**	0.0103	3.10%	0.0094	-6.44%
c5 [J/(m^2.K)]	**6500***	6375	-1.92%	6356	-2.22%

**With 5000 J/(m2.K) for the absorber and the solid materials and 1500 J/(m2.K) for the fluid*

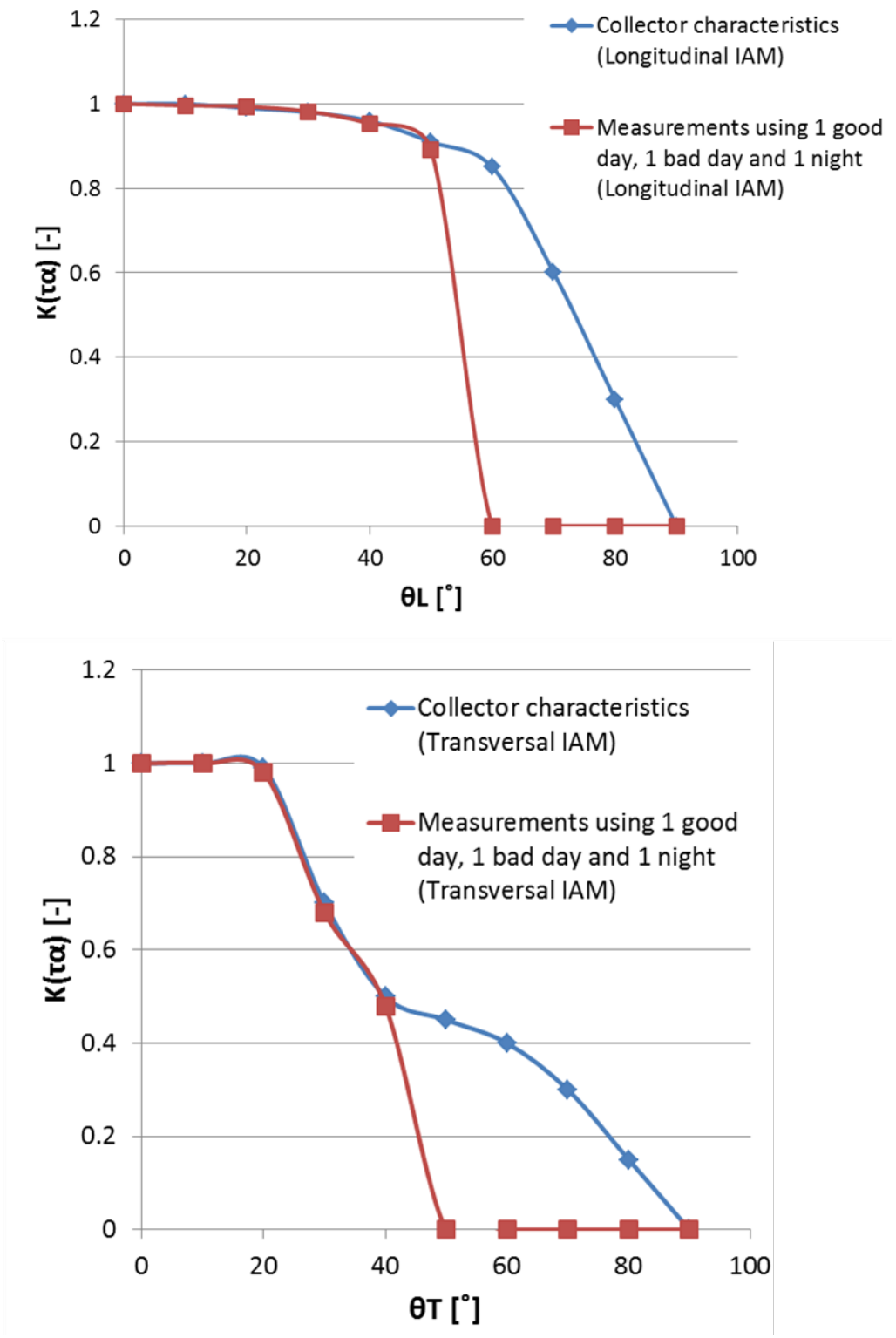

Figure 4.5 Comparison of IAMs between collector characteristics and results from MLR using day and night time measurements on a compound parabolic collector (CPC) –longitudinal IAMs above and transversal IAMs below

The impact of this θ limitation becomes evident when analysing the annual collector output in SEnOCalc, see Table 4.10. Here the IAM dependency for both the transversal and the longitudinal is used as an input and a symmetric

axis is assumed. The diffuse coefficient K(τα)d and the loss factors are taken from the transversal behaviour to simulate the worst case. An underestimation of the collector output for all operating temperatures is observed due to this lack of IAM values for higher incidence angles.

Table 4.10 Collector annual output for a compound parabolic collector (CPC) using night time configuration

	Energy output using the reference parameter sets [kWh]	Energy output from MLR with Tin ϵ (25-85°C) using 1 good day, 1 bad day and 1 night [kWh]	Deviation
25°C	**477**	436	-8.69%
50°C	**321**	298	-7.19%
75°C	**210**	205	-2.14%

4.2 EXPERIMENTAL VERIFICATION OF THE THEORETICAL FINDINGS

To verify the theoretical findings that were made, experimental tests were conducted during two weeks in the spring at SP Technical Research Institute of Sweden in Borås, Sweden. Two different types of collectors were tested, one flat plate and one heat pipe evacuated tube collector using a dynamic temperature inlet and night time measurements. Following are results and evaluations of the findings.

4.2.1 DYNAMIC INLET TEMPERATURE CHANGE

The theoretical findings have been tested on a flat plate collector already evaluated by several institutes within a round-robin/inter-laboratory comparison project. The inlet temperature has been varying with a sinusoidal shape of amplitude 15-80˚C and time period of three hours. The collector was tested from the 16th of April to the 2nd of May in order to meet a wide range of weather conditions. For the regression, filtering was done according to the EN 12975 Standard and the obtained results are shown in Table 4.11 and Figure 4.6. Since the exact parameters of the collector are unknown, the measurements of 2012 have been compared with results from SP's previous tests and median value for the steady-state coefficients obtained in the round-robin project.

Table 4.11 Comparison of a dynamic inlet temperature tests with previous tests performed at SP and round-robin project for a flat plate collector

Parameters	Results from 2012 measurements	Results from SP tests in 2010		Results from SP tests in 2011		Median value of all the results from the round-robin project	
	Sinusoidal variation of the inlet temperature from 15˚C to 85˚C	4 different constant inlet temperature levels (20˚C, 40˚C, 60˚C, 90˚C)				Steady-State measurements and QDT converted to Steady-State	
	Results	Results	Deviation	Results	Deviation	Results	Deviation
F´(τα)n [-]	**0.72**	0.72	0.58%	0.73	2.26%	-	-
Kταd [-]	**0.98**	0.89	-8.88%	0.91	-7.71%	-	-
b0 [-]	**0.319**	0.341	6.63%	0.376	17.82%	0.288	-9.87%
c1 [W/(m^2.K)]	**3.15**	3.21	1.72%	3.12	-1.23%	-	-
c2 [W/(m^2.K^2)]	**0.008**	0.014	73.75%	0.009	6.76%	-	-
c3 [W.s/(m^3.K)]	**0.25**	0.13	-48.56%	0.30	21.80%	-	-
c5 [J/(m^2.K)]	**4088**	5488	34.24%	6093	49.03%	-	-
Steady-State η0 [-]	**72.9%**	71.6%	-1.81%	71.1%	-2.44%	72.2%	-0.97%

As seen, the deviations remain small (<10% for most of the main contributors) when it comes to the determination of $F'(\tau\alpha)_n$ and the IAMs. It can be argued that a significant deviation is observed for IAMs at high angles but those factors have a small impact on the performances of the collector (see *4.1.3 Night time measurements*) and can deviate significantly due to measurements uncertainties (such as a trees shading the pyranometer or collector at sunset and sunrise). Moreover, the IAMs at low angles are higher than 1 which contradicts the theory for a flat plate collector design (see *3.1.3 The models*). These slight deviations, as well as the high value for $K_{\tau\alpha d}$ are further investigated in the following chapter *4.2.2 Higher angular resolution.* Except from those small errors, the new results globally match with the previous tests. This match confirms the theoretical findings, showing that thanks to the dynamic inlet temperature change, $F'(\tau\alpha)_n$ and the IAMs can be determined accurately without the need for measurement points at $(T_{f,av} - T_a) = 0$ for the tested flat plate collector design.

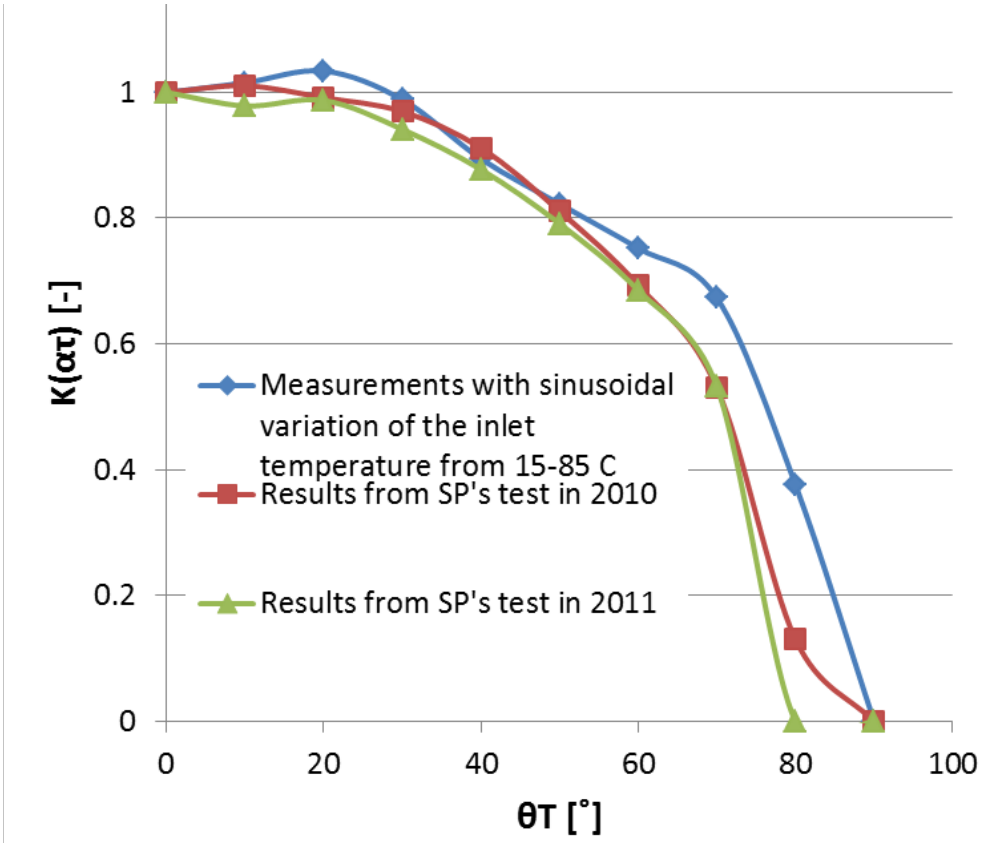

Figure 4.6 Comparison of IAMs for a dynamic inlet temperature test with previous tests performed at SP on a flat plate collector

The main difference is observed for $(m * C)_n$. In this case, the value obtained for the dynamic inlet temperature is expected to be more relevant than the one obtained for the constant inlet temperature, as explained in *3.3.1 Dynamic inlet temperature change*.

When investigating the statistical factors, as seen in Appendix A.1 Table A.2, Figure A.4 and Figure A.5, $R^2 > 0{,}99$, the t-stat values show that each parameters are significant, the residuals remain below 60 W/m^2 and the fitting of $Q_{collmodel}$ remains valid even for extreme output values. It can also be observed in Table 4.12 that the yearly output for previous tests remain acceptable on the whole. However, a deviation of 12% is observed and can be considered out of an acceptable range. The reason for this offset is presented in the following section.

Table 4.12 SEnOCalc calculations for comparison of yearly output between dynamic inlet temperature tests and previous tests

	Energy output from 2012 measurements results [kWh]	**Energy output from 2010 SP tests [kWh]**		**Energy output from 2011 SP tests [kWh]**	
	Sinusoidal variation of the inlet temperature from 15˚C to 85˚C	4 different constant inlet temperature levels (20˚C, 40˚C, 60˚C, 90˚C)			
		Results	Deviation	Results	Deviation
25°C	614	584	-4.86%	591	-3.76%
50°C	398	370	-7.03%	377	-5.21%
75°C	243	214	-11.81%	227	-6.62%

4.2.2 HIGHER ANGULAR RESOLUTION

Besides the evaluation of complicated designs, increasing the angular resolution can help the analysis of measurement uncertainties when determining the IAMs behaviour with the variation of the incidence angle. Indeed, the measurements results investigated in *4.2.1 Dynamic inlet temperature change* show obvious uncertainties for the determination of the IAMS at high incidence angles, an overestimation of $K_{\tau\alpha d}$, and values for IAMs higher than 1. The same regression has been redone with an angular resolution of 1° to check eventual abnormalities. The resulting IAM behaviour, plotted in Figure 4.7 show measurement causes for uncertainties. Firstly, a value of the IAM is unusually high for 11˚ and has been included in the 10˚ separation of the beam radiation, which might explain the slight dip over 1. This could have been caused by an unexpected partial shading of the pyranometer for example, resulting also in an overestimation of the diffuse incidence angle modifier (as most of the output is considered as the contribution from the diffuse irradiance). Moreover, some of the values at high incidence angles are insignificant and then set to zero. It is probably caused by unexpected partial shading of both the collector and the pyranometer or by the filter criteria stated in the standards taking away low irradiance and output values. This might result in uncertain values of the IAM at angles around 60-80˚ when using the 10˚ separation of the beam radiation. Finally, it can be seen that the curve is not perfectly symmetric as it should be for a flat plate design. This is probably due to a slight tilt of the pyranometer compared with the collector surface and can result in uncertain IAMs and $F'(\tau\alpha)_n$ values.

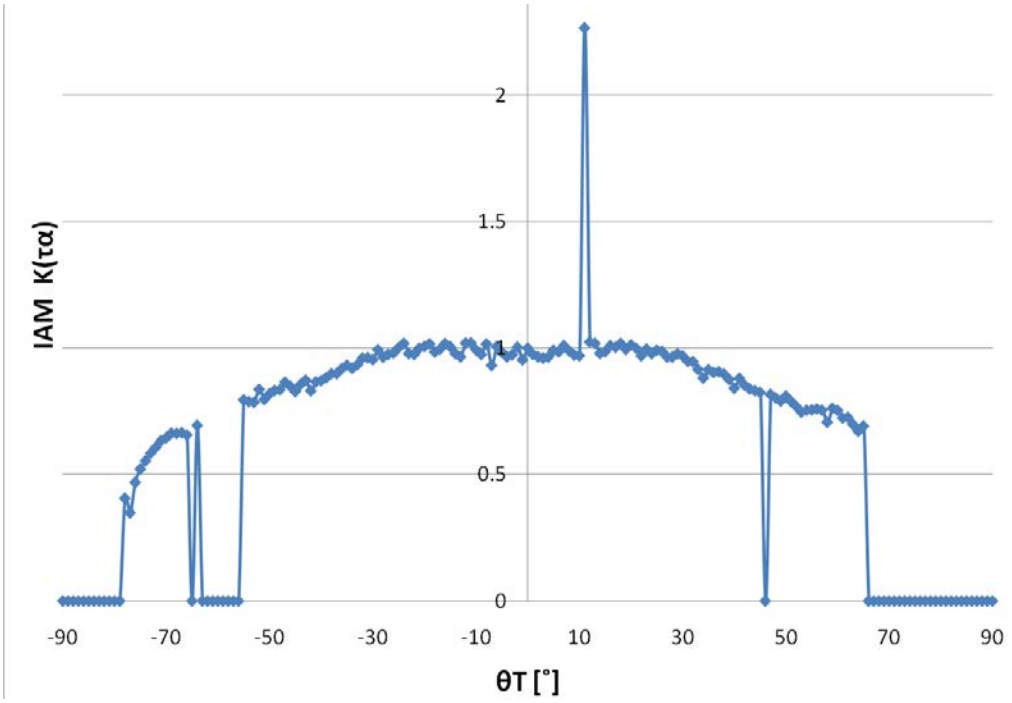

Figure 4.7 Transversal Incidence Angle Modifier for a flat plate collector

When taking away the previous odd values, Table 4.13 and Figure 4.8 shows the impact of this filter on the angular factors. It can be seen that $K_{\tau\alpha d}$ is lowered and the values of the IAMs at low incidence angles are closer to 1, resulting in a more significant value of b_0.

Table 4.13 Comparison of dynamic inlet temperature tests - odd values filtered away - with previous tests for a flat plate collector

Parameters	**Results from 2012 measurements**	**Results from SP tests in 2010**		**Results from SP tests in 2011**		**Median value of all the results from the round-robin project**	
	Sinusoidal variation of the inlet temperature from 15˚C to 85˚C	4 different constant inlet temperature levels (20˚C, 40˚C, 60˚C, 90˚C)				Steady-State measurements and QDT converted to Steady-State	
	Results	Results	Deviation	Results	Deviation	Results	Deviation
F´(τα)n [-]	**0.743**	0.72	-3.10%	0.73	-1.48%	-	-
K(τα)d [-]	**0.93**	0.89	-3.97%	0.91	-2.74%	-	-
b0 [-]	**0.385**	0.341	-11.55%	0.376	-2.27%	0.288	-25.23%
Steady-State η0 [-]	**72.1%**	71.6%	-0.69%	71.1%	-1.33%	72.2%	0.16%

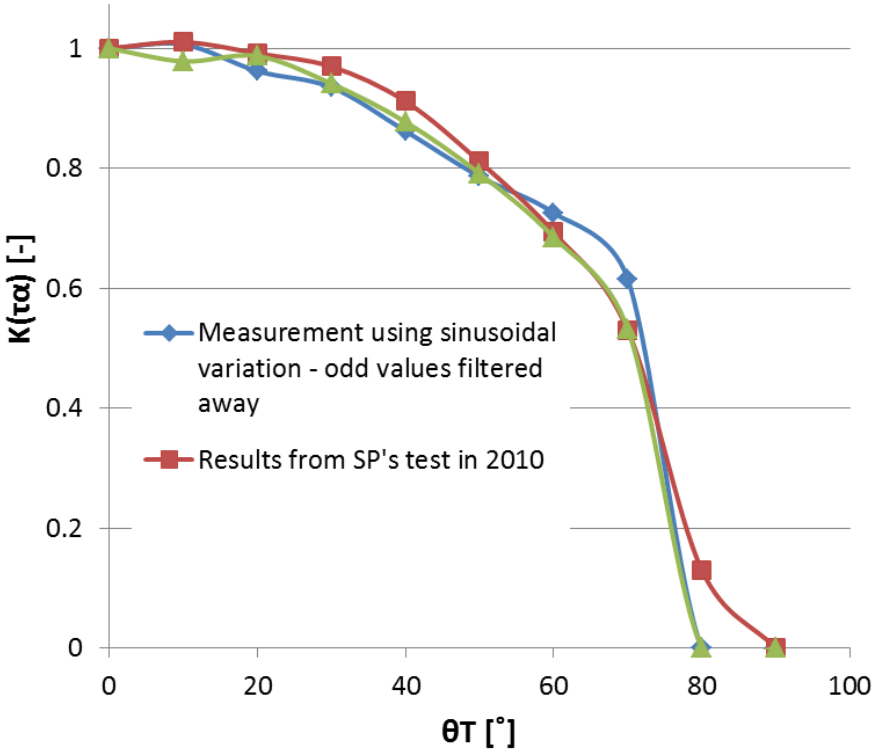

Figure 4.8 Comparison of IAMs for a dynamic inlet temperature test with previous tests performed at SP on a flat plate collector - odd values filtered away

Those new results fit well with the previous tests also when comparing the yearly output with a deviation smaller than 5% for both tests, as it can be seen in Table 4.14. The fitting is still valid since $R^2 = 0{,}994$.

Table 4.14 SEnOCalc calculations for comparison of yearly output between dynamic inlet temperature tests - odd values filtered away - and previous tests for a flat plate collector

	Energy output from 2012 measurements results [kWh]	**Energy output from 2010 SP tests [kWh]**		**Energy output from 2011 SP tests [kWh]**	
	Sinusoidal variation of the inlet temperature from 15˚C to 85˚C **– Odd values filtered away**	4 different constant inlet temperature levels (20˚C, 40˚C, 60˚C, 90˚C)			
		Results	Deviation	Results	Deviation
25°C	579	584	0.87%	591	2.03%
50°C	365	370	1.37%	377	3.35%
75°C	225	214	-4.85%	227	0.75%

4.2.3 NIGHT TIME MEASUREMENTS

Unlike the data simulated in TRNSYS, where the collector design was modelled as a 1-node system; it can also be modelled by a 2-node system making its performance dependent on the heat-flux direction. To illustrate the impact of the heat-flux direction, c1 is separated and a comparison has been made to the characteristics from previous flat plate collector measurements at SP. The results are shown in Table 4.15. Focusing merely on the c_1 variation, it is seen that there is a difference between the two day time measurements on c_1 (case a and b, depending on the heat-flux direction). An even lower value for the heat loss coefficient is achieved using the night measurements, case c. This has been acknowledged in previous studies (Rockendorf, 1993) and is due to the change of heat-flux direction.

Table 4.15 Flat plate collector coefficients comparison using c1 separation for three different cases

Parameters	**Collector characteristics from 2011**	RESULTS using dynamic inlet temperature change - Day & Night measurements when separating c1	
		Result	Deviation
F´(τα)n [-]	**0.732**	0.714	-2.46%
b0 [-]	**0.376**	0.313	-16.76%
Kταd [-]	**0.906**	0.959	5.85%
c1a [W/(m^2.K)]	**3.116**	2.669	-14.34%
c1b [W/(m^2.K)]		2.700	-13.35%
c1c [W/(m^2.K)]		2.643	-15.18%
c2 [W/(m^2.K^2)]	**0.009**	0.015	66.67%
c3 [Ws/(m^3.K)]	**0.304**	0.221	-27.32%
c5 [J/(m^2.K)]	**6093**	3809	-37.49%

Based on the deviation in night and day time estimations of the heat loss coefficient an analysis of the total solar irradiance impact on c_1 were performed. Day and night time data for a flat plate collector during two weeks were used in a regression to get the irradiance term B_{irr} from Equation (3.20). The regression statistics showed that the variable part, B_{irr}, was significant (t-stat = 6.1) in this case and by using Equation (3.21), c_1's dependency on total irradiance was modelled in Figure 4.9.

Figure 4.9 Illustration of c1's dependency on total solar irradiance for a flat plate collector using the Birr estimation

This confirms that the heat loss coefficient c_1 for this particular flat plate collector is not a constant but rather dependent on the total solar irradiance and this can be one explanation to why night time measurements give a lower estimation of the heat loss factor compared to the previously performed quasi-dynamic testing. When analysing the total solar irradiance onto the collector plane as a function of the operating temperature, it can be seen in Figure 4.10 (b) that data points for lower irradiance levels at high operating temperatures are missing. This is caused on one side by the filter criteria that ensure a collector output Q_{coll} higher than 50 W/m^2 to account for any measurement errors initiated by the equipment and on the other, by the condition on the minimum total irradiance sorting away night and low irradiance level data points ($G_{tot} > 100\ W/m^2$). When instead using both day and night measurement and thus disregarding that filter criteria, the data point distribution of solar irradiance as a function of the operating temperature covers a much broader spectrum, see Figure 4.10 (a). By doing this change of filtering criteria, not only does it present more data points but it also gives an estimation of c_1 at lower irradiance levels for higher operating temperatures.

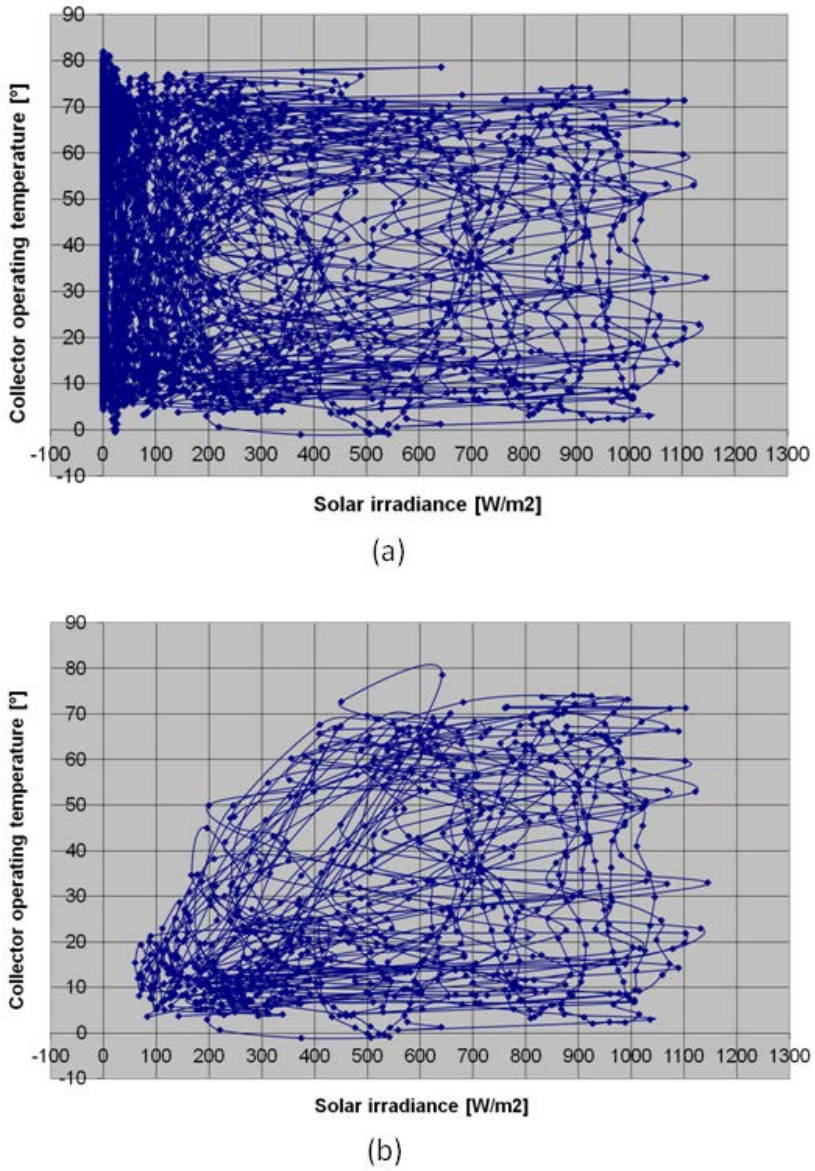

Figure 4.10 Operating temperature as a function of total solar irradiance to the collector plane using the day and night filter (a) and the standard filter (b)

Comparing the regression statistics using one c_1 together with day and night measurement to the ones performed 2011 using the EN 12975-Standard, the t-stat values for the loss factors are higher and thus more significant when using a dynamic inlet temperature change coupled with night time measurements, see Table 4.16.

Appendix A.2 Figure A.9 also shows an illustration of the model fitting using the regression parameters from day and night measurement data. Here it is evident that the model gives a good fitting of the calculated output compared to the measured ones. Even the values at higher outputs are well-fitted as well as the ones around the origin; confirming that the day and night filter is a valid configuration.

Table 4.16 Regression statistic comparison using night time measurements for a flat plate collector and a dynamical inlet temperature

Parameters	**Collector characteristics from 2011**			RESULTS using dynamic inlet temperature change - Day & Night measurements		
	Value	**R-square**	**|t-stat|**	Value	R-square	|t-stat|
c1 [W/(m^2.K)]	**3.12**		**53**	2.64		167
c2 [W/(m^2.K^2)]	**0.009**	**0.9989**	**8**	0.015	0.9979	66
c3 [Ws/(m^3.K)]	**0.30**		**74**	0.23		54
c5 [J/(m^2.K)]	**6093**		**10**	3815		324

To shorten the required test period for the collector characteristics, a regression was performed using only 3 days (2 good days and 1 moderate) together with 2 nights and compared to the previously measured values in 2011, see Table 4.17. Here, one more day was used (compared to the theoretical evaluation) to enable a better coverage of ΔT's dependency on G_{tot} at lower irradiance levels. Deviations in $F'(\tau\alpha)_n$ and b0 can be neglected, the latter as it is really sensitive for small angular changes around 50º. The overestimation of $K_{\tau\alpha d}$ is explained in *4.2.2 Higher angular resolution*, caused by external factors and not by the actual model or test configuration. The underestimation of c_1 when using night measurement can be derived from what has previously been mentioned about the heat-flux distribution and its dependency on the solar irradiance, see Figure 4.9. As the first order heat loss term, c_1, is lowered; some of the collector losses are taken into account in c_2 instead, causing an overestimation of c_2. As previously mention in *4.1.1 Dynamic inlet temperature change* the effective thermal capacity term (c_5) is better estimated using a dynamic inlet temperature variation, this is also validated by the higher t-stat values in Table 4.16.

Table 4.17 Collector characteristics evaluation using 3 days and 2 nights for the tested flat plate collector

Parameters	**Collector characteristics from 2011**	RESULTS using dynamic inlet temperature change - 1 good day (1/5), 1 moderate (19/4), 1 moderate/good (29/4) and 2 nights (17-18/4 and 29-30/4)	
		Result	Deviation
F´(τα)n [-]	**0.732**	0.720	-1.58%
b0 [-]	**0.376**	0.303	-19.41%
Κταd [-]	**0.906**	0.943	4.08%
c1 [W/(m^2.K)]	**3.116**	2.678	-14.05%
c2 [W/(m^2.K^2)]	**0.009**	0.015	61.79%
c3 [Ws/(m^3.K)]	**0.304**	0.224	-26.42%
c5 [J/(m^2.K)]	**6093**	3788	-37.83%

Deviations in the SEnOCalc comparison when using 3 days and 2 nights can be seen in Table 4.18. Despite an overestimation of the loss factor c_2, a slightly higher annual output is observed for all three operating temperature levels, mainly due to the underestimation of the c_1 loss term. The overestimation increases with increasing operating temperature which confirms the impact of c_1 as it is multiplied with the temperature difference, see Equation (3.7). Its influence is therefore proportional to the temperature change. When analysing the regression statistics of using this configuration with 3 days and 2 nights it is evident that the t-stat and the Multiple-R are higher in that case, see Table 4.19.

Table 4.18 SEnOCalc comparison for the tested flat plate collector using 3 days and 2 nights from 2011's measurements in accordance with the EN 12975 standard

	Energy output from test's at SP in 2011 [kWh/unit]	RESULTS using dynamic inlet temperature change - 1 good day (1/5), 1 moderate (19/4), 1 moderate/good (29/4) and 2 nights (17-18/4 and 29-30/4) [kWh/unit]	Deviation
25˚C	**591**	617	4.52%
50°C	**378**	407	8.21%
75°C	**227**	246	8.48%

Table 4.19 Regression statistics of the loss factors when using 3 days and 2 nights for collector characteristic determination for the tested flat plate collector

Parameters	**Collector characteristics from test's at SP in 2011**			RESULTS using dynamic inlet temperature change - 1 good day (1/5), 1 moderate (19/4), 1 moderate/good (29/4) and 2 nights (17-18/4 and 29-30/4)		
	Value	**R-square**	**|t-stat|**	**Value**	**R-square**	**|t-stat|**
c1[W/(m^2.K)]	**3.12**		**53**	2.68		88
c2[W/(m^2.K^2)]	**0.009**		**8**	0.015		34
		0.9989			0.9994	
c3 [Ws/(m^3.K)]	**0.30**		**74**	0.22		28
c5 [J/(m^2.K)]	**6093**		**10**	3789		176

5 DISCUSSION

It can be seen from previous parts that the experiments confirm the theory for most of our findings. However, a main issue restricts the validity of the experimental findings; the lack of time and material resulting in the test of only two collector designs at a single period of the year. To guarantee the validity of these findings, more tests need to be performed to ensure the reproducibility of the results.

While the test of the flat plate collector gives satisfying results, the other test conducted using dynamic inlet temperature change on a heat pipe design provides insignificant values, as illustrated in Table A.3 in Appendix A.1. For instance, the value of the first order heat loss factor, c_1 is negative. This might be the result of a positive output significantly high even when there is low irradiance, see Equation (3.7), changing the loss terms into input factors. One possible solution to this problem could be to use a temperature cycle with a much lower cycle time to cope with the high inertia. However, this needs further investigation before applied.

As previously mentioned; the findings for the flat plate collector have only been tested for one type and need to be tested for other types of flat plate collectors as well to confirm its validity. Indeed, it has been seen previously that the value of the loss factors can vary depending on the direction of the heat flow (see *3.3.3 Night time measurements*). This variation will greatly depend on the value of the internal resistance of the collector. In the previous case, the difference in the loss factor, c1, between a positive irradiance and no irradiance is quite small and B_{irr}, introduced by Rockendorf (1993), remains low but still significant. It would therefore be more relevant to study the behaviour of this factor and the loss parameters for different types of absorber constructions and materials and thus, different internal thermal resistances.

As mentioned before, the testing period was also a limiting criterion, especially due to the Swedish weather. It took a lot of rainy days to finally get a few days of perfect clear sky that were useful for testing. It would have been interesting to prolong the testing during the summer in order to have a wider range of weather conditions with more data points. This confirms that the QDT method today is very weather dependent for getting good estimations of all collector parameters; something that is hard to get around. We have managed to shorten the test period by using only a few days and nights, but these days have been selected manually based on their output and are seldom following consecutive in reality. These trials should therefore be seen as a proof that the setup of day and night measurements together can give a good estimation of the collector parameters.

When performing the test and investigating the changes in the factors, it has been found that many features can greatly influence the results. The first obvious reason for result deviation is the quality of the test installation. Indeed, each sensor must be calibrated carefully and in particular the pyranometers that have a huge impact on the values of the incidence angular factors. It has also been proved that just a small tilt of the pyranometer compared to the collector surface can significantly influence the value of the IAMs and $F'(\tau\alpha)_n$ resulting in misleading results. Moreover, when measuring the diffuse radiation, the position of the shadow ring above the pyranometer must be checked, especially during the spring/early summer where the trajectory of the sun can vary substantially from one day to another. Furthermore, as investigated in *4.2.2 Higher angular resolution*, unexpected events or conditions can also influence the results which emphasize the need for checking the installation and surrounding during the testing to eliminate all these external factors.

The eventual errors can also be illustrated by the intercept at the origin. In theory, the intercept should be set to zero since it represents no output when there is no input; system equilibrium. In the present case, when allowing an intercept, as seen in Table A.4, Appendix A2, there is an offset in the output of 9.35 W/m^2 between the model and the actual output. It can be observed that this small offset results in deviations in the collector factors, up to about 34%. This emphasizes the need to get lower this offset by performing the test as carefully as possible for measuring an accurate behaviour of the collector.

Another source of errors can come from the standards filtering. Indeed, a restriction of $T_{out} - T_{in} \geq 1\,K$ is imposed by the EN 12975 Standard for temperature sensors uncertainty. However, the need for this restriction can be argued since current sensors used in our tests can have an accuracy up to $0{,}05\,K$. When changing this filter, the value for c_1 can vary significantly and the number of data points for ΔT as a function of G_{tot} becomes less restricted, see *4.2.3 Night measurements*.

FURTHER INVESTIGATIONS

As mentioned above, the main findings need to be checked for more designs of collectors. When it comes to flat plate collectors, it can be interesting to evaluate the influence of the internal resistance on the results and generalize the QDT equation to a model valid for both day and night measurements. It would also be interesting to further investigate the behaviour of complicated designs for dynamic inlet temperature such as the heat pipe collector type.

It has also been seen that the interval of the inlet temperature can be narrowed down during the test and still achieve acceptable results regarding the collector characteristics determination. Since it can bring benefits for practical

considerations, it could be interesting to investigate the possibility of further reduction of this interval and its impact on the accuracy of the regression.

An investigation of the offset between the collector output and its model could be useful to evaluate its impact on the results and the possible options for restricting this deviation.

The impact of the filtering conditions should also be studied. As seen in *4.2.3 Night measurements*, a lack of scatter when plotting ΔT as a function of G_{tot} can influence the value of the results from the regression. It might be of interest to conduct a sensitivity analysis comparing the possible impact of a lack of data points with the deviations caused by sensor errors that are not taken away by the filter.

Results from the test of a dynamic inlet temperature for evacuated tubes using heat pipes gave misleading results. As mentioned before, one possible way to solve this problem and still make use of the dynamic inlet is to use longer cycle times.

6 CONCLUSION

Using a dynamic inlet temperature change to cover a broader interval of the measurement data has been proven valid both analytically and experimentally for the tested flat plate collector. This configuration enables a better parameter fitting using a multiple linear regression, especially for the thermal capacitance term c_5. It is also a self-regulated system that does not require measurements close to $\Delta T \sim 0$ to give a good estimation of η_0, i.e. it does not entail live inlet temperature control and predictions of the weather. However, expected problems have been encountered when trying a dynamic inlet temperature change on heat pipe evacuated tube collectors.

Increasing the angular resolution in the collector evaluation stage is useful for detecting unexpected errors caused by external factors and thus optimizing the model. This gives a chance to remove unwanted measurement errors. By increasing the angular resolution, assuming that there are sufficient measurement points, it is possible to get a more accurate determination of the incidence angle modifier even for non-symmetrical collectors with an irregular behaviour (CPC). The findings have been confirmed both analytically and experimentally. As a disadvantage, more data points must be gathered for the regression, more extensive calculations have to be performed requiring other calculation tools, making the regression more time consuming.

Combining a dynamic inlet temperature change with the use of night time measurements enables a shortening of the required test period for the thermal performance evaluation of solar collectors. This has been proven valid analytically for four different types of collectors; flat-plate, evacuated tube (U-pipe), unglazed and the compound parabolic collector (CPC). Indeed, the test period has been shortened down from a few weeks to 3 days and 2 nights with promising results. This has also been proven suitable in reality through experimental trials for one type of flat-plate collector. A small deviation is observed in the heat loss terms and is partially due to a change of heat-flux direction. This offset, that is dependent on the internal resistance of the collector, can however be estimated thanks to the irradiance dependency of first order heat loss factor c_1.

To conclude, these findings help the optimization of the QDT method for evaluating the thermal performance of solar collectors through error seeking, better accuracy and shortening of the required test period. Hence, they are worth being considered as an alternative test configuration and subject for further investigation and possible implementation in the future collector testing standards.

NOMENCLATURE

$(mC)_n$	effective thermal capacitance including piping for the collector array	$[J/(m^2K)]$
$(\tau\alpha)_n$	transmittance-absorption at normal incidence angle	[-]
ΔT	temperature difference	[°]
a_1	steady state first order loss factor	$[W/(m^2.K)]$
a_2	steady state second order loss factor	$[W/(m^2.K^2)]$
A_p	aperture area	$[m^2]$
A_r	receiver area	$[m^2]$
A_{coll}	collector area	$[m^2]$
b_0	incident angle modifier coefficient	[-]
B_w	wind dependence in Zero Loss Efficiency	[W/ms]
c_1	heat loss coefficient, modeled as F'U0	$[W/(m^2K)]$
c_2	temperature dependence of heat loss coefficient, modeled as $F'U_1$	$[W/(m^2K^2)]$
c_3	wind speed dependence of heat loss coefficient, modeled as $F'U_w$	$[Ws/(m^3K)]$
c_4	sky temperature dependence of the heat loss coefficient, modeled as $F'U_{sky}$	$[W/(m^2K)]$
c_5	effective thermal capacity, modeled as $(mC)_e$	$[J/(m^2K)]$
c_6	wind speed dependence in the Zero Loss Coefficient, modeled as	[W/ms]
C	thermal heat capacity	[J/(kgK)]
CPC	Compound Parabolic Collector	[-]
CR	concentration ratio	[-]
D	diameter of circular reciever	[m]
dTf/dt	mean time derivative for T_f within the time step	[K/s]

E	correction factor for the solar time	[min]
E_L	long wave irradiance	[W/m^2]
f	distance from vertex to the focal point	[m]
F	control function	[-]
F’	collector efficiency factor	[-]
F’$(\tau\alpha)_n$	Zero Loss Efficiency for direct radiation at normal incidence angle	[-]
F’U_0	heat loss coefficient at $(T_f - T_a) = 0$	[W/(m^{2}K)]
F’U1	temperature dependence of heat loss coefficient	[W/(m^{2}K^2)]
F’U_w	wind speed dependence of the heat loss coefficient	[Ws/(m^{3}K)]
F’U_{sky}	sky temperature dependence of the heat loss coefficient	[W/(m^{2}K)]
F_R	heat removal factor	[-]
G_b	beam radiation to collector plane	[W/m^2]
G_d	diffuse radiation to collector plane	[W/m^2]
G_{tot}	global hemispherical radiation to the collector plane	[W/m^2]
IAM	Incidence Angle Modifier	[-]
K	incidence angle modifier	[-]
$K_{\tau\alpha b}(\theta)$	incidence angle modifier for direct radiation	[-]
$K_{\tau\alpha d}$	incidence angle modifier for diffuse radiation	[-]
k_1	thermal loss coefficient at the insulation	[W/m^2/K]
k_2	thermal loss coefficient at the absorber tubes	[W/m^2/K]
k_3	thermal loss coefficient for radiation	[W/m^2/K^4]
L_{st}	standard meridian for the local time zone in degrees west	[°]

L_{loc}	longitude of the localization of the observer in degrees west	[°]
$\dot{m}$	mass flow rate	[l/s]
MLR	Multiple Linear Regression	[-]
Q_{coll}	power output from the collector	[W]
$Q_{coll,model}$	regression model power output	[W]
QDT	Quasi-Dynamic Testing	[-]
q'_u	collector array thermal output per unit length	[W/m^2/L]
r_r	focal point radius	[m]
S	absorbed solar radiation per unit area	[W/m^2]
T_f	mean fluid temperature in the collector; $(T_{in} + T_{out})0.5$	[°C]
T_a	ambient temperature near the collector	[°C]
T_{pm}	mean absorber temperature	[°C]
T_s	selective surface temperature	[°C]
T_{sky}	sky temperature	[°C]
T_{in}	inlet temperature	[°C]
T_{out}	outlet temperature	[°C]
U_{int}	internal heat transfer coefficient	[W/(m^2.K)]
U_L	general heat transfer coefficient	[W/(m^2.K)]
U_0	overall heat transfer coefficient	[W/(m^2.K)]
w	wind speed	[m/s]
W	distance between two tubes	[m]
W_r	width of the flat receiver	[m]

GREEK

α_s	solar altitude angle	[°]
α	absorptance, thermal diffusitity	[-]
β	collector slope	[°]

γ	surface azimuth angle	[°]
γ_s	solar azimuth angle	[°]
δ	declination	[°]
η	instantaneous collector efficiency	[-]
η_0	Zero Loss Efficiency at $(T_f - T_a) = 0$	[-]
θ_c	acceptance half angle	[°]
θ_i	incident angle	[°]
θ_L	longitudinal incidence angle	[°]
θ_T	transversal incidence angle	[°]
θ_z	zenith angle	[°]
ρ	energy density	[kg/m^3]
σ	Stefan-Boltzmann's constant	[W/(m^{2}K^4)]
τ	transmittance	[-]
Υ	intercept factor	[-]
ϕ	latitude	[°]
φ_r	rim angle	[°]
ω	hour angle	[°]

SUBSCRIPTS

a	ambient conditions
av	average
b	beam
coll	collector
d	diffuse
ew	east-west
f	fluid
in	inlet
L	longitudinal

n	normal
ns	north-south
out	outlet
p	profile
r	radius
s	sun
T	transversal
z	zenith

BIBLIOGRAPHY

12975:2006, European Standard EN. (2006). *Thermal solar systems and Components - Solar collectors - Part 2: Test methods.* Brussels: CEN.

Brandemuehl, M. J., & Beckman, W. A. (1980). Transmission of diffuse radiation through CPC and flat plate collector glazings. *Solar Energy, Vol. 24*, 511-513.

Duffie, J. A., & Beckman, W. A. (1991). *Solar Engineering of Thermal Processes, Second Edition.* John Wiley & Sons.

Enviko. (2009). *Solar Panels, Heating and Water*. Retrieved March 6, 2012, from Solar Thermal Products, Enviko: http://evacuatedtube.co.uk/

Fischer, S., & Müller-Steinhagen, H. (2009, October 14). Collector efficiency testing - the 2-node collector model ready for implementation in European Standard EN 12975. *ISES Solar World Congress , 11*.

GreenTerraFirma. (2007). *Evacuated Tube Collector*. Retrieved 01 19, 2012, from GreenTerraFirma: http://greenterrafirma.com/evacuated_tube_collector.html

Hardling, G. L., Zhiqiang, Y., & Mackey, D. W. (1985). Heat Extraction Efficiency of Concentric Glass Tubular Evacuated Collector. *Solar Energy Vol. 35, No. 1*, 71-79.

Herrick, C. S. (1982). Optical Transmittance Measurements on Solar Collector Cover of Cylindrical Glass Tubes. *Solar Energy Vol. 28, No. 1*, 5-11.

IEA. (2010). *Key World Energy STATISTICS.* Paris: International Energy Agency.

Löf, G. O., & Duffie, J. A. (1963). Optimization of Focusing Solar-Collector Design. *Transactions of the ASME, 85 A.*

Mandil, C. (2008, March 26). *Our energy for the future*. Retrieved February 28, 2012, from http://sapiens.revues.org/70

Perers, B. (1993). Dynamic Method for Solar Collector Array Testing and Evaluation with Standard Database and Simulation Programmes. *Journal of the Int. Solar Energy Society, Vol. 50, No. 6*, 517-526.

Perers, B. (1995). *Optical Modelling of Solar Collectors and Booster Reflectors under Non Stationary Conditions.* Department of Technology. Stockholm: Almqvist & Wiksell International.

Perers, B. (1997). An Improved Dynamic Solar Collector Test Method for Determination of Non-Linear Optical and Thermal Characteristics with Multiple Regression. *Solar Energy, Vol. 59*, 163-178.

Rockendorf, G. S. (1993). The Difference of Collector Test Results between the Heat Loss Measurement and the Methods with Radiation. (K. E., Ed.) *ISES Solar World Congress, 5*, 323-328.

Sartori, E. (2006). Convection coefficient equations for forced air flow over flat surfaces. *Solar Energy 80*, 1063-1071.

Solar Heating Canada . (2009). *Evacuated Tube Solar Collector*. Retrieved 01 19, 2012, from Solar Water Heating: http://www.solarheatingcanada.com/evacuated-tube-solar-collector.html

Souka, A. F., & Safwat, H. H. (1966). optimum Orientations for the Double Exposure Flat-Plate Collector and Its Reflector. *Solar Energy 10*, 170.

Theunissen, P.-H., & Beckman, W. A. (1985). Solar Transmittance Characteristics of Evacuated Tubular Collectors with Diffuse Back Reflectors. *Solar Energy, Vol. 35, No. 4*, 311-320.

Yong, K., & Taebeom, S. (2007). Thermal Performances Comparisons of the Glass Evacuated Tube Solar Collectors with Shapes of Absorber Tube. *Renewable Energy 32*, 772-795.

A APPENDIX

A.1 DYNAMIC INLET TEMPERATURE

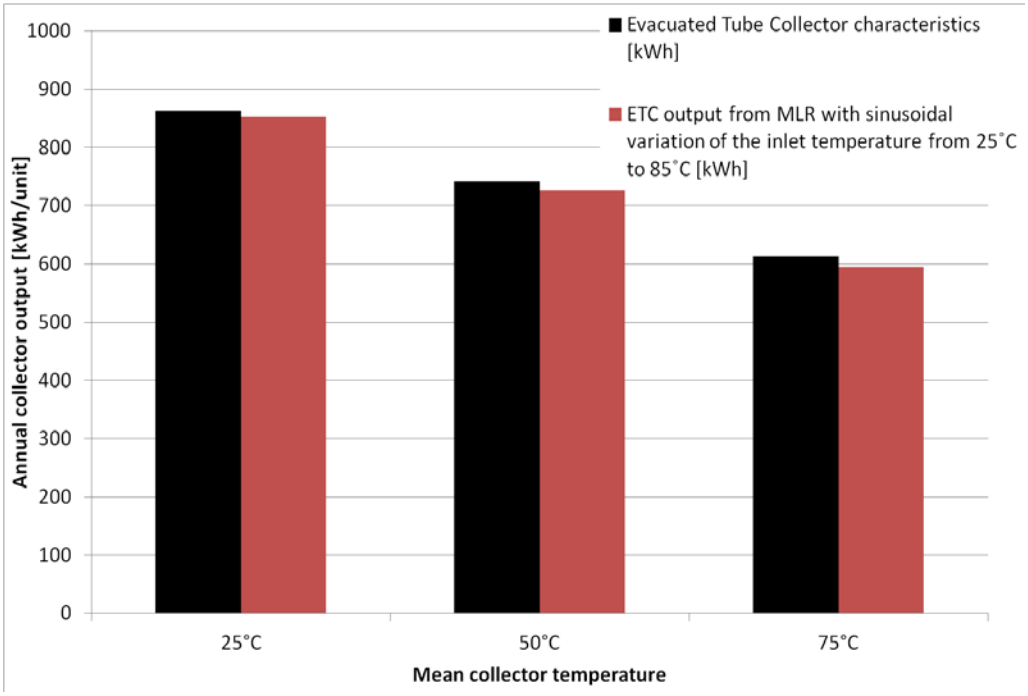

Figure A.1 Collector output comparison for an evacuated tube with and without a dynamic temperature inlet profile assuming a collector area of 1m^2 located in Stockholm, Sweden

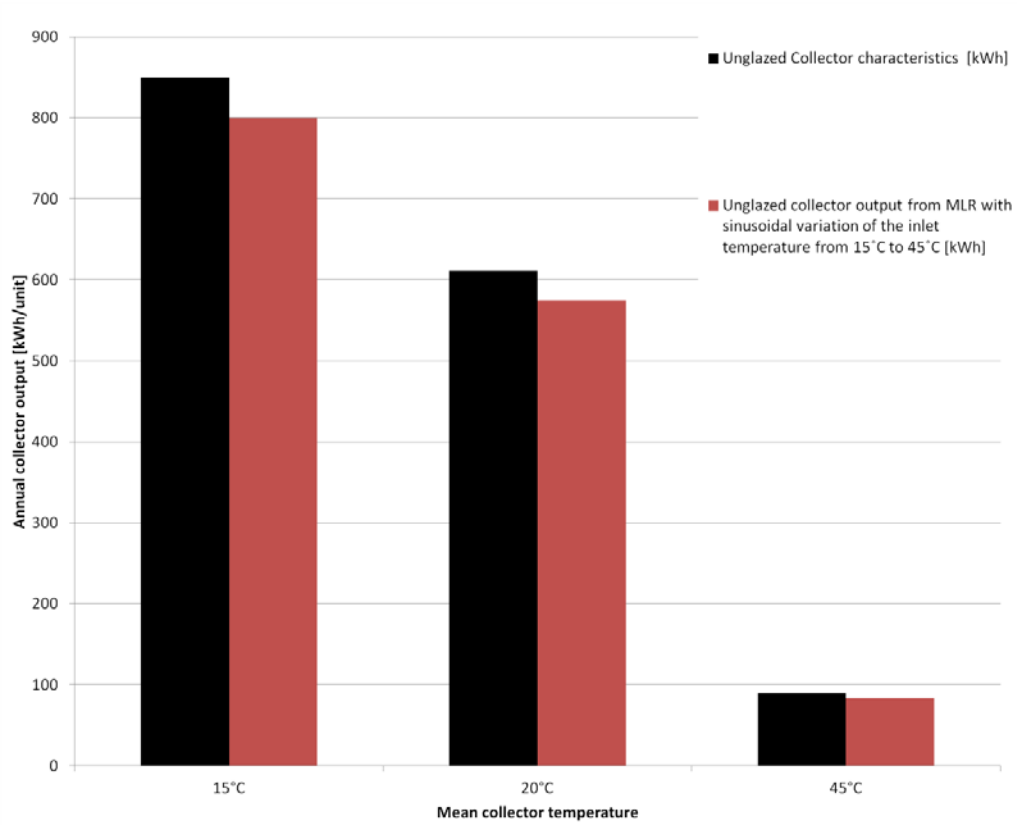

Figure A.2 Output comparison for an unglazed collector with and without a dynamic temperature inlet assuming a collector area of 1m2 located in Stockholm, Sweden

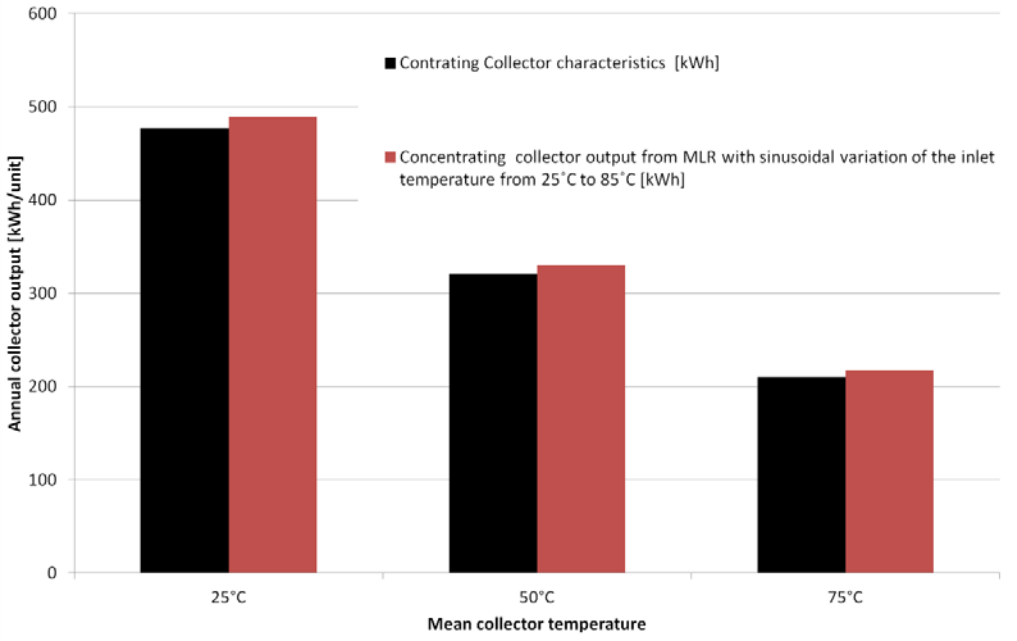

Figure A.3 Output comparison for a CPC collector assuming a collector area of $1m^2$ located in Stockholm, Sweden

Table A.1 Results for dynamic inlet temperature change with evacuated tube, unglazed and concentrating collector types

Parameters*	Units	Evacuated Tube Collector			Unglazed collector			Concentrating collector					
		Collector characteristics	Results from the MLR: Sinusoidal variation of the inlet temperature from 25°C to 85°C		Collector characteristics	Results from the MLR: Sinusoidal variation of the inlet temperature from 15°C to 45°C		Collector characteristics for transversal IAM factors	Results from the MLR: Sinusoidal variation of the inlet temperature from 25°C to 85°C		Collector characteristics for longitudinal IAM factors	Results from the MLR: Sinusoidal variation of the inlet temperature from 25°C to 85°C	
			Results	Deviation		Results	Deviation		Results	Deviation		Results	Deviation
$F'(\tau\alpha)_n$	-	0.70	0.69	-0.95%	0.85	0.85	-0.41%	0.75	0.75	0.35%	0.75	0.75	-0.57%
$K(\tau\alpha)$ (θT=10°)		1.00	1.00	0.13%	-	-	-	1.00	0.99	-1.05%	1.00	1	0.00%
$K(\tau\alpha)$ (θT=20°)	-	1.02	1.02	0.29%	-	-	-	0.99	0.98	-0.83%	0.99	0.99	0.33%
$K(\tau\alpha)$ (θT=30°)		1.12	1.12	-0.01%	-	-	-	0.70	0.69	-1.88%	0.98	0.99	0.93%
$K(\tau\alpha)$ (θT=40°)	-	1.30	1.30	-0.37%	-	-	-	0.50	0.49	-2.31%	0.96	0.98	2.00%
$K(\tau\alpha)$ (θT=50°)		1.50	1.49	-0.86%	-	-	-	0.45	0.52	16.43%	0.91	0.96	5.40%
$K(\tau\alpha)$ (θT=60°)		1.00	1.00	-0.26%	-	-	-	0.40	0.37	-7.52%	0.85	0.90	6.16%
$K(\tau\alpha)$ (θT=70°)		0.70	0.70	-0.70%	-	-	-	0.30	0.19	-36.13%	0.60	0.85	41.66%
$K(\tau\alpha)$ (θT=80°)		0.40	0.42	4.89%	-	-	-	0.15	-	-	0.30	0.49	-
$K(\tau\alpha)$ (θT=90°)		0.00	-	-	-	-	-	0.00	-	-	0.00	0	-
$K(\tau\alpha)d$	-	1.20	1.22	1.71%	0.900	0.904	0.40%	0.60	0.65	8.36%	0.60	0.66	10.57%
b0	-	-	-	-	0.20	0.19	-2.69%	-	-	-	-	-	-
c1 (=F'U0)	$W/(m^2.K)$	1.00	1.08	7.88%	15.00	14.85	-1.02%	2.50	2.56	2.56%	2.50	2.57	2.72%
c2 (=F'U1)	$W/(m^2.K^2)$	0.0100	0.0101	0.59%	0.020	0.023	13.62%	0.010	0.009	-10.60%	0.010	0.009	-10.28%
c3 (=F'Uw)	$W.s/(m^3.K)$	-	-	-	2.00	2.02	1.22%	-	-	-	-	-	-
c4 (=F'Usky)	$W.s/(m^2.K)$	-	-	-	0.500	0.504	0.89%	-	-	-	-	-	-
c5 (=(mC)n)	$J/(m^2.K)$	6500	6378	-1.88%	12000	11928	-0.60%	6500	6450	-0.77%	6500	6397	-1.58%
c6(=Bw)	$W/(m.s)$	-	-	-	0.010	0.0097	-3.04%	-	-	-	-	-	-

**ϑT refers to the transversal incidence angle in all the cases except for concentrating collector when "longitudinal IAM factors" stated*

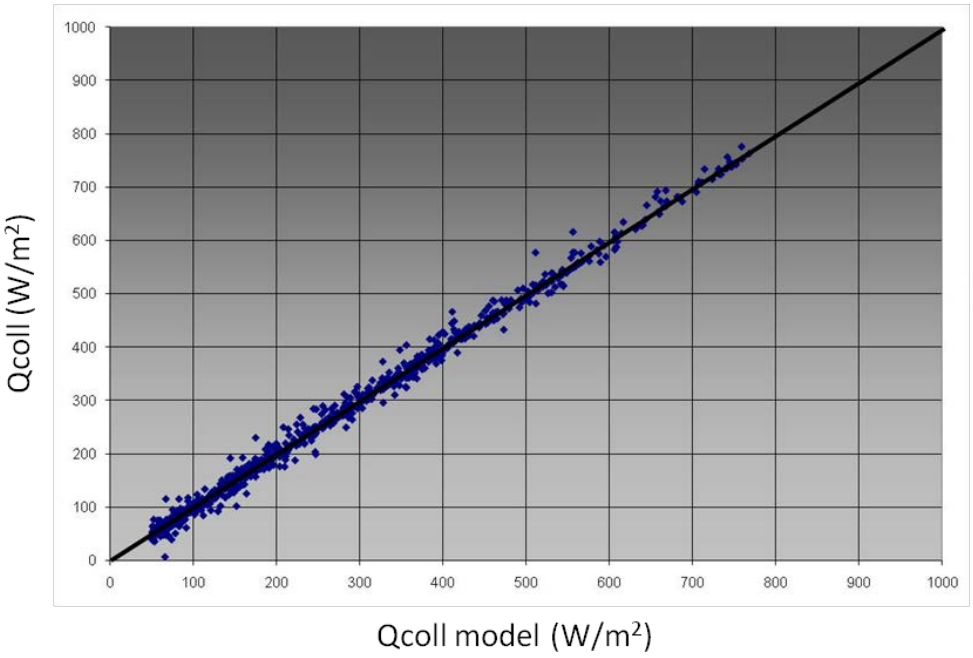

Figure A.4 Power output as a function of regression model predicted output for a flat plate collector with dynamic inlet temperature

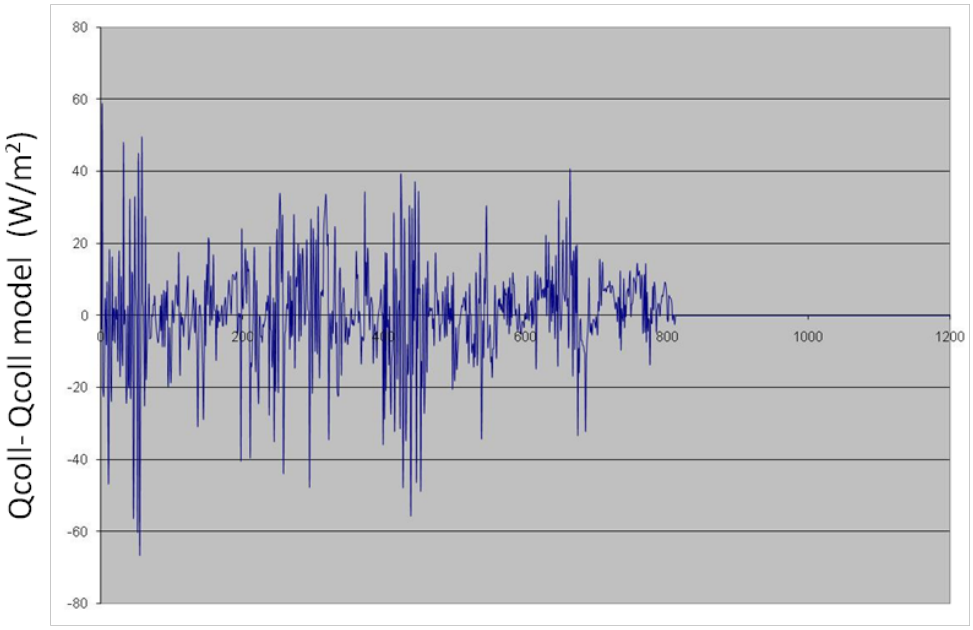

Figure A.5Residuals from the regression model for a flat plate collector with dynamic inlet temperature

Table A.2 Statistical factors from a MLR on test data for a flat plate collector with dynamic inlet temperature

Statistical factors		
Parameters	**|t-stat|**	**R-square**
F´(τα)n [-]	141	
K(τα) (θT=10°) [-]	196	
K(τα) (θT=20°) [-]	156	
K(τα) (θT=30°) [-]	180	
K(τα) (θT=40°) [-]	143	
K(τα) (θT=50°) [-]	113	
K(τα) (θT=60°) [-]	60	
K(τα) (θT=70°) [-]	30	
K(τα) (θT=80°) [-]	6	
K(τα) (θT=90°) [-]	-	**0.99832**
Kταd [-]	152	
c1 [W/(m^2.K)]	29	
c2 [W/(m^2.K^2)]	6	
c3 [Ws/(m^3.K)]	16	
c5 [J/(m^2.K)]	67	

Table A.3 Results and statistical factors from a MLR on test data for an evacuated tube collector

Parameters	**Results from 2012 measurements** Sinusoidal variation of the inlet temperature from 15˚C to 85˚C	R^2 = 0.941	**Results from SP's test in 2010** 4 different constant inlet temperature levels (20˚C, 40˚C, 60˚C, 90˚C)	
	Results	|t-stat|	Results	Deviation
F´(τα)n [-]	0.42	13	0.65	54.49%
K(τα) (θT=10°) [-]	1.35	23	1.03	-23.70%
K(τα) (θT=20°) [-]	1.04	15	1.08	3.42%
K(τα) (θT=30°) [-]	1.53	25	1.16	-23.87%
K(τα) (θT=40°) [-]	1.68	25	1.30	-22.41%
K(τα) (θT=50°) [-]	2.02	25	1.62	-19.61%
K(τα) (θT=60°) [-]	2.09	16	1.55	-25.67%
K(τα) (θT=70°) [-]	1.62	4	1.57	-3.11%
K(τα) (θT=80°) [-]	5.58	1	0.66	-88.26%
K(τα) (θT=90°) [-]	0	-	0.00	-
Kταd [-]	1.67	25	1.13	-32.54%
b0 [-]	-	-	-	-
c1 [W/(m^2.K)]	-3.03	5	0.73	-124.10%
c2 [W/(m^2.K^2)]	0.072	9	0.016	-78.03%
c3 [Ws/(m^3.K)]	-	-	-	-
c5 [J/(m^2.K)]	7458	21	5488	-26.41%
Steady-State η0	53.0%	-	68.8%	29.78%

A.2 NIGHT TIME MEASUREMENTS

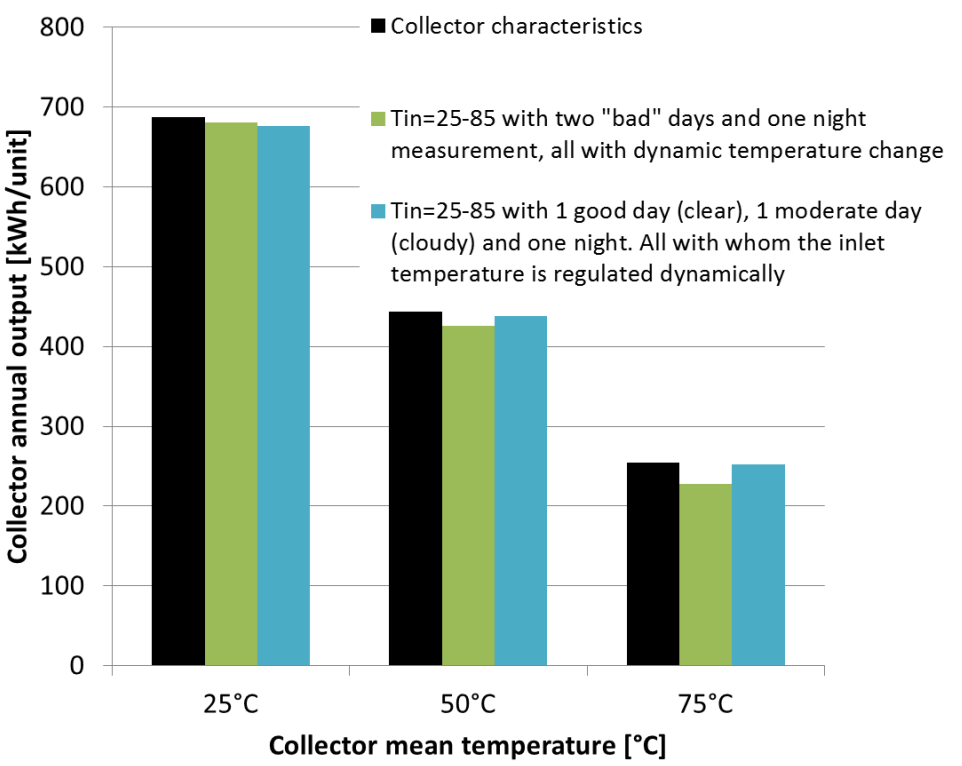

Figure A.6 Results comparison looking at the annual output from SEnOCalc for a flat-plate solar collector, assuming a collector area of 1m2 located in Stockholm, Sweden

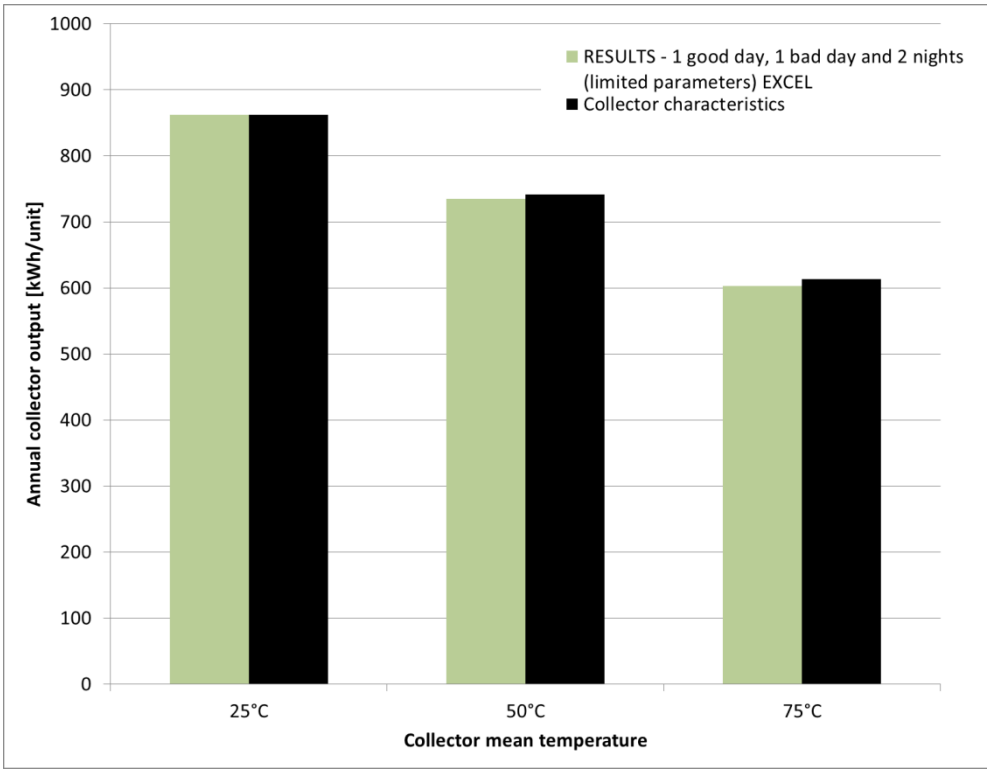

Figure A.7Results comparison of the annual collector output for an evacuated tube collector assuming an aperture area of 1m^2 located in Stockholm,Sweden

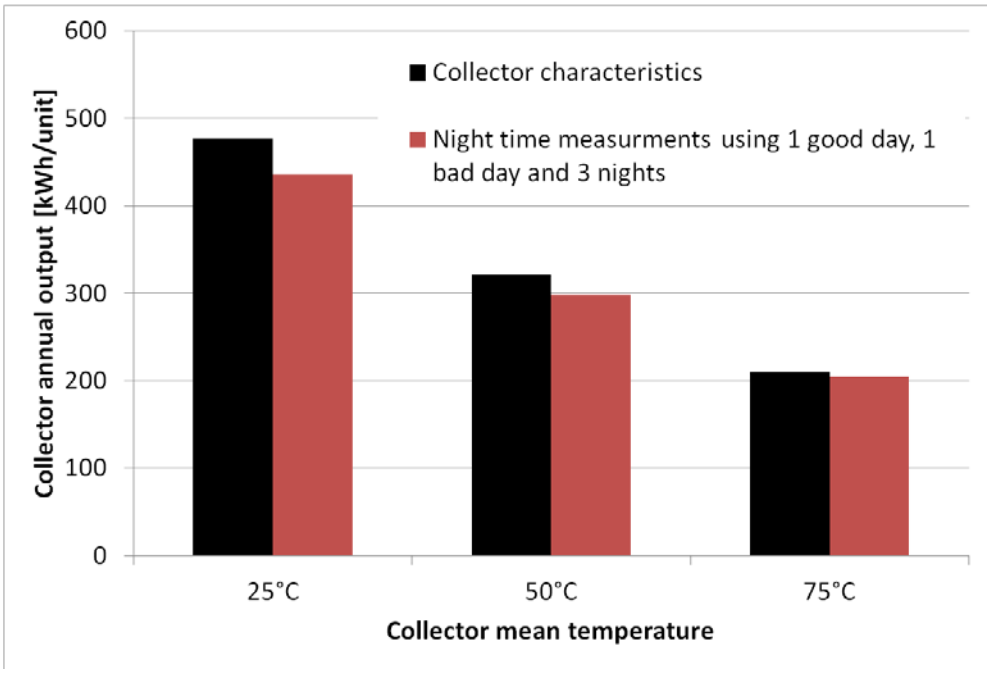

Figure A.8 Results comparison looking at the annual output from SEnOCalc for a CPC solar collector, assuming a collector area of 1m^2 located in Stockholm, Sweden

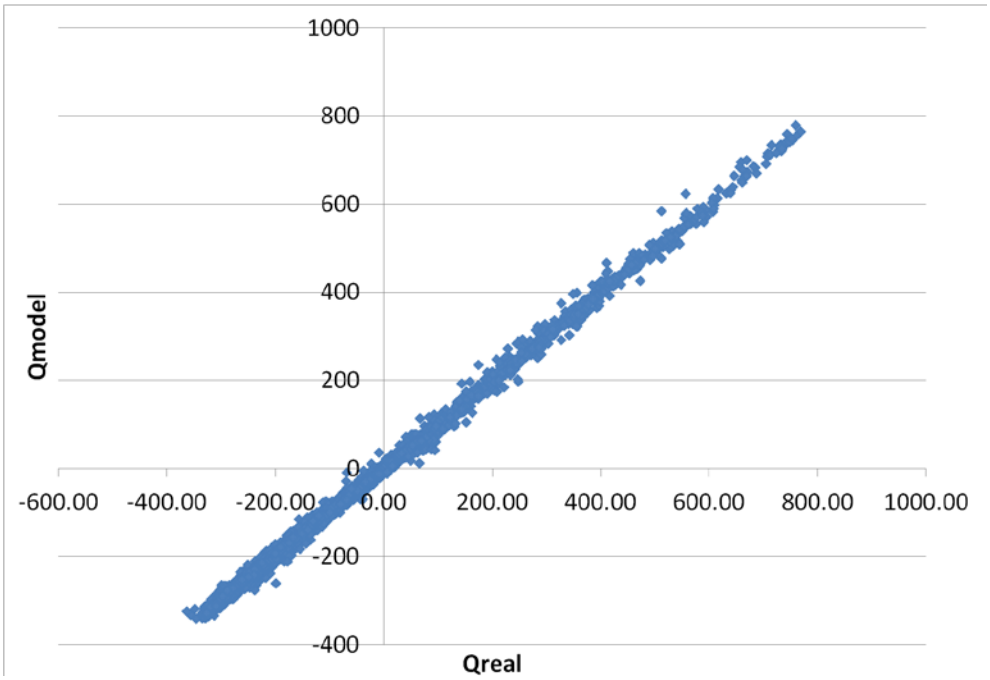

Figure A.9 Qmodel v/s Qreal fitting using measurements from 3 days and 2 nights for a flat plate collector with a dynamic inlet temperature

Table A.4 Evaluation of the impact of the intercept on the MLR factors for a flat plate collector with day and night measurements - dynamic inlet temperature change

Parameters	**Results with no intercept**	**Results with intercept = 9.35 W/m²**	
	Sinusoidal variation of the inlet temperature from 15˚C to 85˚C - Day and Night measurements		
	Results	Results	Deviation
F´(τα)n [-]	**0.72**	0.72	0.84%
K(τα) (θT=10°) [-]	**1.02**	1.01	-0.80%
K(τα) (θT=20°) [-]	**1.00**	1.00	0.54%
K(τα) (θT=30°) [-]	**0.98**	0.97	-0.75%
K(τα) (θT=40°) [-]	**0.88**	0.89	0.37%
K(τα) (θT=50°) [-]	**0.82**	0.82	-0.40%
K(τα) (θT=60°) [-]	**0.71**	0.70	-1.79%
K(τα) (θT=70°) [-]	**0.58**	0.59	0.96%
K(τα) (θT=80°) [-]	**0.39**	0.32	-17.22%
K(τα) (θT=90°) [-]	**0**	0	-
Kταd [-]	**0.94**	0.93	-0.95%
b0 [-]	**0.323**	0.341	5.59%
c1 [W/(m².K)]	**2.64**	3.14	18.81%
c2 [W/(m².K²)]	**0.015**	0.010	-34.32%
c3 [Ws/(m³.K)]	**0.23**	0.21	-6.18%
c5 [J/(m².K)]	**3814**	3809	-0.15%
Steady-State η0	**71.4%**	71.8%	0.58%